MICROCOPY RESOLUTION TEST CHART
NATIONAL BUREAU OF STANDARDS 1963 A

AD-A192 175

OPTICAL SCIENCES CENTER

RESEARCH IN THE OPTICAL SCIENCES

A Final Report Prepared for
The Joint Services Optics Program

88 2 22 296

UNIVERSITY OF ARIZONA
TUCSON, ARIZONA

RESEARCH IN THE OPTICAL SCIENCES

A Final Report Prepared for

The Joint Services Optics Program

Robert R. Shannon, Director

Optical Sciences Center

University of Arizona

Tucson, Arizona 85721

DTIC
ELECTE
FEB 2 3 1988

H

Final Report for Period 1 October 1984 - 30 September 1987

December 1987

REPORT DOCUMENTATION PAGE

Form Approved
OMB No. 0704-0188

1a. REPORT SECURITY CLASSIFICATION	1b. RESTRICTIVE MARKINGS
UNCLASSIFIED	

2a. SECURITY CLASSIFICATION AUTHORITY	3. DISTRIBUTION/AVAILABILITY OF REPORT
	Approved for public release;
2b. DECLASSIFICATION/DOWNGRADING SCHEDULE	distribution unlimited

4. PERFORMING ORGANIZATION REPORT NUMBER(S)	5. MONITORING ORGANIZATION REPORT NUMBER(S)
	ARO 22288.64-PH

6a. NAME OF PERFORMING ORGANIZATION	6b. OFFICE SYMBOL (If applicable)	7a. NAME OF MONITORING ORGANIZATION
Optical Sciences Center		

6c. ADDRESS (City, State, and ZIP Code)	7b. ADDRESS (City, State, and ZIP Code)
University of Arizona Tucson, Arizona 85721	

8a. NAME OF FUNDING/SPONSORING ORGANIZATION Army Research Office Air Force Office of Sci. Res.	8b. OFFICE SYMBOL (If applicable)	9. PROCUREMENT INSTRUMENT IDENTIFICATION NUMBER MIPR ARO 101-8o F49620-85-C-0039

8c. ADDRESS (City, State, and ZIP Code)	10. SOURCE OF FUNDING NUMBERS			
U.S. Army Research Office P.O. Box 12211 Research Triangle Park, NC 27709	PROGRAM ELEMENT NO.	PROJECT NO.	TASK NO	WORK UNIT ACCESSION NO

11. TITLE *(Include Security Classification)*

Research in the Optical Sciences   unclassified

12. PERSONAL AUTHOR(S)
Robert R. Shannon, Director, et al.

13a. TYPE OF REPORT	13b. TIME COVERED	14. DATE OF REPORT (Year, Month, Day)	15. PAGE COUNT
Final	FROM 10/1/84 TO 9/30/87	1987 Dec. 15	171

16. SUPPLEMENTARY NOTATION

17. COSATI CODES			18. SUBJECT TERMS (Continue on reverse if necessary and identify by block number)
FIELD	GROUP	SUB-GROUP	Optics; optical sciences

19. ABSTRACT *(Continue on reverse if necessary and identify by block number)*

This optical science research program has covered many areas of investigation in the physics, technology, and potential application of optics and optical systems. This three-year program involved twenty-two projects from theoretical physics to practical measurements.

20. DISTRIBUTION/AVAILABILITY OF ABSTRACT	21. ABSTRACT SECURITY CLASSIFICATION
☐ UNCLASSIFIED/UNLIMITED ☒ SAME AS RPT ☐ DTIC USERS	Unclassified

22a. NAME OF RESPONSIBLE INDIVIDUAL	22b. TELEPHONE (Include Area Code)	22c. OFFICE SYMBOL
Robert R. Shannon	(602) 621-6997	

DD Form 1473, JUN 86   *Previous editions are obsolete.*   SECURITY CLASSIFICATION OF THIS PAGE

TABLE OF CONTENTS

Page

RESEARCH IN THE OPTICAL SCIENCES

Robert R. Shannon

The research reported here covers the period October, 1984 to September, 1987. The research was performed at the Optical Sciences Center under the Joint Services Optical Program (JSOP). The statistics of the program are impressive. Twenty-two different research programs were carried out by twenty different investigators. Over 160 publications resulted from work done under this contract, as did numerous invited and contributed papers. Students who furthered their educational programs with research work performed under this contract include the recipients of 13 Ph.D. degrees and 10 M.S. degrees.

The work covered a wide range of topics, from theoretical physics to practical measurements in the optical shop. About two-thirds of the work represented the continuation of projects initiated under the previous JSOP contract, with the remaining third being new startups under this contract. Some projects ended during the term of the contract.

A few highlights will be mentioned in this introduction. The reader is referred to the individual research summaries or the publications listed in this report for a full understanding of the work carried out.

A project led by P. Meystre investigated the microscopic behavior of individual atoms in a resonant cavity. These studies have led to an understanding of the development of coherence in a laser and of the relation between classical and quantum descriptions of the operation of a laser.

N. Peyghambarian and students initiated the construction and operation of a facility for the generation and application of femtosecond optical pulses. This contract served as the principal initial source of support for this capability. The facility has been producing measurements with 30-fs pulses for the past year, and has reported detailed measurements of dynamic behavior in the region of the band edge in semiconductors.

A joint program between G. Stegeman and C. Falco carried through the investigation of optical and acoustic properties of metallic superlattice films. The observation of Rayleigh and Stonley waves in these multilayers was accomplished with a theoretical and experimental verification of the elastic constants of these films.

I

Work by D. Sarid investigated nonlinear surface interactions in microcrystallite films, and has led to the development of a continuing program on the nonlinearity of waveguides with dispersed microcrystalline materials. Other work by Sarid on long-range surface plasmons completed a prior program on the propagation of optical signals along metallic boundaries using surface plasmon polaritons.

A major program carried out by the Stegeman group investigated several aspects of the physics and applications of guided waves. Work was done on the theory and experimental verification of grating coupling in films. Low-loss organic waveguides were fabricated and demonstrated. Approaches to optical limiters were investigated both theoretically and experimentally on two programs under JSOP.

A program by C. Falco led to the production of several coatings for x-ray reflectors for application in the soft x-ray region. The success of this program, initiated under JSOP, eventually led to the award to Falco of a University Research Initiative Program grant in the area of x-ray optics.

The use of biased conducting masks during the ion etch process was demonstrated by U. Gibson to have possibilities for the control of edges in the fabrication of waveguides. Additional work carried out by Gibson studied the properties of mixed phase material for the fabrication of nonlinear waveguides. Work by Gibson also investigated the possibilities of using ion beam methods for the coating of plastic optical components.

Considerable progress was made in work directed by M. Sargent on the quantum theory of multiwave mixing. Several publications related results on topics such as quantum squeezing.

A program by H. Gibbs and N. Peyghambarian investigated the use of GaAs etalons as nonlinear decision-making components for potential optical computers. Major achievements under this program included picosecond gating, fabrication of arrays of gates, theoretical and experimental investigation of GaAs band-edge nonlinearities, and demonstration of waveguide electronic nonlinearity. An additional program was directed toward the demonstration of room-temperature operation of bistable GaAS etalons using laser diode sources.

Additional work carried out jointly by Gibbs, Jacobson, Macleod, and Peyghambarian investigated the optical nonlinearities of thin deposited films. Initial work was carried out in developing interference filters of ZnS. The mechanism of the effect was probably thermal and limited in temporal bandwidth, but the results of the work led to several demonstrations of optical decision-making systems.

An attempt to produce densified thin films by ultrasonic excitation during the deposition process was carried out by Jacobson, Macleod and co-workers. Some

2

apparent improvements in film density were noted, along with additional new effects. However, the improvement in film characteristics from ultrasonic excitation appears to be incremental rather than fundamental.

The construction of a device for high-speed wavefront sensing was carried out by C. Koliopoulos. A high-speed heterodyne wavefront phase sensor was constructed and demonstrated using a unique checkerboard beamsplitter approach. Another demonstration of a new sensor was the construction of a direct-readout CCD x-ray intensifier by E. Dereniak and H. Roehrig. This device was fabricated jointly with an industrial organization and demonstrated to operate at high quantum efficiency.

Several methods of measuring the surface figure on an optical element were investigated by R. Parks. The technique of using a bar spherometer has the capability of accurate measurements of principal local curvatures on an aspheric surface in the generation stage. A second approach to obtaining small-scale surface errors by measurement of the intensity distribution in the image plane was also carried out.

Work supervised by R. Shack consisted of a theoretical investigation of the characteristics of aberrated Gaussian beams. This work examined the properties of imperfect transmission of light in the Gaussian beam region.

A program was carried out by B. Seraphin to investigate the possibility of measuring the properties of materials by the use of modulated emittance spectroscopy. Although the technique, which depends upon sychronous detection using computer techniques, appeared to have possibilities, the signal-to-noise ratio possible with available detectors did not lead to a promising result.

In summary, a wide variety of topics was investigated, with a good return in terms of both scientific accomplishments and the development of students.

NONLINEAR DYNAMICS AND CHAOS
IN INTRACAVITY QUANTUM ELECTRODYNAMICS

Pierre Meystre

PUBLICATIONS

P. Filipowicz, J. Javanainen, and P. Meystre, "Theory of a microscopic maser," Phys. Rev. A **34**, 3086 (1986).

P. Meystre and E. M. Wright, "Chaos in the micromaser," in *Chaos, Noise and Fractals*, E. R. Pike and L. Lugiato, eds. (Adam Hilger, Bristol, 1987).

T. A. B. Kennedy, P. Meystre, and E. M. Wright, "The micromaser as a problem in 'quantum chaology'," in *Fundamentals of Quantum Optics II*, F. Ehlotzky, ed. (Springer-Verlag, Heidelberg, 1987).

P. Meystre, "Repeated measurements on a single harmonic oscillator," Opt. Lett. **12**, 669 (1987).

P. Meystre and E. M. Wright, "Measurements-induced dynamics of a micromaser," Phys. Rev. A, in press.

J. Javanainen and P. Meystre, "Single-atom quantum mechanics," in the 1989 McGraw-Hill Yearbook of Science and Technology, in press.

T. A. B. Kennedy and D. F. Walls, "Squeezed quantum fluctuations and macroscopic quantum coherence," Phys. Rev. A, in press.

C. Savage, "Oscillations and quantized second harmonic generation," Phys. Rev. A, in press.

C. Savage and H. J. Carmichael, "Single-atom optical bistability," submitted to Phys. Rev. Lett.

Invited papers

P. Filipowicz, J. Javanainen and P. Meystre, "The micromaser," invited paper, Fourteenth International Quantum Electronics Conference, San Francisco, CA (1986).

P. Meystre, "Chaos in the micromaser," invited paper, International Workshop on Fractals and Chaos, Como, Italy (1986).

P. Meystre, "The micromaser: a true return map in quantum optics," invited paper, Winter Symposium on the Physics of Quantum Electronics, Snowbird, UT (1987).

P. Meystre, "Classical and quantum chaos in the micromaser," invited paper, Second International Seminar on Quantum Optics, Obergurgl, Austria (1987).

T. A. B. Kennedy, P. Meystre, C. M. Savage, and E. M. Wright, "Quantum and classical instabilities in a micromaser," invited paper, International Workshop on Instabilities, Dynamics and Chaos in Nonlinear Systems, Il Ciocco, Lucca, Italy (1987).

P. Meystre, T. A. B. Kennedy, and E. M. Wright, "The micromaser: from cavity QED to quantum chaos," invited paper, Adriatico Research Conference on Vacuum in Nonrelativistic Matter-Radiation Systems, Trieste, Italy (1987).

Contributed paper

T. A. B. Kennedy, P. Meystre, C. Savage, and E. M. Wright, "Chaos in the micromaser," *contributed paper*, Fifteenth International Quantum Electronics Conference, Baltimore, MD (1987).

SCIENTIFIC PERSONNEL

P. Meystre

C. Savage

T. A. B. Kennedy

RESEARCH FINDINGS

Introduction

Intracavity quantum electrodynamics is the study of the interaction between few atoms and the (typically single-mode) fields that can be realized in high-Q microwave cavities. Over the past year, this research has addressed aspects of this problem that are relevant not only in traditional quantum optics (coherence, non-classical fields) but simultaneously make contact with nonlinear dynamics and chaos. A number of novel and unexpected results have been obtained which might have considerable impact and application in quantum electronics, while at the same time contributing to a deeper

understanding of the transition between quantum mechanical and classical dynamics. Specifically, these results will (1) help design lasers with significantly reduced intensity fluctuations, and (2) shed new light on the elusive problem of quantum chaos and on the correspondence between classical and quantum physics.

Lasers with reduced intensity fluctuations

A detailed study of a truly microscopic maser, the micromaser, has been performed. In the process, it has been possible to determine precisely the reasons why conventional lasers and masers produce coherent light; i.e., light with intensity fluctuations ΔI given by $\Delta I = I^{1/2}$, where I is the laser intensity. Somewhat paradoxically perhaps, it is the *incoherent* nature of the loss and pump mechanisms that lead to such an output. Intuitively, this can be understood as follows: at the microscopic level, the dynamics of the atom-field interaction is characterized by a series of Rabi frequencies which scale as the square root of the photon numbers. The "granulated character" of the phases can lead to non-classical fields such as sub-Poissonian or squeezed states. But the fluctuations associated with pump and loss mechanisms "smear out" the quantum mechanical phases. The electrons in the maser or laser act then very much like a classical current, and generate in the best case a Poissonian (coherent) field. But there is no fundamental reason why this should be the case. If cleaner pumping mechanisms are used and losses are minimized, as is the case in the micromaser, it is readily possible to generate sub-Poissonian fields; i.e., fields with reduced intensity fluctuations, $\Delta I < I^{1/2}$.

In the last two years or so, a few groups have independently come to the same realization, and have begun detailed investigations of alternate, "clean" laser-pump mechanisms. These include the New Zealand group of D. F. Walls, who proposes the use of "squeezed pumps,"[1] and Y. Yamamoto et al.[2] in Japan, who propose the use of negative feedback loops to generate amplitude squeezed states. This is a novel, wide-open field of investigation, with a very high potential payoff. Planned future work will extend and generalize our micromaser results toward systems of more practical interest. Various pumping and feedback mechanisms will be investigated and compared. In collaboration with Dr. Walls' group, more exotic schemes, including, for example, the use of squeezed and sub-Poissonian pump mechanisms, will also be considered.

Instabilities in quantum mechanical systems

In a second facet of this work, it has been shown that, in general, the semi-classical version of the micromaser exhibits deterministic chaos: as the cavity damping rate or

6

the interaction time of the atoms with the resonator is varied, the system follows a period-doubling scenario to chaos, followed by an inverse Feigenbaum sequence terminated by a crisis. An extra degree of complexity is provided by a number of coexisting attractors with fractal basins of attraction.

In contrast, it can be shown on the basis of very general theorems that the *quantum mechanical* micromaser always reaches a unique steady state. Hence, it might seem that semi-classical physics exhibits a wealth of possible dynamical behaviors absent from quantum mechanics. Yet, one would like to believe that quantum mechanics includes classical physics as a limit. This, of course, is the central question of quantum chaos.

A hint at the fundamental difference between classical and quantum physics was provided when it was shown that in the micromaser, an average of the semi-classical trajectories over a large random set of initial conditions reproduces at least some of the quantum mechanical features, such as the average maser intensity and thresholds, amazingly well. The point is that in its conventional form, quantum mechanics yields predictions for a large ensemble of identical systems, whereas classically the dynamics are interpreted in terms of single realizations. Even in the classical case, oscillations would not be evident on averaging over an ensemble unless the phase of the oscillations was fixed absolutely, which is not generically the case. Therefore it can be claimed that the paradox is only apparent. What should be considered is the quantum dynamics of a single representative system, which obviously requires including the repeated measurements performed to monitor it.

More precisely, it has been pointed out by W. E. Lamb, Jr.[3] that to study the dynamical behavior of a quantum system, it is necessary to explicitly include the effects of the measurements that must be performed to monitor it. To properly do so requires coupling the system under investigation to a meter system. The measurement process typically produces a back-action on the system which influences its future dynamics. This is quite different from the classical situation, where "any observation of the system would involve some intervention from outside the system, but the structure of the theory is such that the effects of measurements can easily be ignored."[3]

Analyzation of the influence of repeated measurements on a micromaser indicates that they lead to measurement-induced dynamics and instabilities which are not apparent when conventional ensemble-average predictions are considered; i.e., when the system is prepared to a fresh initial state after each measurement, wiping out any memory of the past in the process. Two cases where dynamical information about a single representative system can be extracted from such measurements were

7

explicitly discussed: measurement-induced quantum diffusion between two different mean values of the intracavity intensity, and measurements-induced relaxation oscillations.

It is not suggested that measuring the evolution of a quantum dynamical variable will make it behave in a classical fashion, but rather that in a single realization the dynamics of the system can become evident. In contrast to what is generally assumed in classical dynamics, the observed quantum "trajectories" are measurement-induced and measurement-dependent. Whether it is possible to obtain a classical or semi-classical behavior by performing an appropriate measurement on a quantum dynamical variable is a separate issue that goes beyond the scope of this report.

In an attempt to determine how generic the micromaser results are, research on intracavity second-harmonic generation has also been initiated. Like the micromaser, this system presents the paradox that quantum mechanically, this dissipative system approaches a unique steady state, while its semi-classical version displays oscillations, period-doubling, and chaos. The dilemma is how to reconcile these results.

Another system of considerable interest in this context is single-atom optical bistability, presently being researched in collaboration with H. J. Carmichael at the University of Arkansas.

REFERENCES

1. D. F. Walls, private communication (1987).

2. Y. Yamamoto, S. Machida and T. Yanagawa, "Amplitude squeezing in a semiconductor laser," Paper TuCC2, Technical Digest, XIV International Quantum Electronics Conference, San Francisco, CA (1986).

3. W. E. Lamb, Jr., in *Chaotic Behaviour in Quantum Systems, Theory and Applications*, G. Casati, ed. (Plenum, New York, 1985), p. 353.

GENERATION AND APPLICATION OF FEMTOSECOND LASER PULSES

N. Peyghambarian

PUBLICATIONS

G. R. Olbright, N. Peyghambarian, S. W. Koch, and L. Banyai, "Optical nonlinearities of glasses doped with semiconductor microcrystallites," Opt. Lett. 12, 413 (1987).

G. R. Olbright and N. Peyghambarian, "Interferometric measurement of the nonlinear index of refraction, n_2, of CdS_xSe_{1-x} doped glasses," Appl. Phys. Lett. 48, 1184 (1986).

N. Peyghambarian and S. W. Koch, "Femtosecond and coherent effects in bulk CdSe and $CdSe_xS_{1-x}$ doped glasses," Rev. de Phys. Appl. 22, 61 (1987).

N. Peyghambarian, "A new class of materials for nonlinear optics and nonlinear optical devices," Opt. News 12, 14 (1986). One of twelve papers in the section "Optics in 1986."

N. Peyghambarian, "Femtosecond transients and nonlinear optical effects in $CdSe_xS_{1-x}$ glasses," Proc. SPIE 793, 147 (1986).

N. Peyghambarian, "Materials for fast switching and logic devices," Proceedings SPIE Workshop on Optical Bistability in Digital Optical Computing, Huntsville, AL (1986).

B. Fluegel, N. Peyghambarian, G. Olbright, M. Lindberg, S. W. Koch, M. Joffre, D. Hulin, A. Migus, and A. Antonetti, "Femtosecond studies of coherent transients in semiconductors," Phys. Rev. Lett., in press.

N. Peyghambarian, S. H. Park, S. W. Koch, A. Jeffery, J. E. Potts, and H. Cheng, "Room-temperature excitonic optical nonlinearities of MBE grown ZnSe thin films," Appl. Phys. Lett., in press.

G. R. Olbright, B. D. Fluegel, S. W. Koch, and N. Peyghambarian, "Femtosecond dynamics of electron-hole plasma in semiconductor microcrystallite doped glasses," in *Ultrafast Phenomena*, G. R. Fleming and A. E. Siegman, eds. (Springer-Verlag, New York, 1986).

N. Peyghambarian, "Optical computing and nonlinear optical signal processing," Guest Editorial, Opt. Eng. 26, 1 (1987).

G. R. Olbright and N. Peyghambarian, "Epitaxial growth and x-ray diffraction analysis of single-crystal thin films of CuCl," Solid State Commun. 58, 337 (1986).

N. Peyghambarian, "Recent advances in optical bistability," Fiber and Integ. Opt. 6, 117 (1987).

D. Hulin, A. Mysyrowicz, A. Antonetti, A. Migus, W. T. Masselink, H. Morkoc, H. M. Gibbs, and N. Peyghambarian, "An ultrafast all-optical gate with subpicosecond on and off response time," Appl. Phys. Lett. 49, 749 (1986).

N. Peyghambarian and S. W. Koch, "Experimental and theoretical studies of coherent and nonthermal processes in semiconductors probed by femtosecond laser techniques," United States-Japan Symposium, Monterey, CA (1987).

N. Peyghambarian, "Femtosecond studies of excitons and carriers in semiconductor quantum microstructures," Annual Meeting of the American Physical Society, New York, NY; Bull. Am. Phys. Soc. 32, 392 (1987).

N. Peyghambarian, "Femtosecond transients and nonlinear phenomena in semiconductors," NSF Workshop on High Speed Optical Processes and Optoelectronic Devices Based on Compound Semiconductors, Ann Arbor, MI (1987).

N. Peyghambarian, "Transient and nonlinear effects in GaAs-AlGaAs multiple quantum wells and CdS_xSe_{1-x} doped glasses," Annual Meeting of Electro-Chemical Society, San Diego, CA (1987).

N. Peyghambarian, ed., *NSF Workshop on Optical Nonlinearities, Fast Phenomena and Signal Processing* (University of Arizona, 1986).

H. M. Gibbs, N. Peyghambarian, P. Mandel, and S. D. Smith, eds., *Optical Bistability 3* (Springer-Verlag, Berlin, 1986).

N. Peyghambarian, ed. *Optical Computing and Nonlinear Materials*, Proc. SPIE 88 (1988).

G. R. Olbright, M. Lindberg, B. D. Fluegel, S. W. Koch, F. Jarka, and N. Peyghambarian, "Coherent effects in femtosecond pump-probe spectroscopy of semiconductors," post-deadline paper PD2, IQEC '87, Baltimore, MD (1987).

S. H. Park, A. Jeffery, R. A. Morgan, S. W. Koch, N. Peyghambarian, J. E. Potts, and H. Cheng, "Room-temperature excitonic optical nonlinearities of MBE grown ZnSe thin films," postdeadline paper ThU13, CLEO '87, Baltimore, MD (1987).

G. R. Olbright, B. D. Fluegel, and N. Peyghambarian, "Femtosecond evolution of nonthermal carrier distributions in CdSe microcrystallite doped glasses," OSA Annual Meeting, Seattle, WA (1986).

N. Peyghambarian, G. R. Olbright, and B. D. Fluegel, "Femtosecond dynamics of bandgap renormalization and bandfilling in a CdSe-microcrystallite-doped glass," postdeadline paper PD20, IQEC '86, San Francisco, CA (1986).

G. R. Olbright, N. Peyghambarian, S. W. Koch, and L. Banyai, "Experimental theoretical investigations of the origin of optical nonlinearities of semiconductor-doped glasses," IQEC '86, TUNN2, San Francisco, CA (1986).

S. H. Park, T. Carty, G. R. Olbright, C. T. Seaton, and N. Peyghambarian, "Optimization of optical nonlinearity of semiconductor doped glasses," CLEO 86, WD4, San Francisco, CA (1986).

G. R. Olbright and N. Peyghambarian, "Experimental and theoretical investigation of the optical nonlinearities of CdS_xSe_{1-x} doped glasses," Bull. Am. Phys. Soc. 31, 657 (1986).

G. Olbright and N. Peyghambarian, "Observation of band-filling optical nonlinearity in CdS_xSe_{1-x} doped glasses," OSA Annual Meeting, Washington, DC (1985).

11

SCIENTIFIC PERSONNEL

N. Peyghambarian

G. Olbright (Ph.D. 4/87)

S. H. Park

A. Jeffery (M.S. 6/87)

R. Morgan

S. H. Park and R. Morgan are expected to complete Ph.D. requirements by June 1988.

RESEARCH FINDINGS

Introduction

This project was begun in 1985 and has had two years of funding under this contract. The following report covers accomplishments during the two years.

Objectives

The primary goal of this project was a laser system capable of generating pulses of a few tens of femtoseconds in duration at a repetition rate of $\cong$90 MHz. The pulses were to be amplified to intensities of several hundred gigawatts per square centimeter at repetition rates of a few kilohertz for time-resolved studies of optical nonlinearities in several materials and nonlinear optical switches. In particular, high-speed switching in GaAs-AlGaAs multiple quantum wells (MQWs) were to be investigated, and the dynamics of the optical response of semiconductor-doped glasses and CdSe were to be measured.

Approach

To generate femtosecond pulses, the colliding-pulse passive mode-locking technique found in a ring cavity was proposed. The ring dye laser, which contained a saturable absorber and a saturable gain medium, was pumped by an Ar-ion laser. The cavity incorporated a four-prism sequence to introduce adjustable group velocity dispersion and to allow adjustable pulse durations from several tens of femtoseconds to $\cong$500 fs. The pulses were then to be amplified by a copper vapor laser at $\cong$10 KHz repetition rate to obtain a white light continuum, and for use in pump-probe experiments.

The following techniques were employed to accomplish these goals:

1. *High-Speed Switching Measurement*

    The rapid response time of nonlinear etalon switches may be measured with two or three pulses: a probe pulse and one or two "control" pulses. The devices are made by placing the nonlinear medium between two partially transmitting mirrors. The transmission of the "probe" pulse is the gate output which is controlled by one or two "control" pulses (input to the gate). For example, a NOR gate truth table can be satisfied when the probe wavelength is tuned to the Fabry-Perot peak in the absence of any "control" pulse. The gate output is then initially "high." The application of a "control" pulse shifts the Fabry-Perot peak away from the probe wavelength, forcing the probe transmission to the "low" state. To time-resolve the response of the gate, the speed at which the Fabry-Perot peaks shift in response to the control pulse is measured. Therefore, the probe transmission, which includes the Fabry-Perot peak, is detected with different delays with respect to the "control" pulse.

2. *Pump-Probe Transient Technique*

    In this technique two short pulses with a variable delay are sent into the sample. One of the pulses is usually a weak beam with a broad spectrum to cover the entire absorption region of the material. The second pulse is an intense beam with a narrow spectrum, and tunable to allow excitation at various regions of absorption. The probe pulse is detected either with a combination of a spectrometer and an optical multi-channel analyzer, or with a single photodiode at the narrow slit of a monochromator. By recording the pump-induced changes in the absorption spectrum of the probe pulse as a function of time delay between pump and probe, the evolution of the excited system can be followed.

Accomplishments

Construction of the Femtosecond Laser System

The femtosecond system was built in-house with the following components: a) the colliding-pulse mode-locked ring dye laser which generates pulses of adjustable duration ranging from $\cong 50$ fs to a few hundred fs. The ring cavity contains a four-prism assembly to compensate for the positive group velocity dispersion; b) the amplifier stage which is pumped by a 24 W copper vapor laser operating at $\cong 10$ KHz. The amplifier stage uses a solphorhodamine dye solution for the gain medium and malachite-green dye solution as a saturable absorber medium to remove

13

the fluorescence and unamplified pulses; c) a continuum generator which uses an ethylene glycol jet and produces a white-light continuum ranging from 200 nm to 900 nm in the femtosecond time domain; d) an autocorrelation and a cross-correlation setup which allows measurements of the time duration of the pulses.

This laser system was used in some of the measurements that are summarized in this report. Figures 1 through 4 depict different components of the laser.

Semiconductor-Doped Glasses

The first material studied using the femtosecond laser system was a semiconductor-doped glass. This class of materials is of current interest because of the potential for application in nonlinear devices. The optical nonlinearities in several glasses were time-resolved. A pump-probe experimental technique was employed and is shown schematically in Fig. 5. The differential transmission spectra (DTS) of the samples were measured as a function of time delay between the pump and probe pulses. The DTS is the difference in transmission of the probe pulse in the presence (T) and absence (T_0) of the pump, divided by T_0 (i.e., DTS = $(T-T_0)/T_0$). Figure 6 shows the DTS for a $CdS_{0.8}Se_{0.2}$ glass at 300 K for various time delays between the pump and probe pulses. Negative time delays indicate situations where the probe peak precedes the peak of the pump pulse. A spectral hole is burned at early times. The spectral hole is indicative of a state filling effect where the carriers are in a nonequilibrium state. At later times when the pump and probe overlap increases, the spectral hole broadens and a high-energy shifting of the spectra is observed. This blue shift is the result of a bandfilling effect, which is the main source of nonlinearity of these glasses. The blue shift is more easily recognized if the transmission of the probe is plotted as a function of wavelength. Such spectra at room temperature are shown in Fig. 7. The 1-ps spectrum exhibits the blue shift of the transmission spectrum, clearly demonstrating the bandfilling effect. After 1 ps, the blue shift starts to recover, indicating the onset of the carrier recombination. The carrier recombination lifetime is measured from the recovery of the blue shift of the absorption. This recovery is almost complete in 20 ps. However, a small residual shift remains for times in excess of 500 ps (which is the limit of our femtosecond delay line). This residual shift was attributed to carriers confined to traps. It should be emphasized that the carrier lifetime in glasses is intensity dependent: it is slow at small incident fluences and becomes rapid at higher fluences.
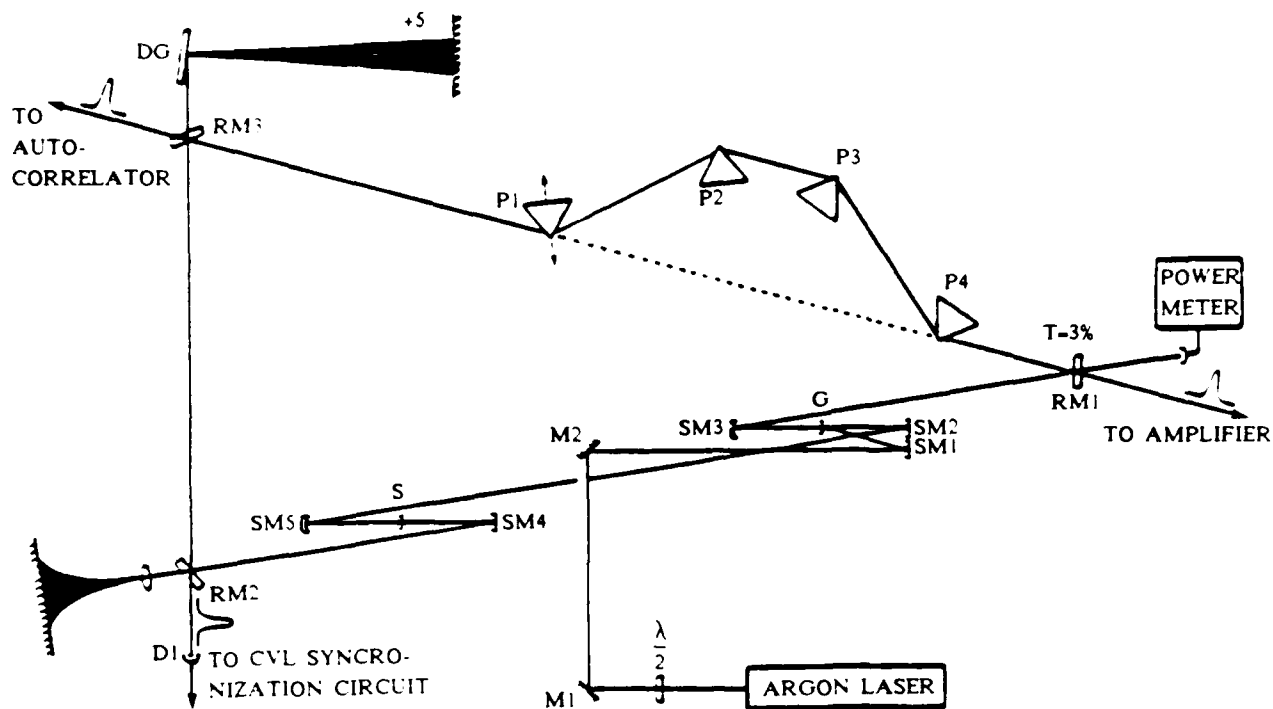
Figure 1. Schematic of the balanced colliding pulse mode-locked (CPM) ring dye laser. RM = ring mirror; SM = spherical mirror; G = gain jet; S = saturable absorber jet; DG = diffraction grating.

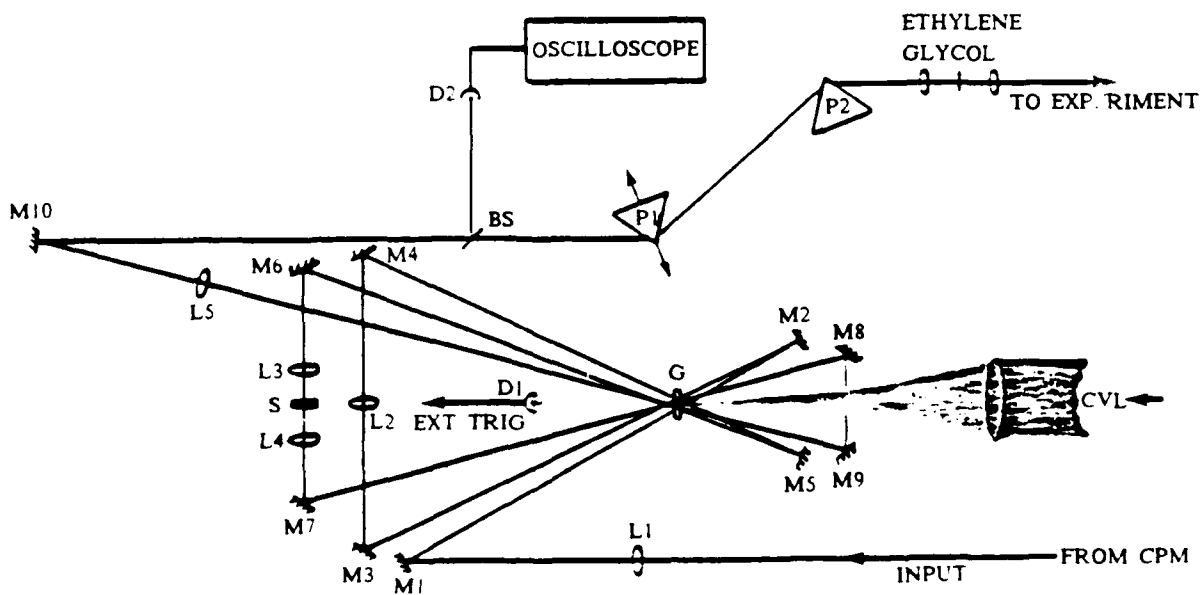Figure 2. Six-stage copper-vapor-laser optical amplifier. P = prism. BS = beamsplitter; G = gain jet, S = saturable absorber jet.

15
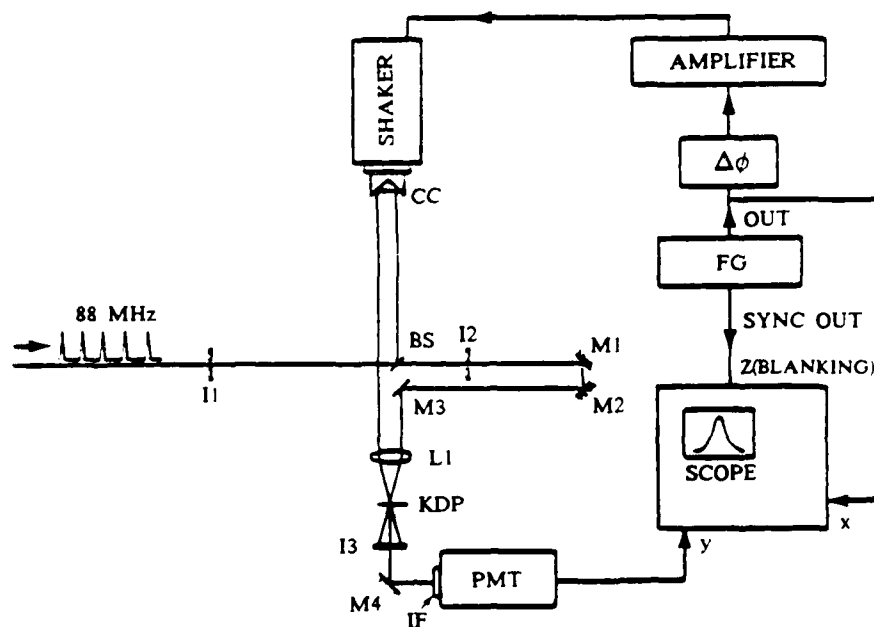
Figure 3. Schematic of the 10-fs-resolution real-time autocorrelator. FG = function generator; CC = corner cube; I = aperture stop; IF = interference filter; PMT = photomultiplier tube; BS = beamsplitter.
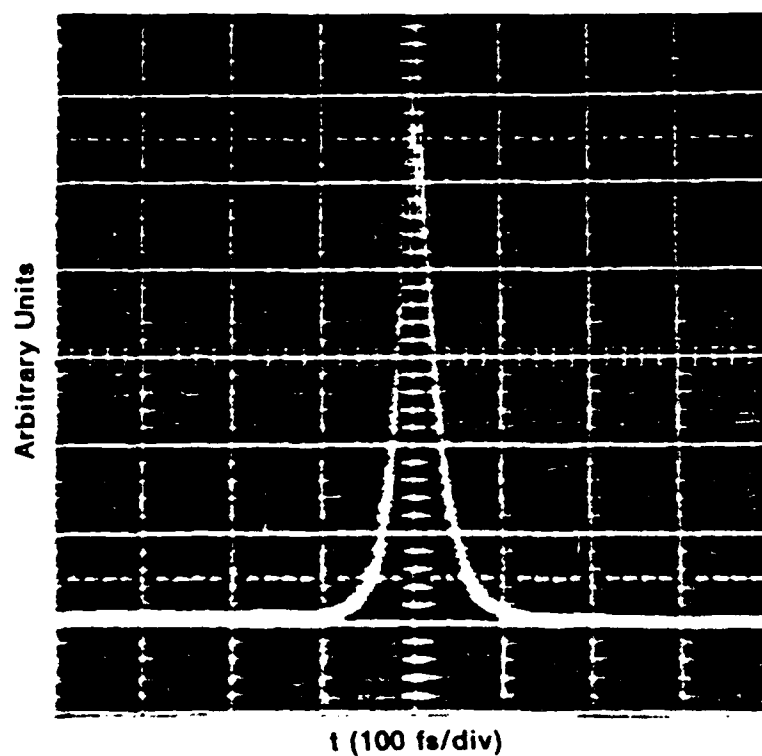
Figure 4. Oscilloscope trace of 35-fs optical pulses.

16
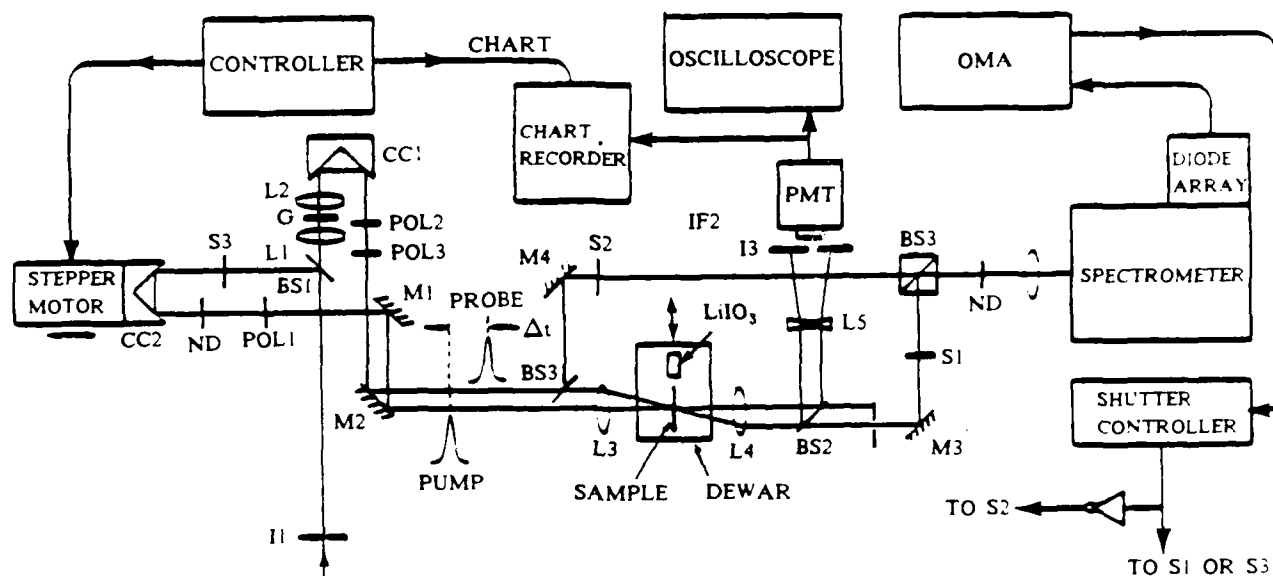
Figure 5. Pump and probe experimental configuration for femtosecond time-resolved spectroscopy. BS = beamsplitter; CC = corner cube; G = continuum jet; I = iris; IF = interference filter; LiIO₃ crystal; L = lens; M = mirror; ND = neutral density; OMA = optical multichannel analyzer; PMT = photomultiplier tube; POL = polarizer; S = shutter.
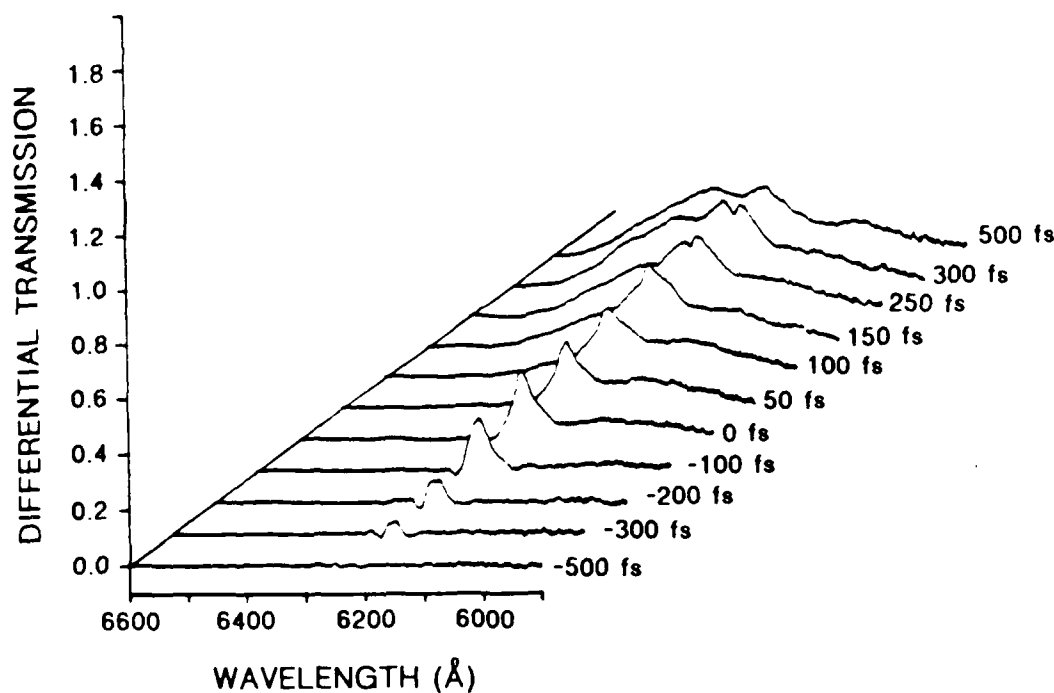
Figure 6. Differential transmission spectra of a CdSe₀.₂S₀.₈ glass at 300 K for various time delays between the pump and probe pulses.

Figure 7. Probe transmission for T = 300 K and pump intensity of 0.5 GW/cm² at various time delays with respect to the pump pulse for a 250 μm CdSe₀.₂S₀.₈ color glass.

Figure 7. Probe transmission for $T = 300$ K and pump intensity of 0.5 GW/cm² at various time delays with respect to the pump pulse for a 250 μm $CdSe_{0.2}S_{0.8}$ color glass.

Ultrafast Switching in GaAs MQW Etalons

Carrier lifetime in nonlinear materials usually limits the switching speed of room-temperature nonlinear optical logic devices because carriers are reponsible for the change in absorption of the material. The carrier lifetime may be shortened by pro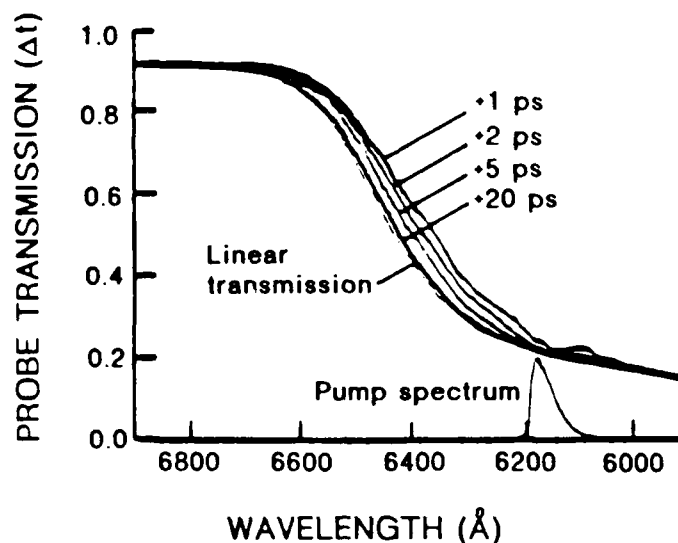ton bombarding of the material, or by applying an electric field (for sweeping the carriers out of the excited region), or by employing surface recombination. The switching time can be shortened further by using the optical Stark effect. The effect is independent of carrier lifetime because the change in absorption is brought about by the electric field of the light. Using the optical Stark effect, optical NOR gate operation was obtained with subpicosecond on and off switching times in a GaAs-AlGaAs MQW. This work was performed in collaboration with the Gibbs group and the researchers at Ecole Polytechnique, ENSTA, France. Figure 8 shows the demonstration of a high-speed NOR gate. Both switch-on and switch-off times were slightly less than 1 ps.

Observation of Optical Stark Effect in Semiconductors

As mentioned above, the optical Stark effect may be employed to obtain subpicosecond switching speeds. The effect is observed in a two-beam experiment where a pump pulse is tuned below the band edge in the transparency region of the semiconductor. The E-field of the pump causes a blue shift of the exciton and band edge. The shift of the exciton or band results in change in the index of refraction.
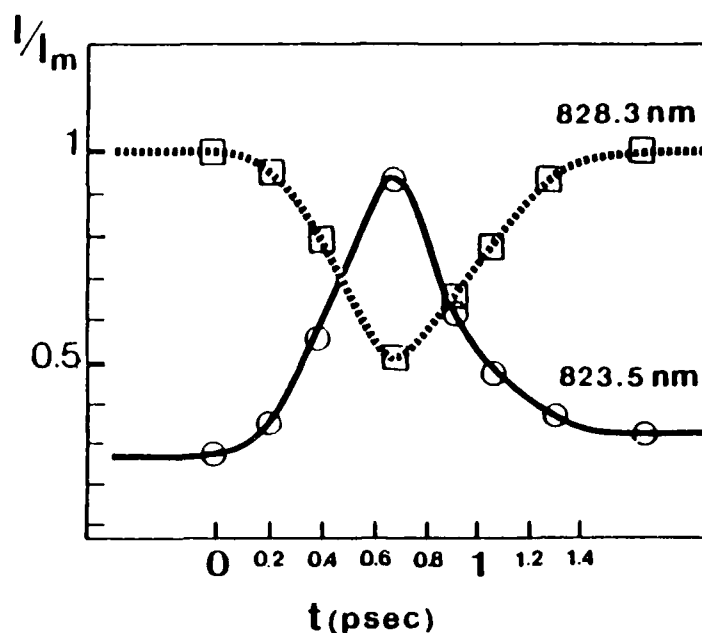
18

Figure 8. The switch-on and switch-off times of a GaAs-AlGaAs MQW etalon working as a NOR gate (dashed line) and OR gate (solid line). The operation of the gate is based on optical Stark effect.

Since the blue shift persists as long as the light field is present, the response time of the nonlinearity is very rapid. The first observation of the bandgap shift arising from the optical Stark effect in CdSe has been made. In addition, the optical Stark shift of the exciton in ZnSe, GaAs, GaAs-AlGaAs MQWs and CdSe has also been observed. The optical Stark shift of excitons in bulk CdSe is shown in Fig. 9.

Optical Nonlinearity of Electronic Origin and Picosecond Response in MBE-Grown ZnSe Thin Films

Large excitonic optical nonlinearities were observed in MBE-grown thin films of ZnSe at T = 300 K and at T = 150 K. The index change for MBE samples (grown at the 3M Company) were measured and a maximum $\Delta n/N$ of $\cong 1.8 \times 10^{-19}$ cm^3 at room temperature and 9×10^{-19} cm^3 at T = 150 K was obtained. $\Delta n/N$ at room temperature is comparable to the value measured for GaAs. The carrier lifetime in these samples was also measured. The exponential fit to these time-dependent data gave a value of $\cong 30$ ps for the carrier lifetime at room temperature for a 0.23-μm sample. The lifetime is lengthened to 166 ps for a 0.68-μm sample. The faster response for thinner samples is attributed to the enhanced surface recombination rate. This fast and large optical nonlinearity will be used to realize low-power, high-speed optical devices. Figure 10 gives the measured response time of a 0.55-μm ZnSe sample at room-temperature.
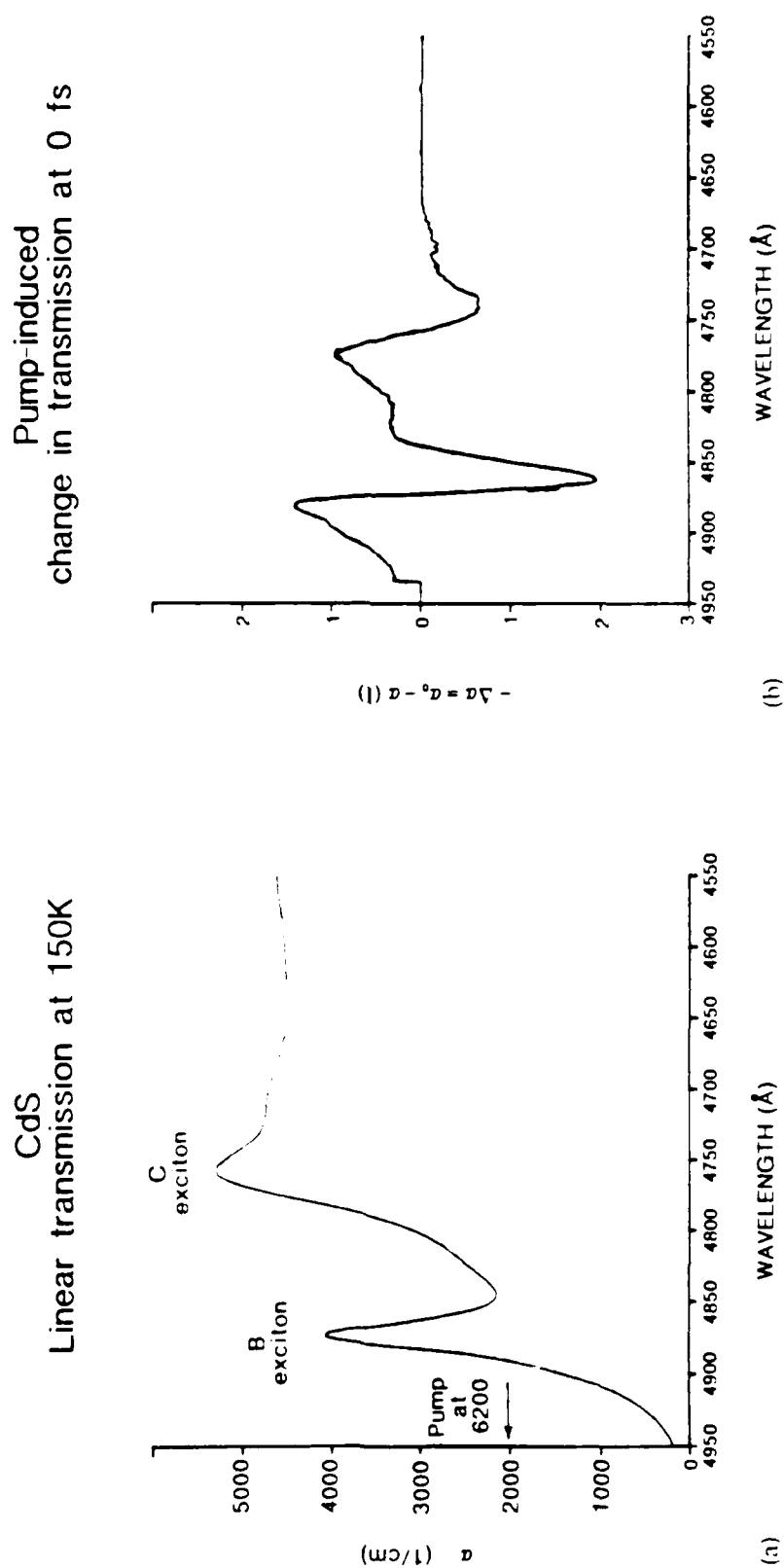
19

Figure 9. Optical Stark shift: (a) transmission of a CdSe thin-platelet at 150 K; (b) optical Stark effect of excitons in CdSe at 150 K.
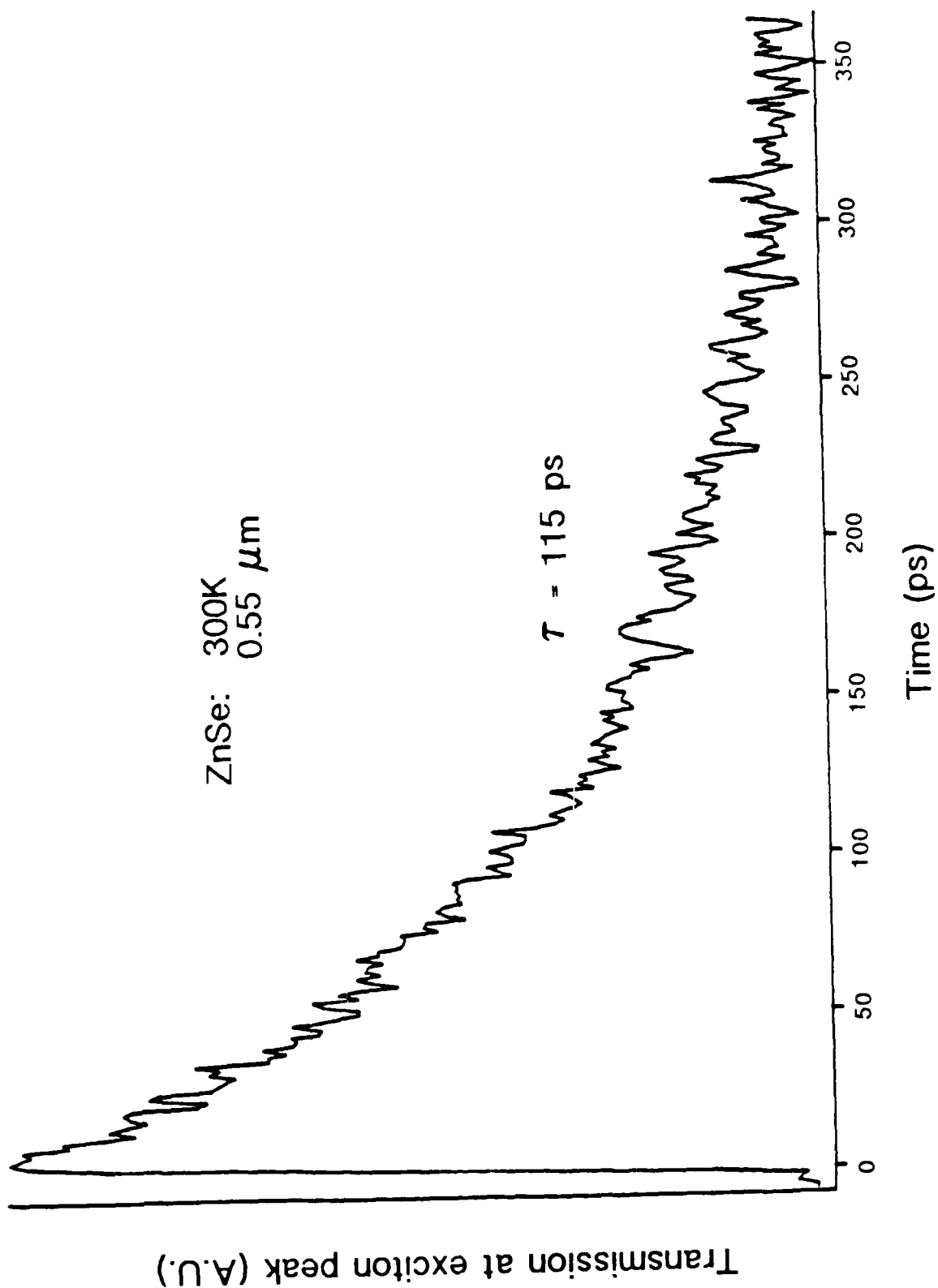
Figure 10. The dynamics of exciton recovery for a 0.55-μm-thick ZnSe thin film at room temperature.

ZnSe: 300K
0.55 μm

τ = 115 ps

Time (ps)

Transmission at exciton peak (A.U.)

21

OPTICAL STUDIES OF METALLIC SUPERLATTICES

G. I. Stegeman, C. M. Falco, and C. T. Seaton

PUBLICATIONS

J. A. Bell, W. R. Bennett, R. Zanoni, G. I. Stegeman, C. M. Falco, and F. Nizzoli, "Elastic constants of Mo/Ta superlattices measured by Brillouin scattering," Phys. Rev. B 35, 4127 (1987).

R. Zanoni, J. Bell, C. T. Seaton, and G. I. Stegeman, "Brillouin scattering from multilayer films," Proceedings of the International Symposium on Surface Waves in Solids and Layered Structures, Vol. III, 166 (Novosibirsk, 1986).

J. A. Bell, W. R. Bennett, R. Zanoni, G. I. Stegeman, C. M. Falco, and C. T. Seaton, "Brillouin scattering from Love waves in Cu/Nb metallic superlattices," Appl. Phys. Lett. 51, 652 (1987).

J. A. Bell, W. R. Bennett, R. Zanoni, G. I. Stegeman, C. M. Falco, and C. T. Seaton, "Elastic constants of, and Stonley waves in molybdenum films measured by Brillouin scattering," Appl. Phys. Lett., in press.

J. A. Bell, W. R. Bennett, R. Zanoni, G. I. Stegeman, C. M. Falco, and C. T. Seaton, "Elastic constants of Cu/Nb superlattices," Solid State Comm., in press.

R. Zanoni, J. Bell, G. I. Stegeman, and C. T. Seaton, "Brillouin spectroscopy: a tool for measuring thin film elastic constants," Thin Solid Films, in press.

G. I. Stegeman, "Surface acoustooptics," Proceedings of the Celebration Meeting for Fiftieth Anniversary of Istituto di Acoustica, Rome, in press.

J. A. Bell, R. Zanoni, W. R. Bennett, C. T. Seaton, G. I. Stegeman, and C. M. Falco, "High resolution Brillouin spectroscopy of Mo/Ta superlattices," APS Annual Meeting, Las Vegas, NV (1986).

J. A. Bell, W. R. Bennett, R. Zanoni, G. I. Stegeman, C. M. Falco, and F. Nizzoli, "Elastic constants of metal superlattices measured by Brillouin scattering," OSA Annual Meeting, Seattle, WA (1986).

J. A. Bell, Brillouin Scattering from Metal Superlattices, Ph.D. dissertation (University of Arizona, March 1987).

SCIENTIFIC PERSONNEL

G. I. Stegeman

C. T. Seaton

C. M. Falco

W. R. Bennett

J. A. Bell (Ph.D. 3/87)

R. Zanoni

RESEARCH FINDINGS

Summary of Technical Progress

Brillouin scattering was used to study the elastic properties of metal films (molybdenum) and superlattices (copper/niobium and molybdenum/tantalum). The superlattice samples consisted of rf-sputtered, alternating layers of the two constituent metals (approximately equal thickness). The key experiments involved measuring the Brillouin spectrum, specifically the Rayleigh and Sezawa modes, as a function of layer thickness. From these the elastic constants were derived.

For superlattice modulation periods of 20 to 50 Å, anomalous softening in the c_{44} (but not the c_{11} or c_{33}) elastic constants was found. Changes of 20% found for C/Nb and 6% for Mo/Ta were linked to the interfacial strain produced between alternate layers due to lattice mismatch. The first observation of Love waves led to the measurement of the c_{12} elastic constant for Cu/Nb, which showed no softening with superlattice period. In addition, the first observation of Stonley waves in molybdenum films led to a comparison of film mechanical properties at the two film surfaces.

Objectives

The goals of this program were:

1. To develop Brillouin spectroscopy as a non-destructive tool for measuring the elastic constants of metal films, concentrating on metallic superlattices.
2. To study the elastic properties of metallic superlattices.

24

Results

Extensive experiments have been carried out on Mo/Ta and Cu/Nb superlattice systems with individual layer thicknesses varying from 10 to 200 Å and total film thicknesses of thousands of angstroms. The observed Brillouin spectrum contained spectral lines attributable to scattering by up to 14 acoustic modes of the superlattice films. Experiments at a single scattering angle yielded the phase velocity for each guided mode for a specific value of $Q_p h$ where h is the film thickness and Q_p is the acoustic wavevector. Both scattering angle and film thickness were varied to map out the dispersion relations; i.e., the phase velocity versus the product $Q_p h$.

Computer programs were developed to deduce the elastic constants from the dispersion relations for films with hexagonal symmetry. Although these films were indeed epitaxial with c-axis normal to the surface, they consisted of crystallites typically thousands of angstroms in size with random orientations in the plane of the surface. This averaging over orientation results in effectively hexagonal crystal film symmetry and the experiments led to a determination of the effective hexagonal elastic constants. Programs were also written to calculate the individual layer elastic constants for crystallites with known elastic constants (those of the constituent superlattice materials) and with random orientation in the plane of the surface. The elastic constants for multilayer films were then calculated using both continuity of strain and stress boundary conditions for comparison with experiment. A program has also been developed, based on scattering theory, to calculate the relative scattering efficiency for the various acoustic modes.

The following results were obtained for Mo/Ta superlattices:

1. There was excellent agreement between scattering theory and the Brillouin spectrum.

2. There is a small (a few percent) softening of the c_{44} elastic constant with decreasing layer thickness.

3. The observed Rayleigh velocity is $\cong 6\%$ smaller than that calculated based on the elastic constants of bulk Mo and Ta.

4. The c_{14} and c_{33} elastic constants were evaluated as a function of superlattice period. A small softening in the c_{33} constant with decreasing period was found.

For the Cu/Nb system, the following results were obtained:

1. Again, there was excellent agreement between scattering theory and experiment.

25

2. As observed previously by others, there is a minimum in the c_{44} elastic constant at a superlattice period of 35 Å. The minimum found in this work was shallower than that of previous researchers.

3. A small (12%) monotonic decrease in c_{33} with bilayer thickness below 3.0 nm was also found.

4. Oxygen contamination during sample growth leads to an increase in the Rayleigh wave velocity.

These results led to one of the principal conclusions of this work, namely that the softening of the c_{44} elastic constant correlates with lattice mismatches for the Mo/Ta and Cu/Nb superlattices. X-ray diffraction has shown that Cu/Nb exhibits a large lattice mismatch whereas Mo/Ta does not. Large mismatches produce strong strains which in turn weaken the lattice.

Brillouin scattering from Love and Stonley waves has also been observed for the first time. In particular, Love waves were measured for the Cu/Nb superlattice system for a range of superlattice periods. These particular modes depend partially on the c_{12} elastic constant, which cannot be measured in any other way and was deduced from the measurements. No significant variation in the c_{12} constant with superlattice period was observed, indicating that interlayer strain does not affect this elastic constant.

Stonley waves are acoustic modes which are guided by the interface between two media, providing a restrictive set of conditions on the relative mechanical properties are satisfied. For a thick film, the Rayleigh and Stonley waves sample the film elastic properties at the film-air and film-substrate interfaces respectively. Both modes were observed experimentally for a molybdenum film on a sapphire substrate for a range of Mo film thicknesses. Evaluating the c_{11} and c_{44} elastic constants from the dispersion curves, the elastic constants at the two film boundaries were found to be identical to within the experimental accuracy of $\cong 1\%$.

This program is now complete.

26

STUDY OF OPTICAL INTERCONNECTS
USING NONLINEAR SURFACE INTERACTIONS

Dror Sarid

PUBLICATIONS/REFERENCES

1. Dror Sarid, N. Peyghambarian, and B. P. McGinnis, "Optical bistability in the presence of spatial dispersion," IEEE JQE, QE-21, 1379 (1985).

2. B. P. McGinnis, Dror Sarid, and N. Peyghambarian, "Reflectivity of a spatially dispersive nonlinear Fabry-Perot," OSA Annual Meeting 1985, Technical Digest, WE4, p.40.

3. Dror Sarid, Bum Ku Rhee, B. P. McGinnis, and Claude J. Sandroff, "Degenerate four-wave mixing from layered semiconductor clusters in the quantum size regime," Appl. Phys. Lett. 49, 1196 (1986).

4. Dror Sarid, Tammy Henson, L. Stephen Bell, and Claude J. Sandroff, "Scanning tunneling microscopy of semiconductor clusters," J. Vac. Science & Tech. A (1988).

5. B. P. McGinnis and Dror Sarid, "Subnanosecond degenerate four-wave mixing in layered semiconductor clusters," to be submitted.

SCIENTIFIC PERSONNEL

Dror Sarid

Brian McGinnis

RESEARCH FINDINGS

Introduction

Highly nonlinear optical materials are necessary to achieve a controllable optical interconnect for signal processing and optical computing. This research has concentrated on the investigation of layered-structure semiconductors in the form of small microcrystallites. These were chosen on the basis of ease of fabrication and room-temperature operation, and because their linear absorption spectra indicated that they exhibit quantum confinement of the charge carriers. Degenerate four-wave

27

mixing studies were performed. The magnitude and temporal response of these microcrystallites suspended as a colloidal solution were analyzed. A theoretical model of the experimental results has been developed which describes the temporal behavior of the system and the efficiency of scattering of the small and large gratings. A large collection of layered-structure semiconductors is now being examined to determine the most promising candidates.

Objectives

The objective of this research was to investigate the nonlinear optical properties of layered-structure semiconductors and to compare these properties with known materials. Experimental study of the magnitude and temporal response of the nonlinearity was of particular interest. Theoretical study of the underlying physics of the mechanisms involved in the nonlinear interaction was also undertaken.

Status

Over the course of the past three years, different materials have been investigated in search of a promising candidate for strong and fast optical nonlinearities. The emphasis of this search has been layered-structure semiconductors and the investigations ranged from bulk samples to small microcrystallites. To evaluate optical nonlinearities, it has been necessary to design and construct a system consisting of lasers, optics, detectors, and a computer data acquisition and analysis system. The magnitude and temporal response of the third-order susceptibility has been analyzed to characterize the nonlinear mechanisms of the investigated materials. The theoretical efforts have covered the effects of spatial dispersion and the thermal response of the nonlinear materials.

The effects of spatial dispersion on the response of an optically bistable etalon were investigated theoretically.[1] It was found that the expected effects were small and would not be noticed in a typical experimental setup at room temperature. The power-dependent spectroscopic reflectivity of a spatially dispersive nonlinear etalon was also investigated.[2] The simulations indicated further similarities between local and spatially dispersive media at high intensities.

The interest in layered-structure semiconductors, having weak van der Waals bonding between adjacent layers, brought to mind analogies with surface-layer effects in multiple-quantum-well structures, and led to an investigation of crystals such as HgI_2 and PbI_2. These semiconductors have pronounced excitonic features and a band edge in the visible region. To probe these materials, a dye laser system was built, pumped by a Nd:YAG laser having an amplifier, doubler, and tripler. Attempts to

28

scan and saturate the exciton in these semiconductors proved unreliable and not consistently reproducible because of severe laser fluctuation problems and an inability to obtain good quality samples with strong reliable excitonic features.

As an alternative approach, layered-structure semiconductor microcrystallites such as PbI_2 and BiI_3 in a colloidal solution were examined (in collaboration with C. Sandroff of Bell Communications Research). These semiconductor clusters exhibited quantum size effects and it was felt, therefore, that they should have large optical nonlinearities. The second harmonic of the Nd:YAG laser was used to perform degenerate four-wave mixing experiments to determine the size of the nonlinearity.[3] The measurement of χ^3 in BiI_3 clusters was found to be larger than that of CS_2 but smaller than those of semiconductor-doped glass.[3]

To better characterize the nonlinear optical response on a subnanosecond time scale, a probing system system was constructed as shown in Fig. 1. A TEA nitrogen laser (LN-1000), purchased from PRA, Inc., produces 800-ps pulses at 337 nm, with 1.25 mJ in a single pulse, and a typical repetition rate of a few hertz. These pulses were used as the optical pump for a home-built grazing-incidence tunable dye laser and a single amplifier stage. This laser produced approximately 500-ps pulses with Coumarin 500 dye, and was tunable from 490 to 530 nm. Pulse energies were typically 40 μJ after spatial filtering.

A degenerate four-wave mixing (DFWM) geometry was used to measure the nonlinear refractive index of the colloidal semiconductor suspensions. The setup has been designed to also investigate the time evolution of the two spatial index gratings formed in the nonlinear material. Isolation of a particular grating was accomplished by rotating the polarization of one pump beam perpendicular to the other pump beam and the signal beam. In holographic terms, the latter two beams act as the writing beams, while the former beam acts as a readout beam. A conjugate beam is formed only if the appropriate third-order diagonal tensor element is finite. By varying the time delay of the readout beam, the nonlinear refractive index could be measured as it evolved in time. The strength of the conjugate signal energy as a function of time delay represents the correlation of the laser pulse and the nonlinear refractive index.

Results of the measurements of the temporal response of the nonlinear refractive index gratings in the colloidal suspension of BiI_3 semiconductor clusters are shown in Figs. 2a and 2b. The insets to these figures indicate the geometry employed in the measurements. The geometry of Fig. 2a results in a grating with a coarse spatial period of 10 μm. The buildup in time of the conjugate energy reflects the very slow response of the optical nonlinearity. The fine-period grating ($\cong 0.25 \mu m$) produced by the geometry shown in Fig. 2b has a markedly different time response.

29
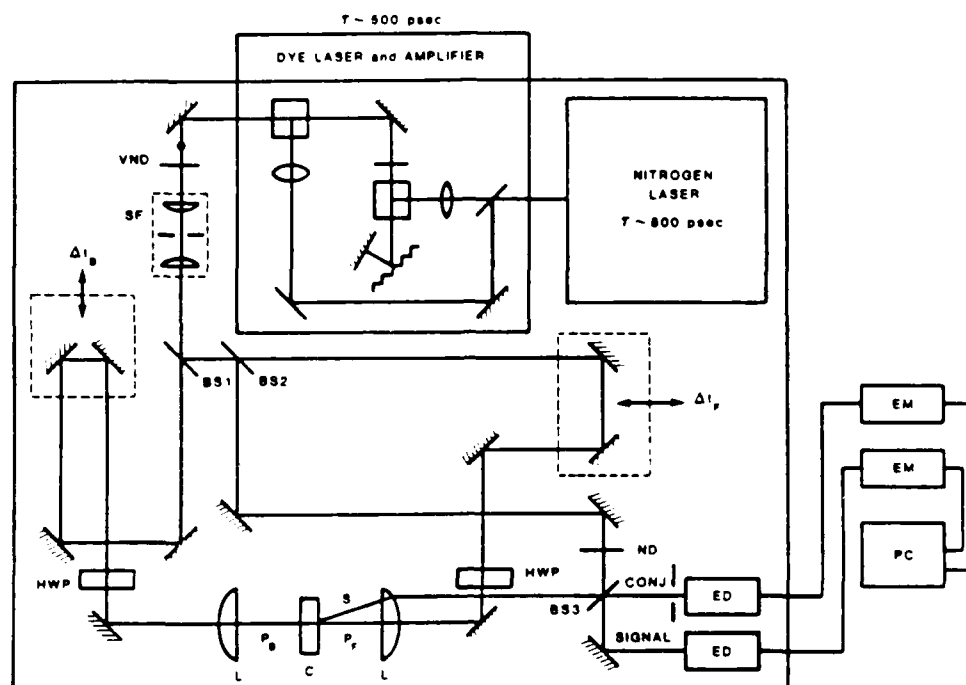
Legends

VND	– variable neutral density filter.
SF	– spatial filter and beam collimator.
BS1, BS2, BS3	– generate backward, forward pump and probe beams with proportions of 1, 1 and 0.5, respectively.
Δt_B, Δt_F	– backward and forward time delays with computer control for fine and manual for coarse motions.
HWP	– halfwave plate for control of beam polarization.
L	– focusing lens.
P_B, P_F	– backward and forward pump beams.
C	– cell containing nonlinear material.
ND	– neutral density filter.
BS3	– 50/50 beamsplitter.
CONJ	– conjugate beam from DFWM.
SIGNAL	– signal beam.
ED, EM	– energy detectors and meters.
PC	– personal computer for data acquisition and analysis.

Figure 1. Experimental setup for time- and polarization-resolved degenerate four-wave mixing.

30
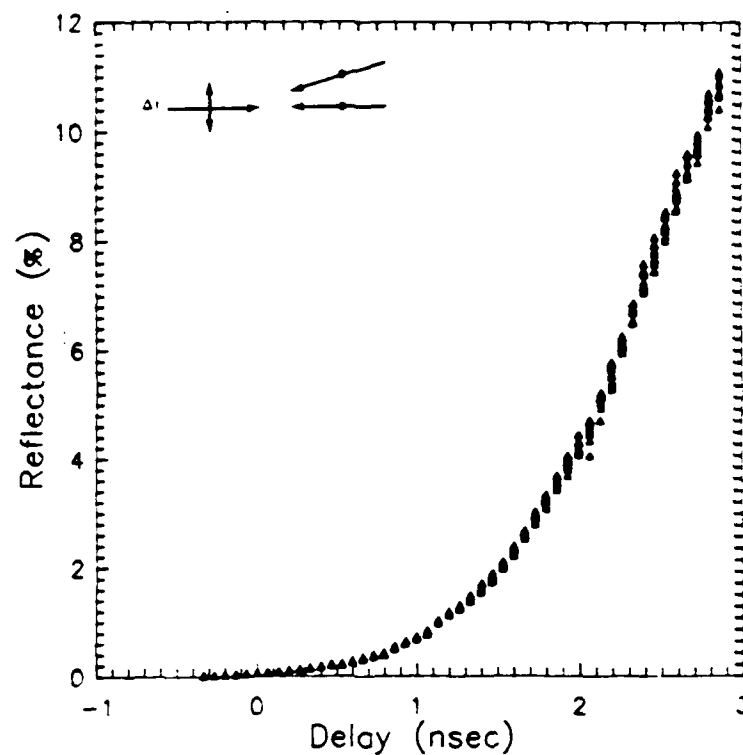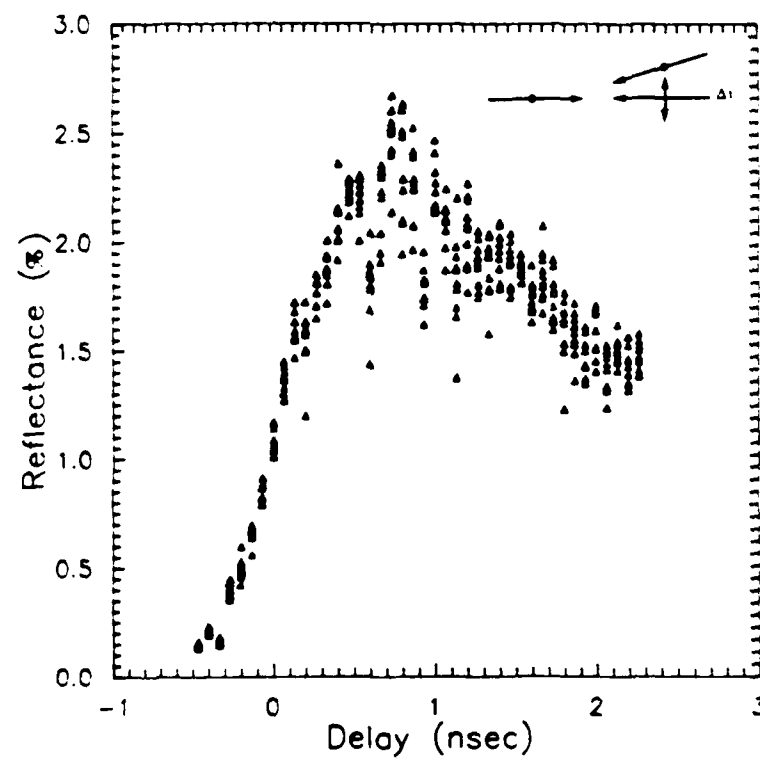
Figure 2. Energy reflectance from a) coarse and b) fine gratings in a colloidal solution of BiI_3 semiconductor clusters.

The origins of the nonlinearity are attributed to the contributions of both electronic and thermal sources. An attempt was made, however, to interpret the observed time responses based on the assumption that the clusters of BiI_3 act as absorbers which convert the incident radiant energy into heat. The temperature increase from this local heating, which results in a change in the refractive index of the solvent, is proportional to the incident intensity of the interference pattern. The slow buildup shown in Fig. 2a reflects the time which is required to convert the incident radiant energy to a thermally-induced refractive index change. Figure 2b reveals the decay of the amplitude of the fine grating due to thermal diffusion.

To describe this interaction, a rate equation analysis was employed which includes thermal diffusion, and the subsequent integral equations were evaluated numerically. The results of this theory are plotted in Fig. 3. The theory gives reasonable agreement only with the faster buildup of the fine grating. The theory and the experiments are being refined to better understand the origins of the nonlinear response of the colloidal suspension. One point to be considered is that any theory involving a local nonlinearity should always predict a contribution from the coarse grating that is greater than or equal to the contribution of the fine grating. Experimentally, a larger contribution from the fine grating than that of the coarse grating was observed for short time periods. This phenomenon can be explained by noting that the light was focused into a very small cross-sectional area ($\cong 50$ μm diameter) to obtain sufficiently high fluences. The grating period for the large grating was approximately 10 μm, and with only five fringes there was insufficient scattering enhancement. This problem did not exist for the fine grating, since its period was 0.25 μm and there were quite a few fringes traversing the length of the focal volume ($\cong 1$ mm). Thus diffraction from the fine grating was much more efficient than the diffraction from the coarse grating.

The short pulse experiments, together with the results of the thermal theory, lead to a better understanding of the results reported from the DFWM with the longer pulse-length YAG laser.[3] In Ref. 3 it was argued that the nearly equal contribution to the conjugate signal from both gratings implied that the nonlinearity was not thermal and thus was due to an electronic mechanism. The focal diameter in that experiment was estimated to be 15 μm with an 8-μm coarse grating period, and the fine grating conjugate signal was found to be three times greater than that of the coarse grating conjugate. Only a reduction in efficiency of the coarse grating due to the small cross-sectional area would explain this effect, assuming a local nonlinearity. Furthermore, this efficiency loss is expected to also outdo the loss in the fine grating efficiency because of thermal diffusion. Any argument based in

32
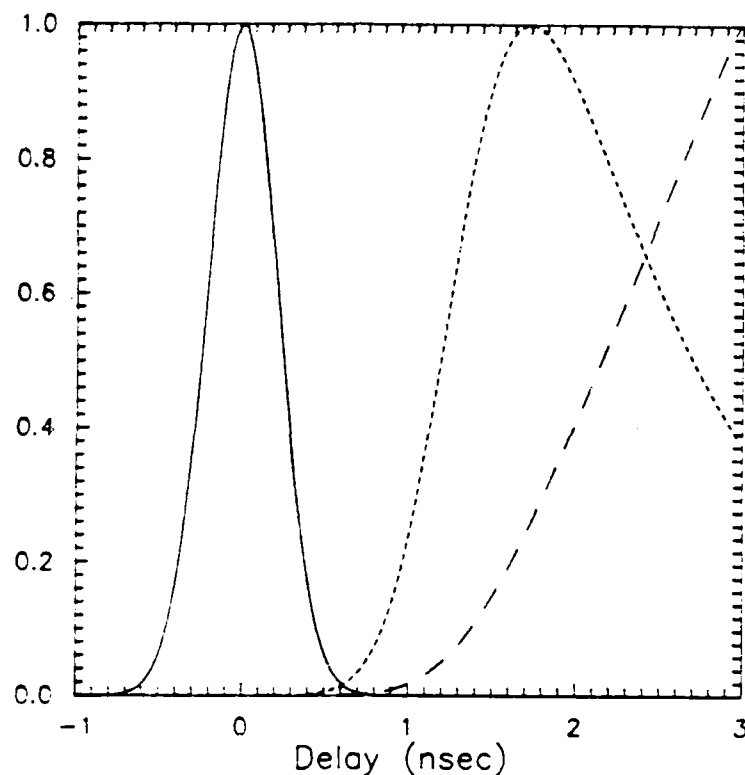
Figure 3. Theoretical normalized plots of laser pulse (solid) and reflected energy for fine (fine dash) and coarse (coarse dash) gratings.

diffraction efficiency must include this effect. In addition, it is now thought that the thermal theory yields a narrowing of the conjugate pulse which is consistent with a slow thermal mechanism. The results of these short pulse experiments, together with the modeling and scanning tunneling microscopy of single clusters,[4] will be shortly submitted for publication.[5] Further work will involve improving the models to better agree with experiment, and emphasis will be on other more promising materials such as MoS_2 and Bi_2S_3.

LONG-RANGE SURFACE PLASMONS

Dror Sarid

PUBLICATIONS

Dror Sarid, "Long-range surface-plasma waves on very thin metal films," Phys. Rev. Lett. **47**, 1927 (1981).

Dror Sarid, R. T. Deck, Alan Craig, Robert Hickernell, and Ralph Jameson, "Optical field enhancement by long-range surface-plasma waves," Appl. Opt. **21**, 3993 (1982).

Dror Sarid, "The nonlinear propagation constant of a surface plasmon," Appl. Phys. Lett. **39**, 889 (1981).

Dror Sarid, R. T. Deck, and J. J. Fasano, "Enhanced nonlinearity of the propagation constant of a long-range surface-plasma wave," J. Opt. Soc. Am. **72**, 1345 (1982).

R. T. Deck and Dror Sarid, "Enhancement of second harmonic generation by coupling to long-range surface plasmons," J. Opt. Soc. Am. **72**, 1613 (1982).

Alan E. Craig, Grieg A. Olson, and Dror Sarid, "Experimental observation of the long-range surface-plasmon polariton," Opt. Lett. **8**, 380 (1983).

Dror Sarid, "Long-range surface-plasmon polaritons," in *Optics '83: A Report on Emerging Technologies* (Optical Society of America, 1983).

Robert T. Deck, Dror Sarid, Grieg A. Olson, and J. M. Elson, "Coupling between finite electromagnetic beam and long-range surface-plasmon mode," Appl. Opt. **22**, 3397 (1983).

Alan E. Craig, Grieg A. Olson, and Dror Sarid, "Novel system for coupling to surface-plasmon polaritons," Appl. Opt. **24**, 61 (1985).

R. A. Booman, G. A. Olson, and Dror Sarid, "Determination of loss coefficients of long-range surface plasmons," Appl. Opt. **25**, 2729 (1986).

Robert. K. Hickernell and Dror Sarid, "Optical bistability using prism-coupled long-range surface plasmons," J. Opt. Soc. Am. **3**, 1059 (1986).

Dror Sarid, "Enhanced surface-magnetoplasma interactions in a semiconductor," Phys. Rev. B 29, 2344 (1984).

Dror Sarid, "Enhanced magnetic interaction of surface-magnetoplasmon polariton," J. Quantum Elect. QE-20, 943 (1985).

Robert. K. Hickernell and Dror Sarid, "Long-range surface magnetoplasmons in thin nickel films," Opt. Lett. 12, 564 (1987).

Alan E. Craig, Surface Plasmon Waves on Thin Metal Films, Ph.D. dissertation (University of Arizona, 1984).

Grieg A. Olson, Coupling Between Finite Electromagnetic Beam and Long-Range Surface-Plasmon Polariton: Experimental Confirmation, M.S. thesis (University of Arizona, 1985).

Richard A. Booman, Determination of Loss Mechanisms in Long-Range Surface Plasmon Modes, M.S. thesis (University of Arizona, 1986).

Robert K. Hickernell, Nonlinear and Magneto-Optic Effects on Long-Range Surface Plasmon Polaritons, Ph.D. dissertation (University of Arizona, 1987).

SCIENTIFIC PERSONNEL

Dror Sarid
A. E. Craig (Ph.D. 1984)
G. A. Olson (M.S. 1985)
R. A. Booman (M.S. 1986)
R. K. Hickernell (Ph.D. 1987)

RESEARCH FINDINGS

This three-year program was a continuation of a previous program which was supported by JSOP, DARPA, and the National Science Foundation. Since 1980, considerable effort has been invested in developing the theory and performing experiments that probed the linear and nonlinear properties of long-range and short-range surface-plasmon polariton modes. These terms, which were coined in 1981 (see the first-listed publication), describe the surface plasma modes which propagate along a thin metallic film bounded by identical or similar dielectrics. The two modes have

35

the distinct property that their propagation distance increases (or decreases) as the thickness of the metal film on which they propagate becomes thinner. The most important characteristic of the long-range mode, which was discovered in 1982, concerns the enhancement of its accompanying electromagnetic fields. Both of these results have been extensively used by this group to explore the following nonlinear phenomena: second-harmonic generation, χ^3, optical bistability, and magneto-optic interactions. Along with the theoretical investigations, experiments were performed in an attempt to verify the theoretical predictions and determine the limitations imposed by imperfect conditions. Among these conditions are films having surface roughness, cermets and inclusions, and light diffraction limitations.

The research in the past three years has been concerned mainly with the properties of surface-plasmon polaritons which propagate in optically nonlinear or magnetic media. Expressions for the electromagnetic fields of a multilayer stack were derived by modification of the Fresnel reflection coefficients. The results on prism-coupled, nonlinear, long-range surface plasmon polaritons, and on bound and prism-coupled, long-range surface magnetoplasmon polaritons in a transversely-applied magnetic field, were compared to previous research on single-interface plasmon polaritons.

The reflectance from prism-coupled nonlinear surface plasmons is analyzed using the infinite plane-wave approximation and a substrate nonlinearity that depends on the square of the transverse-electric field. Bistable switching requires incident intensities two orders of magnitude smaller for the long-range mode than for the single-interface mode. The regime in which the approximations are valid is shown to extend beyond that of first-order perturbation theory to guided waves that are very near cutoff. The sign and location of the nonlinearity become significant for these waves. For positive nonlinearities, nonlinear wave analysis indicates an additional branch of the reflected intensity curve, attributable to self-focusing of the guided wave. Positive and negative nonlinearities exhibit different switching intensities.

The propagation constant of the long-range surface plasmon of a magnetic metal film is shown to shift with the application of a transverse magnetic field. The sign and magnitude of the shift are highly dependent on the metal thickness and the refractive indices of the bounding media. The shift is manifested experimentally as a resonant modulation of the reflectance from the prism-coupled surface plasmon, resulting from changes in the angular position and width of the plasmon resonance. Experimental prism-coupling to the long-range surface magnetoplasmon in thin nickel films confirms the theoretical expectations for a wide variety of sample parameters. The phase of the magneto-optic coefficient is determined from the angular profile of

the reflectance modulation. Although the shift of the propagation constant may be two orders of magnitude smaller for the long-range mode, the modulation signal is the same order of magnitude for long-range and single-interface magnetoplasmons.

PHYSICS AND APPLICATIONS OF SURFACE GUIDED FIELDS

G. I. Stegeman and C. T. Seaton

PUBLICATIONS

C. T. Seaton, J. D. Valera, R. L. Shoemaker, G. I. Stegeman, J. Chilwell, and S. D. Smith, "Anomalous nonlinear guided wave cutoff phenomena," Appl. Phys. Lett. 45, 1162 (1984).

J. D. Valera, C. T. Seaton, G. I. Stegeman, R. L. Shoemaker, Xu Mai, and C. Liao, "Demonstration of nonlinear prism coupling," Appl. Phys. Lett. 45, 1013 (1984).

G. I. Stegeman, C. T. Seaton, and H. G. Winful, "Applications of guided waves to nonlinear optics," Proc. Trans. Roy. Soc. Lond. A 313, 321 (1984).

C. Liao, G. I. Stegeman, C. T. Seaton, R. L. Shoemaker, J. D. Valera, and H. G. Winful, "Nonlinear distributed waveguide couplers," J. Opt. Soc. Am. A2, 590 (1985).

C. T. Seaton, J. D. Valera, B. Svenson, and G. I. Stegeman, "Comparison of solutions for TM polarized nonlinear guided waves," Opt. Lett. 10, 149 (1985).

G. I. Stegeman and C. T. Seaton, "Nonlinear surface polaritons," in *Dynamical Phenomena at Surfaces, Interfaces and Superlattices*, F. Nizzoli, R. Willis, and K. H. Rieder, eds. (Springer-Verlag, Berlin, 1985).

G. I. Stegeman, C. T. Seaton, and J. J. Burke, "Nonlinear integrated optics," in *Integrated Optical Circuits and Components: Design and Application*, L. D. Hutcheson, ed. (Marcel Dekker, New York, 1987), in press.

C. T. Seaton, J. D. Valera, R. L. Shoemaker, G. I. Stegeman, J. Chilwell, and S. D. Smith, "Calculations of nonlinear TE waves guided by thin dielectric films bounded by nonlinear media," IEEE J. Quant. Electron. QE-21, 774 (1985).

G. I. Stegeman and C. T. Seaton, "Nonlinear integrated optics," App. Phys. Rev. (J. Appl. Physics) 58, 57 (1985).

C. T. Seaton, G. I. Stegeman, and H. G. Winful, "Nonlinear planar guided wave interactions and devices," Proceedings of AGARD Conference on Guided Waves in the Military Environment, Istanbul, Turkey (1985).

G. I. Stegeman and C. T. Seaton, "Nonlinear integrated optics," invited paper, Proceedings of Fifth Internation Conference on Integrated Optics and Optical Fibre Communication, Venice, Italy (1985).

C. T. Seaton and G. I. Stegeman, "Intensity-dependent waveguide phenomena," Proceedings of Second Conference on Integrated Optical Engineering, Cambridge (1985).

G. I. Stegeman, J. Ariyasu, C. T. Seaton, and J. V. Moloney, "Nonlinear waves guided by non-Kerr-like media," Proceedings of 1986 Integrated and Guided Wave Optics Conference, A 'anta, GA (1986).

J. D. Valera, C. T. Seaton, G. I. Stegeman, and B. Svensson, "Switching and bistability in liquid crystal cladded waveguides," Proceedings of SPIE Conference on Liquid Crystal and Spatial Light Modulator Materials (1986).

E. M. Wright, C. T. Seaton, G. I. Stegeman, and J. V. Moloney, Proceedings of the Twelfth European Conference on Optical Communication, Barcelona, Spain (1986).

S. Wabnitz, E. M. Wright, C. T. Seaton, and G. I. Stegeman, Proceedings of the Twelfth European Conference on Optical Communication, Barcelona, Spain (1986).

E. M. Wright, G. I. Stegeman, C. T. Seaton, and J. V. Moloney, "Gaussian beam excitation of TE_0 nonlinear guided waves," Appl. Phys. Lett. **49**, 435 (1986).

R. M. Fortenberry, R. Moshrefzadeh, G. Assanto, Xu Mai, E. M. Wright, C. T. Seaton, and G. I. Stegeman, "Power-dependent coupling and switching in prism and grating coupling to ZnO waveguides," Appl. Phys. Lett. **49**, 6987 (1986).

K. W. Steijn, R. J. Seymour, and G. I. Stegeman, "Attenuation of far infrared surface plasmons on overcoated metal," Appl. Phys. Lett. **49**, 1151 (1986).

E. M. Wright, G. I. Stegeman, C. T. Seaton, J. V. Moloney, and A. D. Boardman, "Multi-soliton emission and optical limiting in a nonlinear waveguide," Phys. Rev. A **34**, 4442 (1986).

39

G. I. Stegeman and C. T. Seaton, "Numerical and experimental studies of nonlinear EM guided waves," Proceedings of Second International Conference on Surface Waves in Plasmas and Solids, Ohrid, Yugoslavia (1986).

L. Thylen, E. M. Wright, G. I. Stegeman, C. T. Seaton, and J. V. Moloney, "Beam propagation method analysis of a nonlinear directional coupler," Opt. Lett. 11, 739 (1986).

S. Wabnitz, E. M. Wright, J. V. Moloney, C. T. Seaton, and G. I. Stegeman, "Instabilities and all-optical phase-controlled switching in a nonlinear directional coherent coupler," Appl. Phys. Lett. 49, 838 (1986).

G. I. Stegeman, C. T. Seaton, A. Boardman, and P. Egan, "Nonlinear guided waves," in Proceedings of NATO Summer School on Surface Electromagnetic Excitations, R. F. Wallis and G. I. Stegeman, eds., (Springer-Verlag, Berlin, 1986); also in Proceedings of NATO Summer School on Nonlinear Optics: Materials and Devices, (Springer-Verlag), in press.

G. Assanto, R. M. Fortenberry, K. Rochford, E. M. Wright, C. T. Seaton, and G. I. Stegeman, Proceedings of the Twelfth European Conference on Optical Communication, Barcelona, Spain (1986).

M. Gubbels, E. M. Wright, G. I. Stegeman, C. T. Seaton, and J. V. Moloney, "Effects of absorption on TE_0 nonlinear guided waves," Opt. Commun. 61, 357 (1987).

G. I. Stegeman, C. T. Seaton, A. C. Walker, C. N. Ironside, and T. J. Cullen, "Nonlinear directional couplers with integrating nonlinearities," Opt. Commun. 61, 277 (1987).

G. I. Stegeman, C. T. Seaton, C. N. Ironside, T. J. Cullen, and A. C. Walker, "Effects of saturation and loss on nonlinear directional couplers," Appl. Phys. Lett. 50, 1035 (1987).

G. I. Stegeman, C. T. Seaton, and R. J. Zanoni, "Organic films in nonlinear integrated optics structures," Thin Solid Films 152, 231 (1987).

R. Moshrefzadeh, B. Svensson, Xu Mai, C. T. Seaton, and G. I. Stegeman, "Chirped gratings for efficient coupling into nonlinear waveguides," Appl. Phys. Lett. 51, 390 (1987).

40

G. I. Stegeman and C. T. Seaton, "Nonlinear waves guided by multilayer media," Proceedings of the International Symposium on Surface Waves in Solids and Layered Structures, Novosibirsk, USSR (1986).

R. Moshrefzadeh, X. Mai, C. T. Seaton, and G. I. Stegeman, "Efficient grating couplers for polymer waveguides," Appl. Opt., in press.

M. Gubbels, E. M. Wright, G. I. Stegeman, C. T. Seaton, and J. V. Moloney, "Numerical study of soliton emission from a nonlinear waveguide," JOSA B, in press.

G. Assanto, R. M. Fortenberry, C. T. Seaton, and G. I. Stegeman, "Theory of pulsed excitation of nonlinear distributed prism couplers," JOSA B, in press.

R. M. Fortenberry, G. Assanto, R. Moshrefzadeh, C. T. Seaton, and G. I. Stegeman, "Pulsed excitation of nonlinear distributed coupling into ZnO optical guides," JOSA B, in press.

G. I. Stegeman, G. Assanto, R. Zanoni, C. T. Seaton, E. Garmire, A. A. Maradudin, R. Reinisch, and G. Vitrant, "Bistability and switching in nonlinear prism coupling," submitted to Appl. Phys. Lett.

R. M. Fortenberry, G. Assanto, R. Moshrefzadeh, C. T. Seaton, and G. I. Stegeman, "Nonlinear distributed coupling into guided waves," Proceedings of the USA-USSR Binational Symposium on Laser Optics of Condensed Matter, in press.

D. R. Heatley, E. M. Wright, J. Ehrlich, and G. I. Stegeman, "Nonlinear directional coupler with a diffusive Kerr-type nonlinearity," submitted to Opt. Lett.

J. D. Valera, Nonlinear Guided Waves and Nonlinear Prism Coupling in Thin Film Waveguides with Liquid Crystal Cladding, Ph.D. dissertation (University of Arizona, June 1986).

C. Naselli, Thermally Induced Order-Disorder Transitions in Langmuir-Blodgett Films Studied by Fourier Transform Infrared Spectroscopy, M.S. thesis (University of Arizona, December 1986).

R. M. Fortenberry, Nonlinear Optical Phenomena in ZnO Waveguides, Ph.D. dissertation (University of Arizona, December 1986).

R. Moshrefzadeh, Nonlinear Guided Wave Grating Couplers, Ph.D. dissertation (University of Arizona, March 1987).

SCIENTIFIC PERSONNEL

G. I. Stegeman

C. T. Seaton

C. Naselli (M.S. 12/86)

L. Li

R. M. Fortenberry (Ph.D 12/86)

J. Erhlich

E. M. Wright

J. D. Valera (Ph.D. 6/86)

RESEARCH FINDINGS

Introduction

Research was performed in three different areas:

1. Gratings were fabricated in semiconductor and dielectric surfaces using a modified Lloyd's interference fringe approach and reactive ion milling. Gratings with depth-to-period ratios as large as unity and periods varying from 0.18 μm to 5.0 μm were made. Nonlinear coupling into guided waves was demonstrated for a variety of materials, including dielectrics, semiconductors, and organics. Preliminary results on a nonlinear distributed-feedback grating have been obtained in InSb.

2. Thin nonlinear organic films have been made by spinning and casting. Low-loss waveguides using grating coupling have been demonstrated in a variety of materials. Nonlinear coupler and nonlinear distributed-feedback experiments were initiated.

3. Two approaches to optical limiters were developed. Large decreases in coupling efficiency were obtained when coupling into ZnO thin-film waveguides. This phenomenon has been theoretically analyzed with excellent agreement between experiment and theory. It was also shown theoretically that hard optical limiting is obtained for a thin film bounded by a self-defocusing medium.

42

Objectives

The objective of this research program was to investigate the use of electromagnetic waves incident onto, or guided by, surfaces to probe the fundamental properties of thin films and surfaces, as well as to perform various optical device operations.

Summary

Guided Wave Interactions with Gratings

The initial goals were to fabricate gratings for coupling into nonlinear waveguides and to optically tune the Bragg condition for a distributed-feedback grating and hence the reflectivity of a grating imbedded in a nonlinear waveguide.

High quality gratings have been fabricated in InSb films produced by sputtering both at Arizona and the University of Illinois (Champaign-Urbana), and by MBE at ATT Bell Labs. InSb films with deep gratings (mark-space ratios of unity) have been fabricated by holographic writing of gratings in photoresist and subsequent ion milling. The key to reproducible high quality gratings was to monitor both the exposure of the photoresist during developing and the ion milling of the InSb in real time. The films that were rf sputtered at Arizona had both bad stochiometry and "dissolved" Ar atoms, and proved unusable as waveguides because of large losses. Although the Illinois films were supposedly epitaxial and single crystal, the ion-milling process revealed numerous grain boundaries and defects, also rendering the waveguides unusable. The Bell Labs MBE samples proved to be of high quality, and low propagation losses have been obtained. Linear coupling losses have led to precision (± 0.001) measurements of the refractive index of the films for various wavelengths.

Angular and power-dependent switching due to thermal nonlinearities has been obtained for grating couplers fabricated on amorphous InSb films. The angular dependence of the coupling efficiency into the waveguide was measured. As the incident power was increased, the curve became progressively more asymmetric until switching was obtained on the high angle side. When the incident angle was fixed near the high-power switching angle and the power was varied, switching was obtained at a threshold power. No hysteresis or bistability was observed.

Distributed-feedback gratings have been fabricated in MBE-deposited InSb-film waveguides. Power-dependent changes in the reflectivity have been observed, but as yet bistability has not.

43

Organic Films

The original goal in this part of the program was to fabricate organic films by the Langmuir-Blodgett (L-B) technique, study their properties, and assess and fabricate films for nonlinear applications.

Good films have been fabricated up to 400 monolayers thick, which is about the limit usually quoted for L-B film deposition techniques. X-ray diffraction studies show multiple peaks with widths consistent for a solid-lattice structure. Rutherford backscattering indicates film densities very close to theoretical; that is, very few voids inside the film structure. Unfortunately, we found that the propagation losses in these films when used as waveguides were too large to be useful for waveguiding, and this approach was abandoned.

The nonlinear properties of two organic materials supplied by the Celanese Corporation have been measured by degenerate four-wave mixing using nanosecond laser pulses. The nonlinearity was about a factor of two larger than CS_2 for one, and about a factor of 100 larger for the second. Waveguides have been fabricated by spinning from solution and waveguide losses of 1 db/cm measured. These materials were also studied by the nonlinear coupler technique, using grating couplers, and the dominant nonlinearity was found to be thermal in nature.

Nonlinear grating coupler techniques were developed for organic materials. The approach used was to fabricate the gratings in the substrate and then to overcoat the substrate with the organic film. Coupling efficiencies of up to 40% were obtained with careful and detailed design of the grating parameters. Gratings for waveguide applications are now being supplied to a number of laboratories around the country.

Nonlinear waveguides were fabricated by dissolving MNA in polystyrene. Techniques were developed for including up to 30% MNA in PMMA without crystallizing the MNA. The resulting waveguides had typical losses of 1 db/cm. The decrease in coupling efficiency with increasing power was used to study the nonlinearity with nanosecond laser pulses. Using chirped gratings, it has been demonstrated that high-power pulses can be efficiently coupled into a nonlinear waveguide, despite the nonlinear coupling phenomenon.

Distributed-feedback gratings have also been fabricated under organic films and essentially 100% linear reflectivity has been demonstrated. Nonlinear distributed-feedback experiments are underway.

44

Optical Limiters

The last two years of this program, originally funded through MICOM, have been funded partially through this JSOP task.

Grating and prism coupling of high-power nanosecond and picosecond laser pulses into a ZnO (very low loss, ≅1 db/cm) thin-film waveguide have been investigated. Optical limiting action was obtained; that is, a reduction in coupling efficiency by a factor greater than 20 was obtained with increased laser power. At high powers, all-optical switching phenomena on a sub-nanosecond time scale were observed within the pulse envelopes. In apparent contradiction to this result, the relaxation time of the nonlinearity was measured directly under the coupler to be ≅1 μs, identifying it as thermal in origin.

All of the phenomena described above were successfully interpreted in terms of a nonlinear traveling wave interaction between an incident field and a guided wave, characterized by a power-dependent wavevector. The switching phenomena is caused by a nonlinearly produced phase mismatch between the two fields, and the switching time is determined solely by the pulse power and not the nonlinearity relaxation time.

The properties of waves guided by thin films bounded by self-focusing media were pursued further. It had previously been established that for two self-focusing bounding media, it is possible to have three stable field distributions, all characterized by the same guided-wave power. It has been established through numerical propagation studies that all three can be independently excited by focusing Gaussian beams onto the endface of a nonlinear waveguide. The Gaussian beam parameters, positioned relative to the film center and half-width, are different for each of the three waves.

Another numerical experiment focused a Gaussian beam onto the waveguide endface with beam parameters chosen for optimum coupling to low-power guided waves. As the incident power was increased, there was an upper value to the power guided by the film. If larger powers are incident, the additional power is emitted in the form of spatial solitons, the number of solitons being determined by the limiting value of the power which can be guided by the film. An additional, preliminary calculation has established that a soliton can be partially trapped by a thin-film waveguide when it is incident upon it. This makes possible logic devices based on soliton emission and capture.

45

OPTICAL ELEMENTS FOR X-UV
and
PRODUCTION OF HIGH REFLECTIVITY MIRRORS

C. M. Falco

PUBLICATIONS

F. E. Fernandez and C. M. Falco, "Sputter deposited multilayer V-UV mirrors," Proc. SPIE **563**, 195 (1985).

F. E. Fernandez and C. M. Falco, "Multilayer reflectors for the 200 Å region," Proc. SPIE **688**, 104 (1987).

C. M. Falco, F. E. Fernandez, P. Dhez, A. Khandar-Shahabad, L. Nevot, B. Pardo, and J. Corno, "Normal incidence X-UV mirrors," Proc. SPIE **733**, 343 (1987).

F. E. Fernandez, C. M. Falco, P. Dhez, A. Khandar-Shahabad, L. Nevot, B. Pardo, J. Corno, and B. Vidal, "Characterization of multilayers for extended ultraviolet optics," *Appl. Phys. Lett.* **51**, 880 (1987).

F. E. Fernandez, Multilayer Reflectors for Soft X-Rays, Ph.D. dissertation (University of Arizona, 1987).

C. M. Falco, F. E. Fernandez, P. Dhez, A. Khandar-Shahabad, L. Nevot, B. Pardo, J. Corno, and B. Vidal, "Metallic multilayers for x-ray optics," Proc. Metall. Soc., in press.

C. M. Falco, "Fabrication and future of metallic superlattices," J. de Phys., in press.

C. M. Falco, "Growth of metallic and metal-containing superlattices," in *Physics Fabrication and Applications of Multilayered Structures*, P. Dhez, ed. (Plenum, New York, in press).

C. M. Falco, F. E. Fernandez, P. Dhez and A. Khandar-Shahabad, "Properties of multilayers for soft x-ray optics," J. of Superlattices and Microstructures, in press.

J. Boudry, C. Riedel, B. Edwards, M. Lagally, R. Redaelli, F. Cerrina, C. Falco, F. Fernandez, J. H. Underwood, and M. Hettrick, "A beamline for layered synthetic microstructure studies," submitted to Nucl. Instr. Methods.

46

Conference Presentations

F. E. Fernandez and C. M. Falco, "Characteristics of sputter-deposited multilayers," American Vacuum Society, Arizona Chapter, Scottsdale (1985).

F. E. Fernandez and C. M. Falco, "Sputter-deposited multilayer V-UV mirrors," Symposium on Applications of Thin-Film Multilayered Structures to Figured X-Ray Optics at the Annual Meeting of the Society of Photo-Instrumentation Engineers, San Diego, CA (1985).

F. E. Fernandez and C. M. Falco, "X-ray characterization of sputter-deposited multilayer materials," American Physical Society, Las Vegas, NV (1986).

F. E. Fernandez and C. M. Falco, "Multilayer reflectors for the 200 Å radiation region," Symposium on X-Ray Optics at the Annual Meeting of the Society of Photo-Optical Instrumentation Engineers, San Diego, CA (1986).

C. M. Falco, F. E. Fernandez, P. Dhez, and A. Khandar, "Normal incidence X-UV mirrors," International Conference on Soft X-Ray Optics and Technology, Berlin (1986).

C. M. Falco, F. E. Fernandez, P. Dhez, A. Khandar-Shahabad, L. Nevot, B. Pardo, J. Corno, and B. Vidal, "Metallic multilayers for x-ray optics," Symposium on Metallic Multilayers and Epitaxy at the Joint American Society for Metals and Metallurgical Society Meeting, Denver, CO (1987).

F. Fernandez, C. M. Falco, P. Dhez, A. Khandar, L. Nevot, B. Pardo, J. Corno, and B. Vidal, "Multilayer mirrors for soft x-rays," Seventh Annual Symposium of the Arizona Chapter of the American Vacuum Society, Tempe (1987).

D. Schulze and C. M. Falco, "Application of molecular beam epitaxy (MBE) for the production of x-ray optical coatings," Seventh Annual Symposium of the Arizona Chapter of the American Vacuum Society, Tempe (1987).

C. M. Falco, "Metal-metal, metal-semiconductor and metal dielectric superlattices," NATO Advanced Study Institute on Physics, Fabrication and Application of Low Dimensional Structures, Ile de Bendor, France (1987).

C. M. Falco, F. E. Fernandez, P. Dhez, and A. Khandar-Shahabad, "Fabrication and future of metallic superlattices," Third International Conference on Modulated Semiconductor Structures, Montpellier, France (1987).

C. M. Falco, "Artificial metallic superlattices for x-ray optics," Third International Conference on Superlattices, Microstructures and Microdevices, Chicago, IL (1987).

SCIENTIFIC PERSONNEL

C. M. Falco

F. E. Fernandez (Ph.D. 8/87)

D. Schulze

RESEARCH FINDINGS

Summary

The purpose of this work has been to design, fabricate, characterize, and test the optical properties of multilayer coatings for operation in the soft x-ray or extended ultraviolet region of the spectrum (approximately 10 Å to 300 Å, referred to as the X-UV). Normal-incidence mirrors for a variety of wavelengths, beamsplitters, polarizers, and a narrow-pass Fabry-Perot interferometer have been designed. It is believed that this remains the only U. S. university with a complete x-ray optics program, including capabilities for the design, fabrication, characterization, and testing of multilayer coatings for the X-UV.

Results

Several computer programs for calculating the reflectivity of multilayer coatings as a function of wavelength and as a function of incidence angle, with and without interfacial roughness, have been implemented. These programs have been completely tested by reproducing theoretical results in the literature for the X-UV reflectivity of various multilayer mirrors, and by performing design calculations which were subsequently verified by fabricating the appropriate multilayers in this laboratory and testing them at a synchrotron.

A data base has been assembled, consisting of a complete set of optical constants (real and imaginary parts) for all elements from 1 to 94, and for wavelengths between 6 and 124 Å. For a few materials of particular interest (e.g., crystalline and amorphous Si, W, Mo) this has been extended to longer wavelengths.

48

During the past year, several types of multilayer coatings were fabricated, including beamsplitters, polarizers, a Fabry-Perot etalon, and reflectors for several incidence angles. Operational wavelengths for these structures range from 31.6 to 210 Å. A set of Si/W normal-incidence reflectors for 210 Å radiation, and a Si/Mo normal-incidence Fabry-Perot reflector for 150 Å, were tested with synchrotron radiation. The remainder of this section briefly describes the fabrication procedure used for the Si/W mirrors, as well as results of an extensive series of characterization measurements, model fitting, and synchrotron tests on the Si/W samples. It is believed that this is the first time such a comprehensive set of characterization techniques has been applied to a multilayer x-ray coating. As shown in Fig. 1, reflectances for ~200 Å, calculated using the results from these various characterization techniques, were found to agree very well with measurements obtained with synchrotron radiation. Thus, it has been demonstrated that the use of a suitable set of complementary characterization techniques can determine in detail the properties of the as-deposited films in a multilayer (i.e., prediction of layer thicknesses, interface roughness, chemical contamination, and oxidation of the outermost layer) and therefore enable prediction of the performance when operated in the X-UV. This development is felt to be a significant contribution to the field of multilayer x-ray optics.
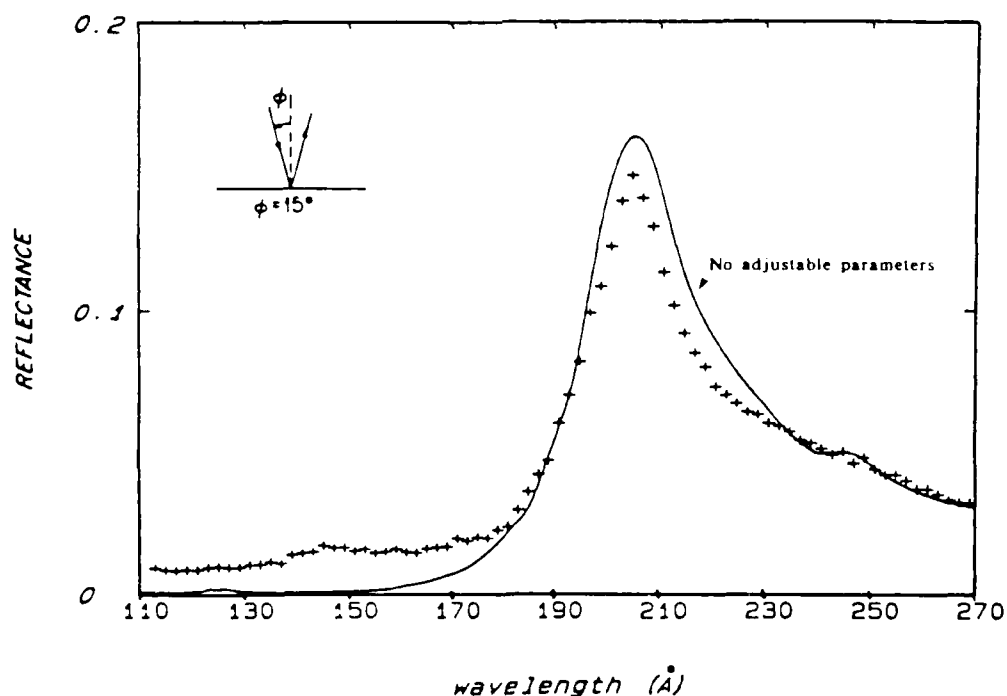

Figure 1 Measured and calculated near-normal incidence reflectivity for a Si/W multilayer mirror. The solid curve is calculated from measured quantities, without any adjustable parameters.

Carbon has been the "spacer" of choice for much of the X-UV spectrum because of its generally low absorption and the smooth interfaces that form when interlayered with many metals. However, interest in the use of silicon as a spacer is justified for several reasons. Silicon has lower absorption than carbon at wavelengths just below the carbon K-edge at 44 Å, and also at wavelengths immediately above the silicon L-edge at 124 Å. There are important potential applications for normal-incidence optics in both these regions; for example, for x-ray lasers where light amplification at 206.3 and 209.6 Å has recently been demonstrated, and for free-electron lasers (FEL) operating in this wavelength range. For wavelengths below 44 Å, there is additional interest in soft x-ray microscopes for use in biological research.

The study of Si/metal multilayers is also of interest because of the possible fabrication of fully crystalline multilayers which could withstand the effects of high-intensity radiation much better than polycrystalline or amorphous ones. Recrystallization could not occur, thus eliminating an effect which greatly increases surface roughness or even destroys the layered structure in a multilayer. The unique (in the x-ray optics field) molecular beam epitaxy (MBE) capability available here, will allow, for the first time, investigation of possible improvements in the performance of multilayers based on crystalline Si.

The deposition system used to date in this laboratory for the fabrication of the Si/W samples described here is built around magnetically-confined dc-sputtering guns. The sputtering rates are feedback-controlled through an empirical relationship between sputtering rate, target voltage and current, target size, and substrate-to-target distance. The motion of the substrates over the guns is governed by a servo-controlled motor operated by a microprocessor. These combine to allow layer thickness control of better than 0.3%.

Under the deposition conditions used in this sputtering system, smooth layers of amorphous Si and of oriented polycrystalline W with layer-thickness-limited crystallite size were obtained. A cross-section transmission electron micrograph (TEM) of one of the Si/W samples is shown in Fig. 2.

The characterization techniques applied to the multilayer coatings were low-angle x-ray diffraction with Cu and C radiation, Bragg-Brentano and Seemann-Bohlin diffraction, Read camera studies, transmission electron microscopy, and Rutherford backscattering spectroscopy (RBS). The characterization procedure developed over the past several years using these techniques has been very useful in determining how to modify an initial design or the deposition procedure, to improve the reflectance characteristics. This work has demonstrated that the performance of such coatings,

50

Figure 2. Cross-sectional TEM of one of the Si/W samples.

and the causes for deviations from ideal behavior, can now be fully understood.

RBS was used to determine the oxygen and argon content in the interior of these particular samples, demonstrating that the chemical quality of the samples was very good. X-ray diffraction measurements in $\theta2\theta$ configuration and at grazing incidences were performed for one sample on the low-angle diffractometer of the Institut d'Optique (Universite de Paris XI, Orsay). The bilayer spacing ($\Delta = dW + dSi$) was determined accurately from the Bragg peak positions and, by fitting model calculations to the measured curve, the thickness ratio ($\gamma = dW/\Delta$), rms roughness of the layers, and the thickness of oxide on the top W layer were deduced.

With high-angle x-ray scans of the samples using the Bragg-Brentano diffraction geometry, it was determined that both Si and W were deposited with very small crystallite sizes, since no diffraction peaks were observed. Wide-film Debye-Scherrer

(Read) camera exposures of the samples exhibited broad lines corresponding to polycrystalline tungsten and to amorphous Si. Using an x-ray diffractometer in the Seemann-Bohlin configuration, the crystallite size in the W layers was determined to be 37 Å for the multilayer, strongly suggesting that the crystallites are limited in size by the thickness of the tungsten layers in the sample (39 Å).

From the above data, the density of the W in the sample was calculated and found to be almost 10% less than bulk density. From the fitting procedure for the low-angle x-ray data, the layer thicknesses were determined to be dSi = 73.0 Å and dW = 39.4 Å. This value for dW is 4.8% higher than the intended thickness of 37.6 Å, which is the amount to be expected when the W density in the multilayer is lower than bulk. This points out the necessity of careful structural characterization of the multilayers.

To summarize, various complementary techniques were applied to determine the detailed structure of the multilayer mirrors. These allowed calculation of the expected performance of the mirror without requiring adjustable parameters for the structure. It is believed that this was the first time such a set of characterization techniques were applied to a multilayer x-ray mirror.

The same Si/W multilayers which were characterized in detail were tested at several incidence angles using synchrotron radiation in the 120 to 280 Å region. These tests were performed at the ACO Synchrotron at L.U.R.E., Universite de Paris XI, Orsay. The multilayers were tested at various angles of incidence between 5^0 and 45^0.

One set of reflectance measurements has been shown in Fig. 1, together with values calculated using the results of the structural characterization procedure, without any adjustable parameters. Considering the uncertainties in the optical constants for Si in the 200 Å region, the agreement between calculation and measurement is excellent.

The research described above, conducted in this laboratory during the past three years, has shown how both multilayer densities and layer thicknesses can be accurately determined by combining RBS and low-angle x-ray diffraction results. The complete characterization procedure described here has removed uncertainties in the structure and resulted in excellent agreement between measured and calculated results for the X-UV performance. The present limit is imposed by uncertainties in the available optical constants for the X-UV.

With JSOP support, the capability to design, fabricate, characterize, and test multilayer coatings for the X-UV has been developed. It is felt that there is no better-equipped university laboratory in the world for this type of research.

52

NOVEL ION-BEAM MILLING TECHNIQUES FOR INTEGRATED OPTICS

U. J. Gibson

PUBLICATIONS

G. Assanto, B. Svensson, D. Kuchibhatla, U. J. Gibson, C. T. Seaton, and G. I. Stegeman, "Prism coupling into ZnS waveguides: A classcial example of a non-linear coupler," Opt. Lett. 11, 644 (1986).

D. Kuchibhatla and U. Gibson, "Technique for edge profile modification of optical waveguides using ion milling," to be submitted.

SCIENTIFIC PERSONNEL

Ursula Gibson

Dilip Kuchibhatla (M.S. 1/87)

RESEARCH FINDINGS

The use of biased conducting masks during the ion etching process to control the edge roughness and the edge profile of photolithographically defined features was investigated. An Al-glass-ZnS-Al structure as shown in Fig. 1 was used to assess the process for the formation of optical rib waveguides. A positive voltage on the upper electrode deflected the incoming ions in the vicinity of the stripe, altering the edge profile.
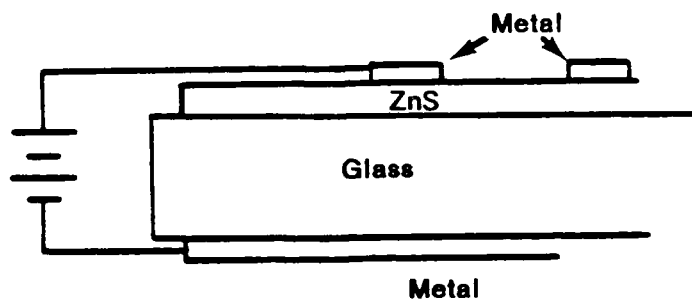
Figure 1. Schematic of biased ion milling sample.

Early results on Ni-glass-ZnS-Ni structures were encouraging, despite extreme roughening of the edges of the waveguides. Since beginning the project, the processing technique has been substantially improved, confirming the early results on edge-profile modification, with spinoff improvements in the quality of planar ZnS waveguides.

Experiments have been performed on ZnS waveguides on both oxidized Si and glass substrates ($\geq$0.5 mm thick), with Al masking electrodes. Four stripes, with widths of 50 to 100 μm, were spaced 5 mm apart on each substrate, to minimize crosstalk between adjacent electrodes. The voltage, applied between a ground plane on the reverse side of the substrate and the electrode above the waveguiding layer, was varied between 0 and 400 V. The angle between the substrate surface and the waveguide edge could be varied from near normal incidence to less than 65° by argon ion milling in the presence of the field. Data for contact angle and sidewall roughness versus applied voltage are shown in Fig. 2. The contact angle obtainable was limited by the increase in milling time required for large applied voltages. (Larger angles should be attainable by reducing the substrate thickness and using lithographically defined ground stripes to increase the field gradient at the electrode edges.) Smooth top surfaces of the guide, and acceptably smooth edges were obtained. Examples of the milled edges are shown in Figs. 3a and 3b, for applied voltages of 0 and 300 V, respectively. Propagation losses in the guides, illuminated with 0.628 μm light, were comparable to those observed in planar guides, as would be expected because of the large width of the stripes. Smaller stripe widths will be required to make a detailed assessment of value of the technique for loss reduction.

As part of the project, it was necessary to develop ZnS films resistant to the wet-chemical processing involved in photolithography. Thick films of ZnS (>1.0 μm), required for waveguiding, are highly stressed, and typically delaminate from the substrate. Using ion precleaning of the substrate, and concurrent ion bombardment of the first 1000 Å of ZnS that was deposited, thick films with good adherence properties were obtained.
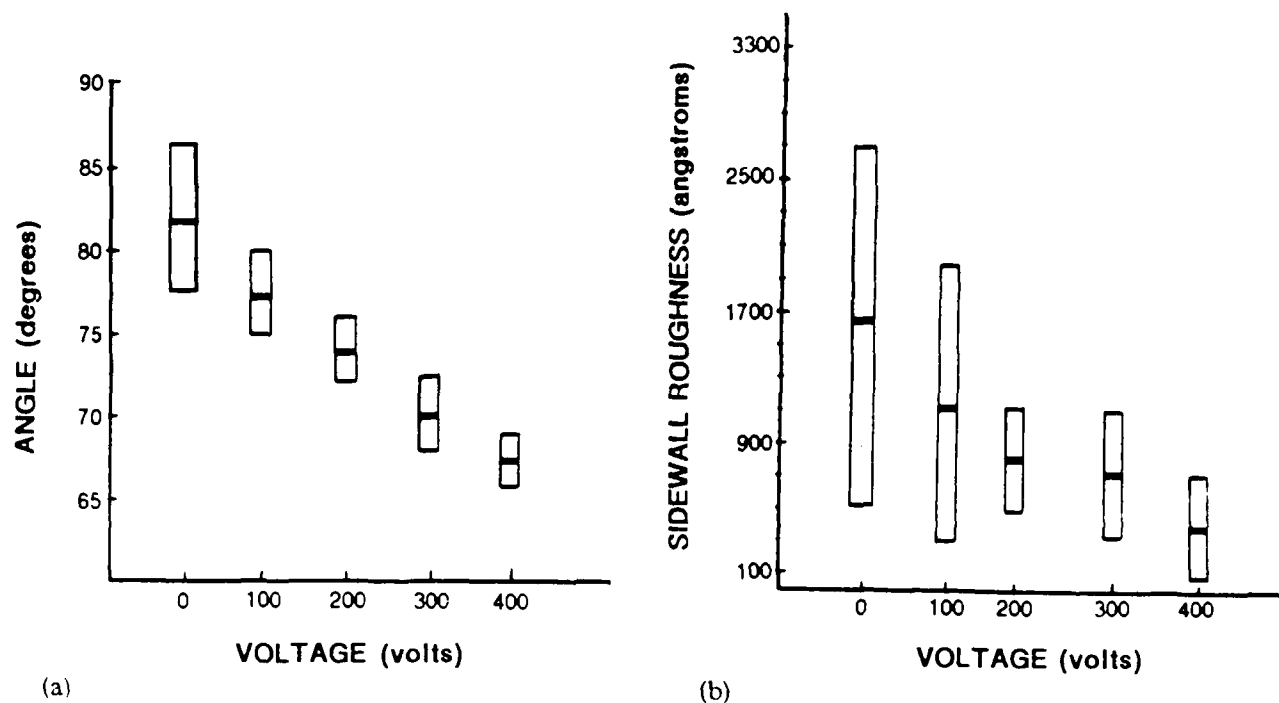
Figure 2. (a) Contact angle and (b) sidewall roughness as a function of applied voltage. The heavy bar indicates the mean value, and the box indicates the range of values served.
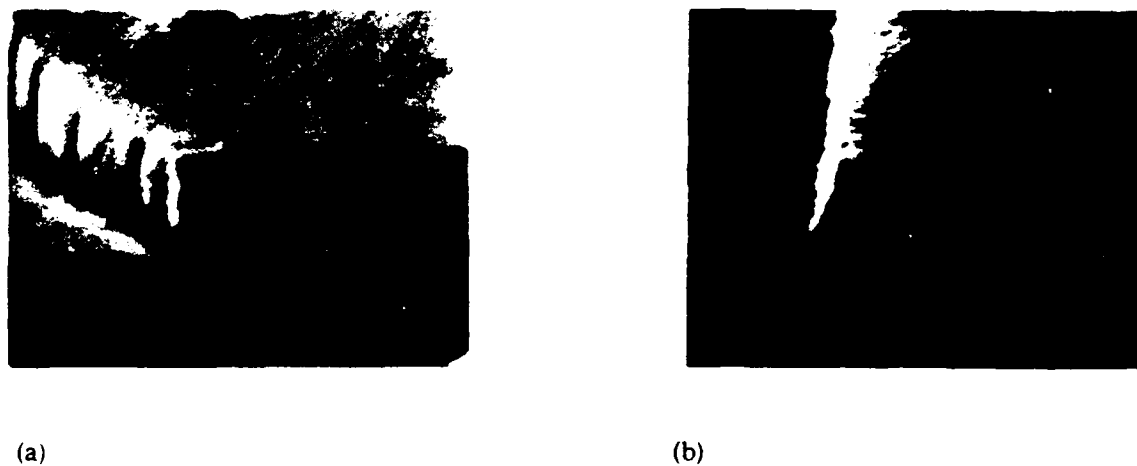

(a)

(b)

Figure 3. (a) Sidewall of reference (θ applied voltage) sample. Foot is due to incomplete milling; (b) sidewall of 300 V biased sample; θ ≅ 70°.

OPTICAL PROPERTIES OF INHOMOGENEOUS MEDIA

U. J. Gibson

SCIENTIFIC PERSONNEL

U. J. Gibson

J. A. Ruffner

RESEARCH FINDINGS

Objectives

Prepare and characterize the linear optical properties of mixed-phase materials that are of potential use in nonlinear applications.

Use effective medium theory to calculate optical properties for comparison with experiment.

Progress

In the first nine months of this contract, calculations of the optical properties of semiconductor-metal (ZnS/Au and ZnS/Zn) and semiconductor-dielectric (CdS/glass) mixtures have been made, and initial film depositions have been performed. In the case of the metal-semiconductor mixture, it is anticipated that the resonant absorption at long wavelengths may be used for efficient driving of the thermal nonlinearity of the semiconductor host. In addition, it is expected that second-harmonic generation will be enhanced because of symmetry breaking at the surface. The characteristic band-edge absorption for the small semiconductor particles in the dielectric host may also be used for probing nonlinear properties of the material.

Film depositions corresponding the the first set of calculations revealed difficulties in precipitating gold into particles, so the system in use now is Zn on ZnS. Depositions of this mixture have been made, but experiments on second-harmonic generation (SHG) in alumina thin films demonstrated that minute amounts of anisotropy in thin films, due to deposition conditions, affect the SHG signal significantly. Therefore an investigation of the sensitivity of ZnS (without metal particles) to deposition conditions is underway to eliminate spurious effects. Since ZnS is non-centrosymmetric, the SHG is extremely sensitive to film structure, and it has been necessary to upgrade the deposition system to include an optical monitor and residual gas analyzer. Once the required repeatability in the production phase

has been achieved, meaningful studies of SHG in ZnS may be made and compared to both the calculations and to metal/ZnS mixtures.

Early attempts to deposit CdS/oxide mixtures to create semiconductor precipitates were unsuccessful, because of the formation of CdO. Experiments with production of CdS/ZnS are now underway.

Funded 1/87 to 10/87.

QUANTUM THEORY OF MULTIWAVE MIXING

Murray Sargent III

PUBLICATIONS

D. A. Holm and M. Sargent III, "Quantum theory of multiwave mixing VII. Connection to quantum Langevin theory," Phy. Rev. A **33**, 4001 (1986).

D. A. Holm, M. Sargent III, and B. A. Capron, "Generation of squeezed states by nondegenerate multiwave mixing in two-level media," Opt. Lett. **11**, 443 (1986).

B. A. Capron, A. S. Marathay, and M. Sargent III, "Theory of two-photon Doppler-broadened probe absorption," Opt. Lett. **11**, 70 (1986).

B. A. Capron and M. Sargent III, "Effects of ionization and cascade decay on two-photon two-level interactions," Phys. Rev. A **34**, 3051 (1986).

B. A. Capron and M. Sargent III, "Effect of Doppler broadening on two-photon multiwave mixing," Phys. Rev. A **34**, 3034 (1986).

D. A. Holm, Sunghyuck An, and M. Sargent III, "Solution of the quantum coupled mode equations," Opt. Comm. **60**, 328 (1986).

D. A. Holm and M. Sargent III, "Quantum theory of multiwave mixing VIII. Squeezed states," Phys. Rev. A **35**, 2150 (1987).

B. A. Capron, D. A. Holm, and M. Sargent III, "Quantum theory of multiwave mixing IX. Squeezed states in two-photon media," Phys. Rev. A **35**, 3388 (1987).

S. An, B. A. Capron, and M. Sargent III, "Nondegenerate phase conjugation with no pump spatial holes," Opt. Comm. **64**, 307 (1987).

R. W. Boyd and M. Sargent III, "Population pulsations and the dynamic Stark effect," J. Opt. Soc. Am. B (1988), special issue edited by the authors.

G. Khitrova, P. Berman, and M. Sargent III, "Theory of pump-probe spectroscopy," J. Opt. Soc. Am. B (1988).

M. Sargent III. "Instabilities due to quantum multiwave mixing." Opt. News 12, 111 (1986).

B. A. Capron, D. A. Holm, and M. Sargent III, "Squeezing in nondegenerate two-photon two-level media," Opt. News 12, 144 (1986).

D. A. Holm and M. Sargent III, "Quantum theory of multiwave mixing in two-photon two-level media," Opt News 12, 144 (1986).

M. Sargent III, "Efficient entry of mathematical equations," Opt. News 12, 212 (1986).

S. An, B. A. Capron, and M. Sargent III, "Phase conjugation without spatial holes," Opt. News 12, 216 (1986).

B. A. Capron and M. Sargent III, "Nondegenerate two-photon phase conjugation," Opt. News 13, 101 (1987).

G. Khitrova, P. Berman, and M. Sargent III, "New lineshape profiles in two-wave mixing," Opt. News 13, 139 (1987).

G. Khitrova, P. Berman, and M. Sargent III, "Theory of pump-probe spectroscopy," J. Opt. Sci. Am. B (1988).

S. An and M. Sargent III, "Generation of squeezing in two-photon three-level media," submitted to Opt. Lett.

Presentations

D. A. Holm and M. Sargent III, "Squeezed states in nondegenerate four-wave mixing," XIV International Conference on Quantum Electronics, San Francisco, CA (1986).

B. A. Capron and M. Sargent III, "Generalized two-photon multiwave mixing," XIV International Conference on Quantum Electronics, San Francisco, CA (1986).

M. Sargent III, "Squeezing and the quantum beat laser," XV Winter Colloquium on Quantum Electronics, Snowbird, UT (1987).

D. A. Holm and M. Sargent III, "Effects of quantum noise on phase conjugation," XV International Conference on Quantum Electronics, Baltimore, MD (1987).

M. S. Zubairy, M. O. Scully, and M. Sargent III, "Generation of squeezing in the quantum beat laser," XV International Conference on Quantum Electronics, Baltimore, MD (1987).

M. Sargent III, "Optical instabilities due to quantum multiwave mixing," International Workshop on Instabilities, Dynamics, and Chaos in Nonlinear Optical Systems, Lucca, Italy (1987).

SCIENTIFIC PERSONNEL

M. Sargent III

D. A. Holm

B. A. Capron (Ph.D. 1986)

S. An (Ph.D. 1988)

RESEARCH FINDINGS

Considerable progress has been made over the past year. The minor discrepancies between our formulations and those of Reid and Walls[1] have been resolved; the groups all now predict squeezing in various tuning regions in two-level media, in agreement with the experiments of Slusher and others.[2] The theory for the two-photon two-level model has been developed, predicting nearly perfect squeezing even for near degenerate operation with small pump intensities. This is attributable to the fact that four-wave mixing occurs in fourth-order in the atom-field interaction energy, while spontaneous emission requires eight orders and a correspondingly larger pump field.

The two-photon results could provide a squeezer using atomic beams that works considerably better than those achieved in beams to date. The small pump intensities required also can be described by relatively simple theory. This understanding may be applicable to the physics of semiconductor lasers. It is also conceivable that the media studied here may provide methods to increase the signal to noise in critical measurements; if so, these methods will have considerable impact.

The author also coedited a special issue of the Journal of the Optical Society of America dedicated to population pulsations and the dynamic Stark effect. This issue will appear in January 1988. These phenomena are responsible for the generation of squeezing in two-level media, as well as a host of other phenomena.

REFERENCES

1. R. E. Slusher, L. W. Hollberg, B. Yurke, J. C. Mertz, and J. F. Valley, Phys. Rev. Lett. 55, 2409 (1985).

2. M. D. Reid and D. F. Walls, Phys. Rev. A 34, 4929 (1986).

ETALON LOGIC AND TWO-DIMENSIONAL ARRAYS

H. M. Gibbs and N. Peyghambarian

PUBLICATIONS/REFERENCES

1. A. Migus, A. Antonetti, D. Hulin, A. Mysyrowicz, H. M. Gibbs, N. Peyghambarian, and J. L. Jewell, "One-picosecond optical NOR gate at room temperature with a GaAs-AlGaAs multiple-quantum-well nonlinear Fabry-Perot etalon," Appl. Phys. Lett. **46**, 70 (1984).

2. T. Venkatesan, P. J. Lemaire, B. Wilkens, L. Soto, A. C. Gossard, W. Wiegmann, J. L. Jewell, H. M. Gibbs, and S. S. Tarng, "All-optical data switching in an optical-fiber link using a GaAs optical bistable device," Opt. Lett. **9**, 297 (1984).

3. H. M. Gibbs, J. L. Jewell, N. Peyghambarian, M. C. Rushford, K. Tai, S. S. Tarng, D. Weinberger, A. C. Gossard, W. Wiegmann, and T. Venkatesan, "Advances in optical bistability of semiconductors: GaAs-AlGaAs superlattices, bulk GaAs, CuCl, ZnS, ZnSe, and GaSe," Proceedings of the Royal Society Meeting, London (1984); and "Semiconductor nonlinear etalons," Phil. Trans. R. Soc. Lond. A **313**, 245 (1984).

4. J. L. Jewell, M. C. Rushford, H. M. Gibbs, and N. Peyghambarian, "Optical logic on a single etalon," Proceedings of the Royal Society Meeting, London (1984); and J. L. Jewell, M. C. Rushford, H. M. Gibbs, M. Warren, N. Peyghambarian, A. C. Gossard, and W. Wiegmann, "Optical logic on a single etalon," Phil. Trans. R. Soc. Lond. A **313**, 375 (1984).

5. N. Peyghambarian and H. M. Gibbs, "Optical nonlinearity and bistability in semiconductors," invited paper, Proceedings of the International School on Nonlinear Phenomena in Solids, Varna, Bulgaria (1984); and in *Nonlinear Phenomena in Solids*, A. F. Vavrek, ed. (World Scientific Publishing, Singapore, 1984).

6. A. Mysyrowicz, D. Hulin, A. Migus, A. Antonetti, H. M. Gibbs, N. Peyghambarian, and J. L. Jewell, "Blue shift of the exciton resonance due to exciton-exciton interactions in a multiple-quantum-well structure," postdeadline paper PD-C6, Proceedings of the XIII International Conference on Quantum Electronics (IQEC, 1984).

7. J. L. Jewell, S. Ovadia, N. Peyghambarian, S. S. Tarng, H. M. Gibbs, A. C. Gossard, and W. Wiegmann, "Room-temperature excitonic optical bistability in bulk GaAs," Conference on Lasers and Electro-Optics, IEEE Technical Digest, 120 (1984).

8. H. M. Gibbs, J. L. Jewell, Y. Lee, G. Olbright, S. Ovadia, N. Peyghambarian, M. C. Rushford, M. Warren, and D. A. Weinberger, "Controlling light with light using semiconductor etalons," invited paper, AVP Specialists meeting on Optical Circuit Technology, Munich, West Germany (1984).

9. N. Peyghambarian, H. M. Gibbs, D. Hulin, A. Mysyrowicz, A. Migus, A. Antonetti, and J. L. Jewell, "Evidence for exciton-exciton interaction in a GaAs-AlGaAs multiple-quantum-well from dynamical studies with subpicosecond resolution," paper ThJ7, OSA Annual Meeting, San Diego, CA (1984).

10. J. L. Jewell, Y. H. Lee, M. Warren, H. M. Gibbs, N. Peyghambarian, A. C. Gossard, and W. Wiegmann, "Low-energy fast optical logic gates in a room-temperature GaAs etalon," paper ThF6, OSA Annual Meeting, San Diego, CA (1984).

11. S. Ovadia, H. M. Gibbs, N. Peyghambarian, D. Sarid, J. L. Jewell, A. C. Gossard, and W. Weigmann, "Evidence that room-temperature GaAs optical bistability is excitonic," paper WM5, OSA Annual Meeting, San Diego, CA (1984).

12. N. Peyghambarian, H. M. Gibbs, J. L. Jewell, A. Antonetti, A. Migus, D. Hulin, and A. Mysyrowicz, "Blue shift of the exciton resonance due to exciton-exciton interactions in a multiple-quantum-well structure," Phys. Rev. Lett. 53, 2433 (1984).

13. N. Peyghambarian and H. M. Gibbs, "Optical bistability for optical signal processing and computing," invited paper, Opt. Eng. 24, 68 (1985).

63

14. N. Peyghambarian, H. M. Gibbs, J. L. Jewell, A. Migus, A. Antonetti, D. Hulin, and A. Mysyrowicz, "A study of exciton and carrier dynamics and a demonstration of one-picosecond optical NOR gate operation of a GaAs-AlGaAs device," paper ThA2, Proceedings of the Topical Meeting on Picosecond Electronics and Optoelectronics, Lake Tahoe, NV (1985); and in *Picosecond Electronics and Optoelectronics* G. A. Mourou, D. M. Bloom, and C. H. Lee, eds. (Springer-Verlag, Berlin, 1985), p.148.

15. D. Hulin, A. Migus, A. Antonetti, A. Mysyrowicz, H. M. Gibbs, N. Peyghambarian, H. Morkoc, and W. T. Masselink, "Exciton interaction in GaAs, GaAlAs superlattice," postdeadline paper PDP1, Picosecond Electronics and Optoelectronics Topical Meeting, Incline Village, NV (1985); and D. Hulin, A. Migus, A. Antonetti, A. Mysyrowicz, H. M. Gibbs, N. Peyghambarian, H. Morkoc, and W. T. Masselink, "Exciton-exciton interaction in GaAs-GaAlAs superlattices," in *Picosecond Electronics and Optoelectronics* (Springer-Verlag, Berlin, 1985), p.151.

16. H. M. Gibbs and N. Peyghambarian, "Nonlinear optical mechanisms and devices for optical computing," invited paper MC1, Topical Meeting on Optical Computing, Lake Tahoe, NV (1985).

17. J. L. Jewell, Y. H. Lee, M. Warren, H. M. Gibbs, and N. Peyghambarian, "Low-energy, fast, thermally-stable optical NOR gate in a room-temperature GaAs etalon," paper MD1, Topical Meeting on Optical Computing, Incline Village, NV (1985).

18. N. Peyghambarian, H. M. Gibbs, J. L. Jewell, D. Hulin, A. Mysyrowicz, A. Migus, and A. Antonetti, "Femtosecond dynamics of excitons and evidence for exciton-exciton interaction in a two-dimensional superlattice of GaAs-AlGaAs," Bull. Am. Phys. Soc. **30**, 454 (1985).

19. N. Peyghambarian and H. M. Gibbs, "Material requirements for optical logic and bistable devices," invited paper, Proceedings of the APS Topical Meeting on Basic Properties of Optical Materials, Gaithersburg, MD (1985).

20. N. Peyghambarian and H. M. Gibbs, "Optical nonlinearity, bistability, and signal processing using semiconductors," invited paper, J. Opt. Soc. Am. B **2**, 1215 (1985).

64

21. S. Ovadia, H. M. Gibbs, J. L. Jewell, D. Sarid, and N. Peyghambarian. "Evidence that room-temperature optical bistability is excitonic in both bulk and multiple-quantum-well GaAs," Opt. Eng. 24, 565 (1985).

22. A. Migus, A. Antonetti, D. Hulin, A. Mysyrowicz, H. M. Gibbs, N. Peyghambarian, and J. L. Jewell, "One-picosecond optical NOR gate at room-temperature with a GaAs-AlGaAs multiple-quantum-well nonlinear Fabry-Perot etalon," Appl. Phys. Lett. 46, 70 (1985).

23. J. L. Jewell, Y. H. Lee, M. Warren, H. M. Gibbs, N. Peyghambarian, A. C. Gossard, and W. Wiegmann, "3-pJ, 82-MHz optical logic gates in a room-temperature GaAs-AlGaAs multiple-quantum-well etalon," Appl. Phys. Lett. 46, 918 (1985).

24. N. Peyghambarian and H. M. Gibbs, "Nonlinear optical devices," invited article, Sixth ed., Encyclopedia of Science and Technology (McGraw-Hill, New York, 1985).

25. H. M. Gibbs, Optical Bistability: Controlling Light with Light (Academic Press, New York, 1985).

26. T. Venkatesan, B. Wilkens, Y. H. Lee, M. Warren, G. R. Olbright, H. M. Gibbs, N. Peyghambarian, J. S. Smith, and A. Yariv, "Fabrication of arrays of GaAs optical bistable devices," Appl. Phys. Lett. 48, 145 (1986).

27. Y. H. Lee, M. Warren, G. R. Olbright, H. M. Gibbs, N. Peyghambarian, T. Venkatesan, J. S. Smith, and A. Yariv, "Streak-camera observation of 200-ps recovery of an optical gate in a windowless GaAs etalon array," Appl. Phys. Lett. 48, 754 (1986).

28. Y. H. Lee, M. Warren, G. Olbright, H. M. Gibbs, N. Peyghambarian, T. Venkatesan, J. S. Smith, and A. Yariv, "200-ps recovery of an optical gate in a GaAs etalon array," paper FU5, OSA '85.

29. H. M. Gibbs, "Central role of thin films in nonlinear optical signal processing," invited paper ThN2, OSA '85.

30. A. Migus, A. Antonetti, D. Hulin, A. Mysyrowicz, N. Peyghambarian, and H. M. Gibbs, "An ultrafast GaAs all-optical logic gate," paper MC4, OSA Topical Meeting on Optical Bistability, Tucson, AZ (1985); and A. Migus, D. Hulin, A. Mysyrowicz, A. Antonetti, N. Peyghambarian, H. M. Gibbs, W. T. Masselink, and H. Morkoc, "An ultrafast GaAs all-optical logic gate," in *Optical Bistability III*, H. M. Gibbs, P. Mandel, N. Peyghambarian, and S. D. Smith, eds. (Springer-Verlag, Berlin, 1986), p.42.

31. M. Warren, Y. H. Lee, G. R. Olbright, H. M. Gibbs, T. Venkatesan, B. Wilkens, J. S. Smith, and A. Yariv, "Fabrication and characterization of arrays of GaAs all-optical logic gates," paper MC3, OSA Topical Meeting on Optical Bistability, Tucson, AZ (1985); and M. Warren, Y. H. Lee, G. R. Olbright, B. P. McGinnis, H. M. Gibbs, N. Peyghambarian, T. Venkatesan, B. Wilkens, J. S. Smith, and A. Yariv, in *Optical Bistability III*, H. M. Gibbs, P. Mandel, N. Peyghambarian, and S. D. Smith, eds. (Springer-Verlag, Berlin, 1986), p.39.

32. D. Sarid, W. M. Gibbons, H. M. Gibbs, M. E. Warren, S. W. Koch, and L. Banyai, "Optical waveguides in bulk and multiple-quantum-well structures," in *Optical Bistability III*, H. M. Gibbs, P. Mandel, N. Peyghambarian, and S. D. Smith, eds. (Springer-Verlag, Berlin, 1986), p.91.

33. H. M. Gibbs, P. Mandel, N. Peyghambarian, and S. D. Smith., eds., *Optical Bistability III* (Springer-Verlag, Berlin, 1986). Proceedings of the Topical Meeting, Tucson, AZ (1985).

34. D. Hulin, A. Mysyrowicz, A. Antonetti, A. Migus, W. T. Masselink, H. Morkoc, H. M. Gibbs, and N. Peyghambarian, "Two-dimensional nature of the blue shift of excitons in GaAs multiple-quantum-well structures," paper WDD5, Conference on Lasers and Electro-Optics Technical Digest, IEEE (1986).

35. Y. H. Lee, H. M. Gibbs, J. L. Jewell, J. F. Duffy, A. C. Gossard, W. Wiegmann, J. H. English, and T. Venkatesan, "Speed and effectiveness of windowless GaAs etalons as optical logic gates," paper FK2, Conference on Lasers and Electro-Optics Technical Digest, IEEE (1986); and submitted to Appl. Phys. Lett.

36. A. Chavez-Pirson, Y. H. Lee, H. M. Gibbs, A. C. Gossard, and W. Wiegmann, "Limiting and other nonlinear optical behavior of a GaAs/AlGaAs distributed feedback structure," postdeadline paper PD13, XIV International Conference on Quantum Electronics (1986).

66

37. S. W. Koch, Y. H. Lee, A. Chavez-Pirson, H. M. Gibbs, J. Morhange, S. H. Park, T. Carty, A. Jeffery, N. Peyghambarian, B. Batdorf, L. Banyai, A. C. Gossard, and W. Wiegmann, "Room-temperature optical nonlinearities in GaAs," postdeadline paper PD14, XIV International Conference on Quantum Electronics (1986).

38. A. Migus, D. Hulin, A. Mysyrowicz, A. Antonetti, W. T. Masselink, H. Morkoc, H. M. Gibbs, and N. Peyghambarian, "An ultrafast all-optical gate with subpicosecond on and off response time," paper ThU9, OSA Topical Meeting on Ultrafast Phenomena, Snowmass, UT (1986).

39. Y. H. Lee, A. Chavez-Pirson, S. W. Koch, H. M. Gibbs, S. H. Park, J. Morhange, A. Jeffery, N. Peyghambarian, L. Banyai, A. C. Gossard, and W. Wiegmann, "Room-temperature optical nonlinearities in GaAs," Phys. Rev. Lett. 51, 2446 (1986).

40. H. M. Gibbs, N. Peyghambarian, Y. H. Lee, M. Warren, A. Chavez-Pirson, S. W. Koch, A. C. Gossard, and W. Wiegmann, "Room-temperature bulk GaAs: dominant nonlinearities, fast-recovery gates, arrays for parallel processing," NSF Workshop on Optical Nonlinearities, Fast Phenomena and Signal Processing, Tucson, AZ (1986).

41. H. M. Gibbs, N. Peyghambarian, Y. H. Lee, M. Warren, A. Chavez-Pirson, S. H. Park, J. Morhange, A. Jeffery, S. W. Koch, A. C. Gossard, and W. Wiegmann, "Room-temperature bulk GaAs, dominant nonlinearities, fast-recovery gates, arrays for parallel processing," International School of Electro-Optic and Photorefractive Materials, Erice, Sicily (1986).

42. N. Peyhambarian, H. M. Gibbs, D. Hulin, A. Antonetti, A. Migus, and A. Mysyrowicz, "Overview of optical switching and bistability," Conference on High Speed Electronics, Stockholm (1986).

43. H. M. Gibbs and N. Peyghambarian, "Bistability, gating, and pattern recognition using GaAs etalons and ZnS interference filters," invited paper, OSA'86.

44. Y. H. Lee, B. K. Rhee, A. Chavez-Pirson, H. M. Gibbs, A. C. Gossard, and W. Wiegmann, "Direct measurement of dispersive nonlinearities in GaAs," OSA'86.

67

45. J. F. Morhange, S. H. Park, N. Peyghambarian, A. Jeffery, H. M. Gibbs, Y. H. Lee, A. Chavez-Pirson, S. W. Koch, A. C. Gossard, J. H. English, M. Masselink, and H. Morkoc, "Measurements of the bandgap-resonant nonlinear refractive index of bulk and multiple-quantum-well GaAs at room temperature," OSA'86.

46. Y. H. Lee, A. Chavez-Pirson, B. K. Rhee, H. M. Gibbs, A. C. Gossard, and W. Wiegmann, "Direct measurement of dispersive nonlinearities in GaAs," Appl. Phys. Lett. **49**, 1505 (1986).

47. H. M. Gibbs, N. Peyghambarian, and Y. H. Lee, J. L. Jewell, A. Migus, A. Antonetti, D. Hulin, and A. Mysyrowicz, "High-speed optical logic using GaAs," invited paper, Picosecond Electronics and Optoelectronics Topical Meeting, Incline Village, NV (1987).

48. Y. H. Lee, H. M. Gibbs, S. W. Koch, and N. Peyghambarian, "Physics and nonlinear device applications of bulk and multiple quantum well GaAs," Proc. SPIE, Baypoint, FL (1987).

49. M. E. Warren, S. W. Koch, and H. M. Gibbs, "Theory of all-optical GaAs logic devices," Second Topical Meeting on Optical Computing, Lake Tahoe, NV (1987).

50. M. Warren, W. Gibbons, K. Komatsu, D. Sarid, D. Hendricks, and H. M. Gibbs, "Electronic optical bistability in a GaAs/AlGaAs channel waveguide," postdeadline paper, IQEC' 87.

51. M. Warren, W. Gibbons, K. Komatsu, D. Sarid, D. Hendricks, and H. M. Gibbs, "Electronic optical bistability in a GaAs/AlGaAs strip-loaded waveguide," Appl. Phys. Lett. **51**, 1209 (1987).

52. N. Peyghambarian and H. M. Gibbs, "Semiconductor optical nonlinearities and applications to optical devices and bistability," in *Nonlinear Optical Properties of Semiconductors*, H. Huag, ed. (Academic Press, in press).

53. S. W. Koch, N. Peyghambarian, and H. M. Gibbs, "Band-edge nonlinearities in direct-gap semiconductors and their application to optical bistability and optical computing," Appl. Phys. Rev. (review article).

54. M. E. Warren, S. W. Koch, and H. M. Gibbs, "Optical bistability, logic gating, and waveguide operation in semiconductor etalons," IEEE Computer.

55. H. M. Gibbs, G. Khitrova, S. Koch, N. Peyghambarian, D. Sarid, A. Chavez-Pirson, W. Gibbons, A. Jeffery, K. Koma su, Y. H. Lee, D. Hendricks, J. Morhange, S. H. Park, M. Warren, A. C. Gossard, W. Wiegmann, and M. Sugimoto, "GaAs etalons and waveguides: Bulk versus multiple-quantum-well material," invited paper, USA-USSR Symposium on Laser Optics of Condensed Matter, Leningrad (1987).

56. H. M. Gibbs, "Optical bistability: Introduction to nonlinear etalons; GaAs etalons and waveguides; regenerative pulsations," Proceedings of NATO Summer School.

57. H. M. Gibbs, G. Khitrova, S. Koch, N. Peyghambarian, D. Sarid, A. Chavez-Pirson, W. Gibbons, A. Jeffery, K. Komatsu, Y. H. Lee, D. Hendricks, J. Morhange, S. H. Park, M. Warren, A. C. Gossard, W. Wiegmann, and M. Sugimoto, "GaAs etalons and waveguides: Bulk versus multiple-quantum-well material," invited paper, People's Republic of China Meeting on Optical Bistability, Beijing (1987).

58. S. H. Park, J. F. Morhange, A. D. Jeffery, R. A. Morgan, A. Chavez-Pirson, H. M. Gibbs, S. W. Koch, N. Peyghambarian, M. Derstine, A. C. Gossard, J. H. English, and W. Wiegmann, "Investigation of room-temperature bandgap-resonant optical nonlinearities of GaAs/AlGaAs multiple quantum wells and bulk GaAs," submitted to Phys. Rev. B.

SCIENTIFIC PERSONNEL

H. M. Gibbs

N. Peyghambarian

S. Ovadia (Ph.D. 1985)

K. Tai (Ph.D. 1985)

Y. H. Lee (Ph.D. 1986)

R. Jin

M. E. Warren

A. Chavez-Pirson

J. Morhange, Visiting Scientist, Univ. Paris, 1986.

RESEARCH FINDINGS

Goal

Assess the potential of GaAs etalons for nonlinear decisionmaking for optical signal processing and optical computing. Many improvements have been made and some limitations have been found. Major achievements include ps gating, array fabrication, theory/experiment of bulk GaAs band-edge nonlinearities, and waveguide optical bistability by means of an electronic nonlinearity.

One-Picosecond NOR Gate[1,10,14,17,22,23]

It was demonstrated at ENSTA that a GaAs Fabry-Perot can be shifted in 1 to 3 ps; therefore a logic decision can be made in that time period. Thermally stable NOR-gate operation can be achieved; that is, the NOR gate operates properly regardless of pulse sequence.

Exciton Blue Shift[6,9,12,14,15,18,34]

An intriguing shift to higher energy of the free exciton occurs for high exciton density in superlattices with ≥ 50 Å wells and barriers. At ENSTA, femtosecond time-resolved studies of the exciton blue shift and bleaching were performed as a function of well and barrier thickness with the conclusion that the blue shift is a two-dimensional quantum-well effect and not a superlattice effect.

GaAs Arrays[26,31,41,42,43,48,52,54,55,56,57]

A layer of 1.5-μm-thick undoped GaAs was grown by molecular beam epitaxy over an $\cong 0.2$ μm undoped $Al_{0.4}Ga_{0.6}As$ layer at Cal Tech. The top AlGaAs window was eliminated to enhance surface recombination (in all the previous work, the GaAs layer was grown with AlGaAs layers below and above). An array of 9×9 μm^2 pixels was defined by plasma etching in a freon, helium, and oxygen gas mixture. The array, which consisted of over 100×100 devices, was placed between two partially reflecting mirrors, forming a two-dimensional array of nonlinear etalons. Shown in Fig. 1 is a portion of the array, photographed through a microscope. M. Warren traveled to Cal Tech for instruction in plasma etching of arrays, and he aided T. Venkatesan (visiting Cal Tech from Bell Communications Research) in fabricating the device described above. A plasma etcher (purchased with funds provided by a DOD equipment grant) is now in place at OSC. Different masks have been designed and purchased and used for array, waveguide, and quantum dot fabrication in Tucson.

70
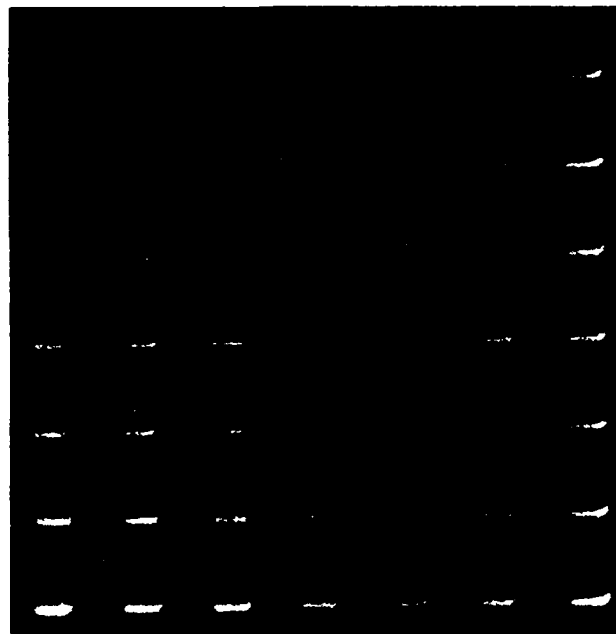
Figure 1   Two-dimensional array of 9×9 µm² pixels prepared by reactive ion etching.

Measurements of the switch-off time of the array were also performed at OSC. The device was studied as an array of optical-logic NOR gates in a pump-probe experiment.   In optical gates, the transmission of a low-intensity probe beam (gate output) is modified by the application of one or two pump beams (input to the gate). Fast recovery time (<200 ps) was observed for a single element of the array at room temperature.   The fast recovery time is attributed to faster surface recombination of carriers at the GaAs-dielectric mirror interface as compared to that at a GaAs-AlGaAs interface.   The streak camera traces of the optical gates for one pixel of the two-dimensional array are shown in Fig. 2.   NOR gate action is also displayed in an arrayless sample that shows a gate recovery time of 300 ps.   The 1-ps switch-on time (reported above for a single GaAs-AlGaAs device) and 200-ps recovery time are the fastest reported for such low-energy nonlinear optical devices.

Bistability has also been observed at 150 K with Nd:YAG-pumped dye pulses of $\cong 10$ ns.   Operation was at relatively low powers ($\cong 5$ mW), but switch-off was not especially fast.

71

ARRAY ARRAYLESS

t (200 ps/div)   t (300 ps/div)
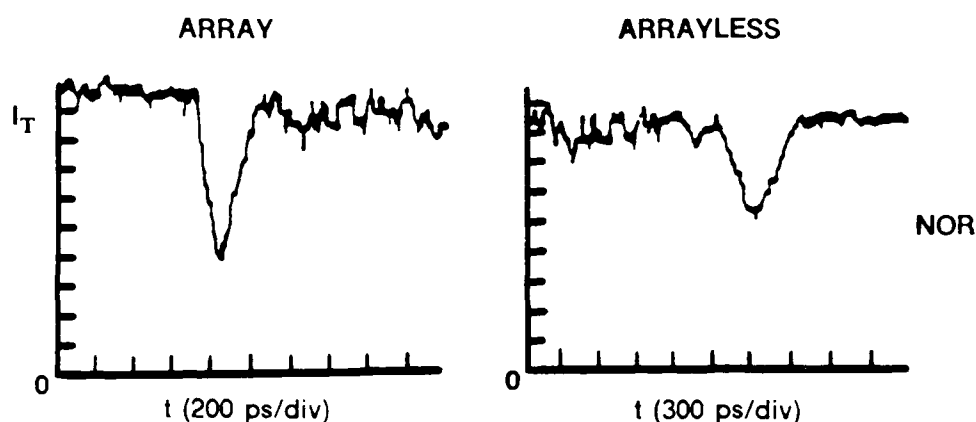
Figure 2. Streak camera trace for NOR gate in GaAs etalon with and without etched array.

Optical-Logic-Gate Recovery Time[27,28,35,47]

Previously described GaAs nonlinear etalon gates have shown 10 to 20 ns (with AlGaAs windows) or $\cong 200$ ps (no top AlGaAs window) recovery time. Proton damage and reduction of the sample thickness to enhance surface recombination have been investigated. Two successive AND gate operations have been performed with a separation of only 70 ps using a 0.3-μm-thick windowless bulk-GaAs etalon: see Fig. 3.
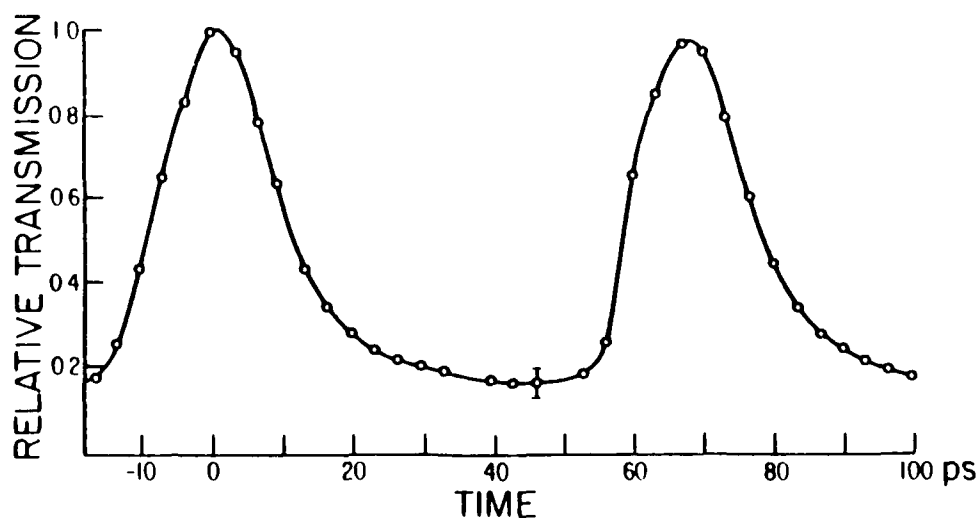
Figure 3. 70-ps cycle time of the 0.3-μm windowless GaAs etalon (20 pJ/input) operated as an AND gate.

72

Gate with Subpicosecond Recovery[30,38,47]

By shining intense light on a multiple-quantum-well sample, it is possible to induce a large blue shift of the excitons through the optical Stark effect. But the wavelength of the light must be in the transparency region to avoid the production of carriers that would give a recovery time of many picoseconds. These experiments, performed at ENSTA, required about 1 pJ/μm^2 (see Fig. 4).
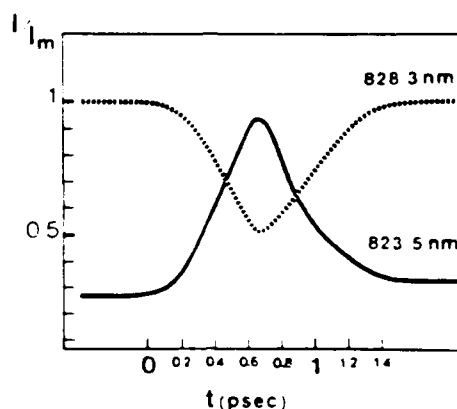
Figure 4. Transmission as a function of time of the etalon at two wavelengths on each wing of the transmission peak. The maximum amplitude has been normalized. Note the incomplete recovery of the high-energy tail.

Direct Measurement of Dispersive Nonlinearities in GaAs[44,46,48]

Nonlinear refractive index changes in GaAs were directly monitored by measuring Fabry-Perot transmission peak shifts. These changes correlate with those obtained by Kramers-Kroning transformations of the nonlinear absorption under identical pumping conditions. The maximum refractive index changes are about -0.06 below the bandgap. Thermal refractive index changes were also measured directly to obtain thermal stability conditions on nonlinear etalon devices based on GaAs.

Room-Temperature Optical Nonlinearities in Bulk GaAs[7,11,21,37,39,40,41,45,48,49,53,55,58]

Quasi-cw pump-probe measurements of room-temperature excitation-dependent absorption spectra of bulk GaAs are reported and compared to the Banyai-Koch plasma theory; see Fig. 5. The good agreement gives some confidence to the theoretical conclusion that band-filling and screening of the continuum-state Coulomb enhancement are the dominant nonlinearities. The absorption change, plus the Kramers-Kronig calculation of the nonlinear index, agrees well with direct measurements made by determining shifts of Fabry-Perot peaks (see preceding subsection). Not only are the results important for understanding band-edge physics, but they will be useful in modeling and optimizing nonlinear devices utilizing these room-temperature nonlinearities; see Fig 6.
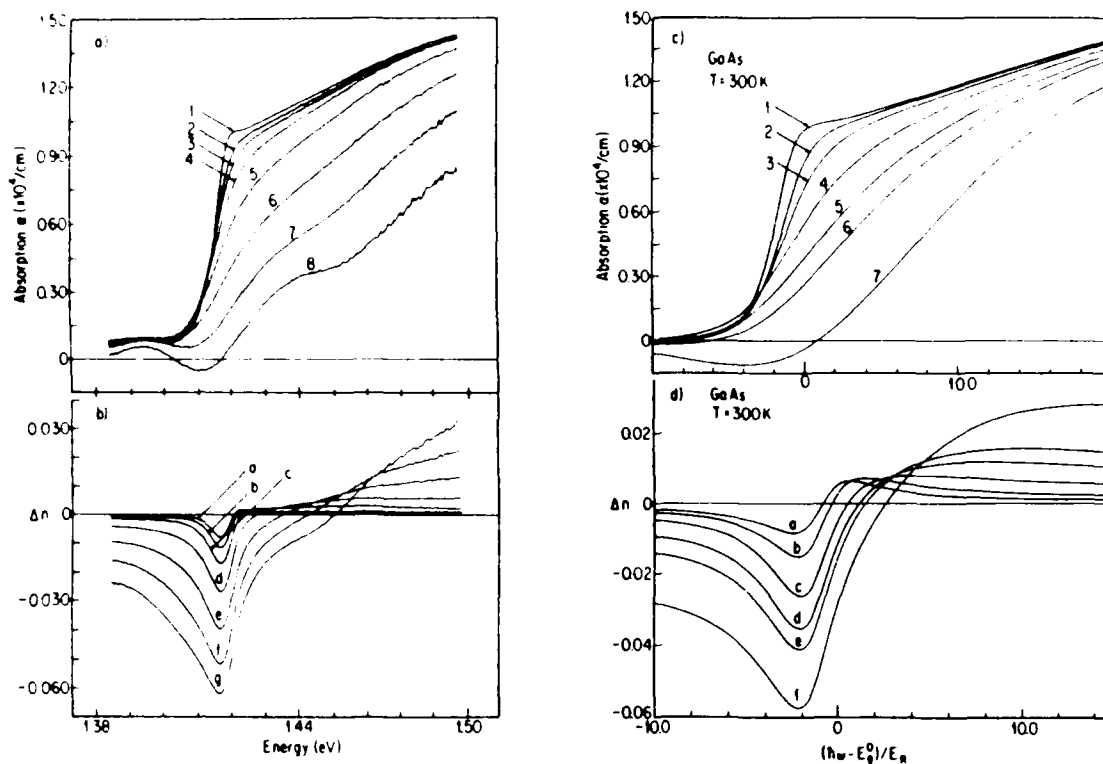
Figure 5. Room-temperature bulk GaAs optical nonlinearities; experiment and theory: (a) experimental absorption spectra for different excitation powers P (mW) - (1) 0; (2) 0.2; (3) 0.5; (4) 1.3; (5) 3.2; (6); 8; (7) 20; (8) 50 on a 15-μm diameter spot; (b) nonlinear refractive index changes corresponding to the measured absorption spectra; the curves (a-g) in Fig. 5(b) are obtained by the Kramers-Kronig transformation of the corresponding experimental data (2-8) in Fig. 1(a); (c) calculated absorption spectra for different electron-hole pair densities N (cm^{-3}) - (1) 10^{15}; (2) 8×10^{16}; (3) 2×10^{17}; (4) 5×10^{17}; (5) 8×10^{17}; (6) 10^{18}; (7) 1.5×10^{18}; E_g^0 = 1.420 eV and E_R = 4.2 meV; (d) calculated nonlinear refractive index changes. The curves (a-f) in Fig. 5(d) are obtained from the curves (2-7) in Fig. 5(c), respectively.
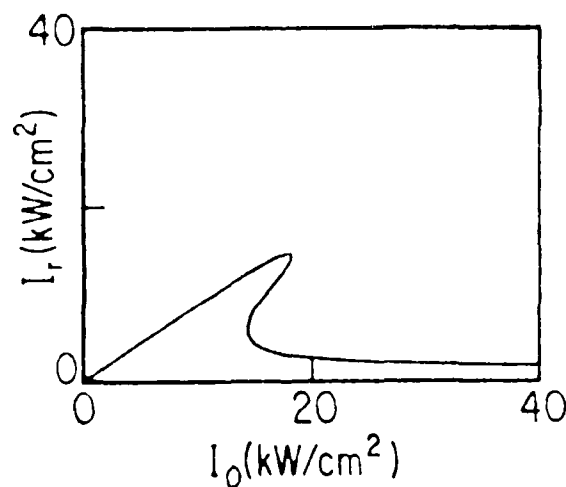
Figure 6. Single-wavelength NOR-gate operation in reflection predicted by computer simulations using the Banyai-Koch plasma theory for the GaAs band-edge nonlinearities.

74

Waveguide Optical Bistability of Electronic Origin[32,50,51,54,55,56,57]

The reactive ion etching research has concentrated on designing and fabricating bulk GaAs and GaAs/AlGaAs multiple-quantum-well (MQW) waveguides and testing their nonlinear properties (see Fig. 7 and Fig. 8). Optical bistability of electronic origin has been observed in strip-loaded waveguides in a GaAs/AlGaAs MQW structure; see Fig. 9. This is an important first step in nonlinear waveguide operation. The addition of a gas channel for use with Cl_2 or BCl_3 was necessary for AlGaAs etching. Future reactive ion etching work will involve fabrication of strip-loaded-waveguide single-channel Fabry-Perots and directional couplers, uniform arrays of nonlinear devices, and quantum-dot structures.
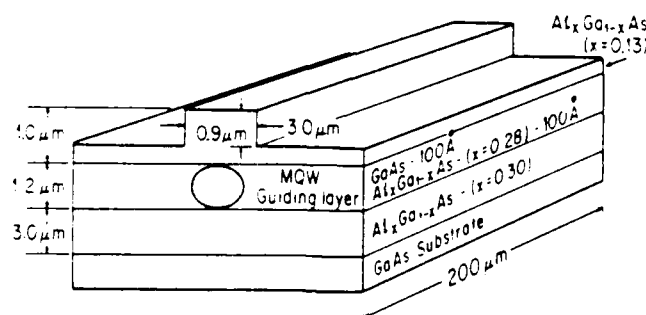
Figure 7. GaAs/AlGaAs MQW strip-loaded waveguide structure.
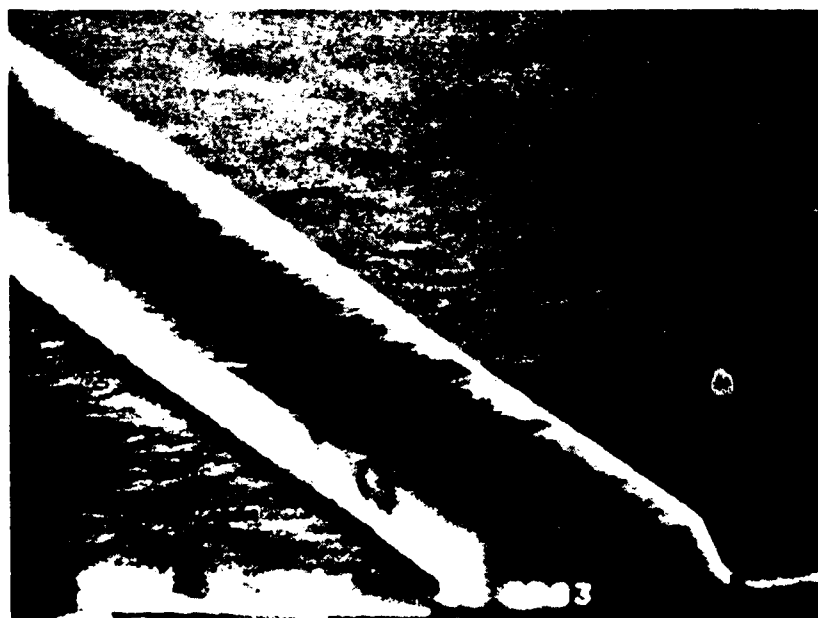
Figure 8. SEM micrograph of strip-loaded waveguide after etching and removal of photoresist layer (some photoresist remains). The scale bar in the micrograph is 5 μm.
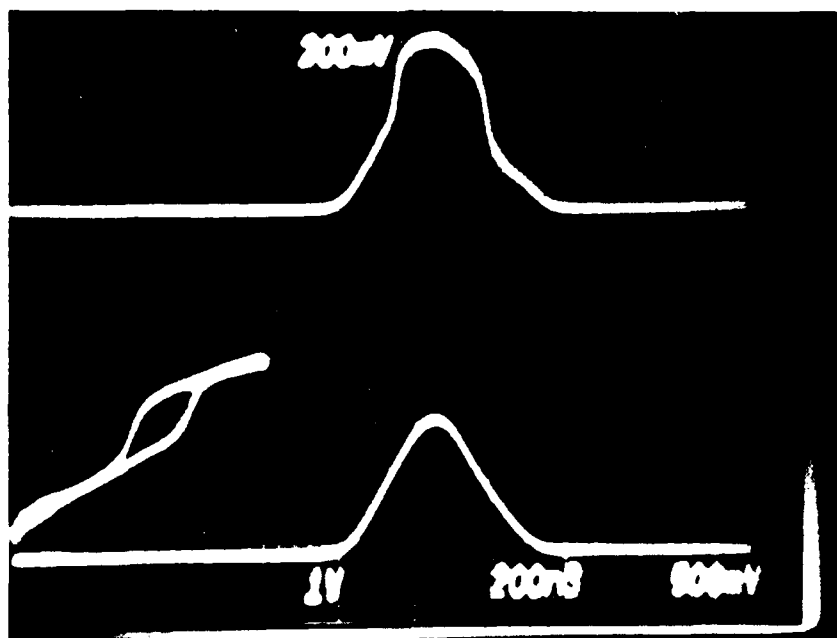
Figure 9. Experimental input-output behavior of a bistable MQW waveguide operating at 867 nm. The upper trace is the output pulse and the lower trace is the input. The trace in the lower left is a plot of output versus input.

OPTICAL NONLINEARITIES OF THIN EVAPORATED FILMS AND COLOR FILTERS

H. M. Gibbs, M. R. Jacobson, H. A. Macleod, and N. Peyghambarian

PUBLICATIONS/REFERENCES

1. G. R. Olbright, N. Peyghambarian, H. M. Gibbs, H. A. Macleod, and F. Van Milligen, "Microsecond room-temperature optical bistability and crosstalk studies in ZnS and ZnSe interference filters with visible light and milliwatt powers." Appl. Phys. Lett. **45**, 1031 (1984).

2. H. M. Gibbs, J. L. Jewell, N. Peyghambarian, M. C. Rushford, K. Tai, S. S. Tarng, D. Weinberger, A. C. Gossard, W. Wiegmann, and T. Venkatesan, "Advances in optical bistability of semiconductors: GaAs-AlGaAs superlattices, bulk GaAs, CuCl, ZnS, ZnSe, and GaSe," Proceedings of the Royal Society Meeting, London (1984); and "Semiconductor Nonlinear Etalons," Phil. Trans. R. Soc. Lond. A **313**, 245 (1984).

3. J. L. Jewell, M. C. Rushford, H. M. Gibbs, and N. Peyghambarian, "Optical logic on a single etalon," Proceedings of the Royal Society Meeting, London, (1984); and J. L. Jewell, M. C. Rushford, H. M. Gibbs, M. Warren, N. Peyghambarian, A. C. Gossard, and W. Wiegmann, "Optical logic on a single etalon," Phil. Trans. R. Soc. Lond. A **313**, 375 (1984).

4. N. Peyghambarian and H. M. Gibbs, "Optical nonlinearity and bistability in semiconductors," invited paper, Proceedings of the International School on Nonlinear Phenomena in Solids, Varna, Bulgaria (1984); and in *Nonlinear Phenomena in Solids*, A. F. Vavrek, ed. (World Scientific Publishing, Singapore, 1984).

5. J. L. Jewell, M. C. Rushford, H. M. Gibbs, and N. Peyghambarian, "Single-etalon optical logic gates," Conference on Lasers and Electro-Optics, IEEE Technical Digest, 184 (1984).

6. H. M. Gibbs, J. L. Jewell, Y. Lee, G. Olbright, S. Ovadia, N. Peyghambarian, M. C. Rushford, M. Warren, and D. A. Weinberger, "Controlling light with light using semiconductor etalons," invited paper, AVP Specialists meeting on Optical Circuit Technology, Munich, West Germany (1984).

7. G. R. Olbright, H. M. Gibbs, H. A. Macleod, N. Peyghambarian, and K. Tai, "Low-power microsecond optical bistability in ZnS interference filters," paper ThF5, OSA Annual Meeting, San Diego, CA (1984).

8. H. M. Gibbs, "Optical bistability and nonlinear optical signal processing," invited paper, LASERS '84, San Francisco, CA (1984).

9. N. Peyghambarian and H. M. Gibbs, "Optical bistability for optical signal processing and computing," invited paper, Opt. Eng. 24, 68 (1985).

10. H. M. Gibbs, G. R. Olbright, N. Peyghambarian, and H. Haug, "Kinks in increasing absorption optical bistability," paper TuM5, Conference on Lasers and Electro-Optics, Technical Digest, IEEE (1985).

11. H. M. Gibbs, G. R. Olbright, N. Peyghambarian, H. E. Schmidt, S. W. Koch, and H. Haug, "Kinks: longitudinal excitation discontinuities in increasing absorption optical bistability," Phys. Rev. A (Rapid Commun.) 32, 692 (1985).

12. H. M. Gibbs, "Central role of thin films in nonlinear optical signal processing," invited paper, paper ThN2, OSA '85.

13. G. R. Olbright, H. M. Gibbs, N. Peyghambarian, H. E. Schmidt, S. W. Koch, and H. Haug, "Longitudinal effects in increasing absorption optical bistability," paper TuA1, OSA Topical Meeting on Optical Bistability, Tucson, AZ (1985).

14. R. Jin, L. Wang, R. W. Sprague, G. R. Olbright, H. Kulcke, G. C. Gigioli, H. M. Gibbs, H. A. Macleod, and N. Peyghambarian, "Simultaneous optical bistable switching of adjacent pixels on a uniform ZnS interference filter," paper MC9, OSA Topical Meeting on Optical Bistability, Tucson, AZ (1985); and R. Jin, L. Wang, R. W. Sprague, H. M. Gibbs, G. C. Gigioli, H. Kulcke, H. A. Macleod, N. Peyghambarian, G. R. Olbright, and M. Warren, "Simultaneous optical bistable switching of adjacent pixels on ZnS and ZnSe interference filters," in *Optical Bistability III*, H. M. Gibbs, P. Mandel, N. Peyghambarian, and S. D. Smith, eds. (Springer-Verlag, Berlin, 1986), p.61.

15. H. M. Gibbs, "Kinks (longitudinal discontinuities) in increasing absorption bistability and Ikeda instabilities in transverse bistability," invited paper, XII National Conference on Coherent and Nonlinear Optics, Moscow (1985).

16. H. M. Gibbs and N. Peyghambarian. "Nonlinear etalons and optical computing," invited paper, SPIE Advanced Institute Series on Hybrid and Optical Computing, Leesburg, VA (1986).

17. H. M. Gibbs. "Approaching the all-optical computer," Optics News 12, 21 (1986).

18. H. M. Gibbs and N. Peyghambarian. "Nonlinear etalons and optical computing," invited paper, U.S.-Japan NSF Workshop on Optoelectronics, Tokyo (1986).

19. H. M. Gibbs and N. Peyghambarian. "Nonlinear etalons and optical computing," invited paper, Proc. SPIE 700, 64 (1986).

20. N. Peyghambarian, H. M. Gibbs, D. Hulin, A. Antonetti, A. Migus, and A. Mysyrowicz, "Overview of optical switching and bistability," Conference on High Speed Electronics, Stockholm (1986).

21. H. M. Gibbs and N. Peyghambarian. "Bistability, gating, and pattern recognition using GaAs etalons and ZnS interference filters," invited paper, OSA'86.

22. R. W. Sprague, G. C. Gigioli, H. M. Chou, M. T. Tsao, L. Wang, R. Jin, H. A. Macleod, and H. M. Gibbs, "Effects of design parameters on ZnS bistable etalons," Proc. SPIE 678, 167 (1986).

23. H. M. Gibbs. "Parallel optical computing and symbolic substitution," Proc. SPIE (1986).

24. M. T. Tsao, L. Wang, R. Jin, R. W. Sprague, G. Gigioli, H. M. Kulcke, Y. D. Li, H. M. Chou, H. M. Gibbs, and N. Peyghambarian. "Symbolic substitution using ZnS interference filters," Opt. Eng. 26, 41 (1987).

25. L. Wang, H. M. Chou, H. M. Gibbs, G. C. Gigioli, G. Khitrova, H-M. Kulcke, R. Jin, H. A. Macleod, N. Peyghambarian, R. W. Sprague, and M. T. Tsao, "Symbolic substitution using ZnS interference filters," Proc. SPIE 752, 14 (1987).

26. H. M. Gibbs. "Two-dimensional arrays of semiconductor optical gates for optical computing," invited paper, Second Topical Meeting on Optical Computing, Lake Tahoe, NV (1987).

27. Galina Khitrova, H. M. Gibbs, and N. Peyghambarian, "Optical computing with nonlinear optics," invited paper, Proceedings of the International Commission for Optics, Quebec (1987).

28. L. Wang, V. Esch, R. Feinleib, L. Zhang, H. M. Chou, R. W. Sprague, H. A. Macleod, G. Khitrova, H. M. Gibbs, K. Wagner, and D. Psaltis, "Interference filters as nonlinear decisionmaking elements for three-spot pattern recognition and associative memories," submitted to Appl. Opt.

29. L. Zhang, R. Jin, G. Khitrova, H. M. Gibbs, C. W. Stirk, and R. A. Athale, "All-optical compare and exchange switches," submitted to J. Lightwave Tech.

SCIENTIFIC PERSONNEL

H. M. Gibbs

M. R. Jacobson

H. A. Macleod

N. Peyghambarian

H. M. Kulcke (M.S. 1986)

R. W. Sprague (M.S. 1987)

D. Hendricks (M.S. 1987)

H. M. Chou (M. S. 1987)

L. Wang

R. Jin

R. Potoff

R. Swenson

RESEARCH FINDINGS

Introduction

The goal of this project was to fabricate ZnS interference filters that were sufficiently uniform to demonstrate optical logic, cascading, fanout, and simple logic circuits with a moderate amount of parallelism. This goal was achieved, but the most impressive demonstrations were made after the termination of JSOP funding for the project.

Growth of Interference Filters[1,7]

An Edwards 24-in. box coater, a venerable system that required considerable work to recommission, was made to operate reliably. About 25 runs were made with this system in the process of optimizing the narrowband filters that incorporate the ZnS and ZnSe. These narrowband filters consist of 17 layers with the following design:

$$\text{Air} \mid [HL]^4 \text{ HHHH } [LH]^4 \mid \text{Substrate}$$

where H denotes a high-index quarterwave optical thickness of ZnS or ZnSe and L denotes a low-index quarterwave of chiolite ($5(NaF) \cdot 3(AlF_3)$). The exponents indicate that the sequence in the square brackets is repeated four times, and the four H layers in the middle represent one full-wave layer, the spacer layer. The substrates were 2-in. squares of glass.

Optical and quartz crystal monitors controlled the thickness. For the ZnSe films, the source for the optical monitor was a HeNe laser at 6328 Å. For the ZnS films, an optical fiber carried a beam of laser light at 5145 Å from another lab. The base pressure for the chamber was about 3.5×10^{-6} torr. Thermal sources with tantalum or molybdenum boats evaporated the zinc chalcogenides, after which the vapor moved 30 cm to the substrates, which were not intentionally heated.

After deposition, the transmittance and reflectance of the coatings were measured on a Cary 14 spectrophotometer.

Switching Power versus Spacer Thickness[22]

The goal was to determine the effect of cavity length on the optical performance, particularly the minimum power and detuning. Keeping the finesse of the cavity constant, the order number, m, which is the number of halfwaves in the cavity, was varied. Cavities of 1, 2, 3, 4, and 6 halfwaves of optical thickness with a design wavelength of 514.5 nm were produced.

The filters were deposited at ambient temperature using an Airco-Temescal Supersource electron beam gun operating at 9.6 kV. The optical monitor used an air-cooled Ar^+ ($\cong 30$ mW) laser as the light source. The simple rotating substrate holder was a flat plate in which the center substrate was directly monitored.

The films were sealed by cementing a coverslip with Norland 61 cement and cured for 24 hours under mild UV irradiation. This procedure retards moisture penetration and subsequent drift and degradation of the filter. Both the substrate and the coverslip were 50×50 mm Kodak slide cover glasses.

The linear, low-power characteristics of the sample were then determined with a Cary 14 spectrophotometer. By sampling various locations, the transmittance uniformity of the filter was determined. Figure 1 shows a typical transmission curve

for two locations on a filter separated by 10 mm. The peak transmittance is adequate, but less variation in the passband wavelength would be required for simultaneous operation of a large number of spots.
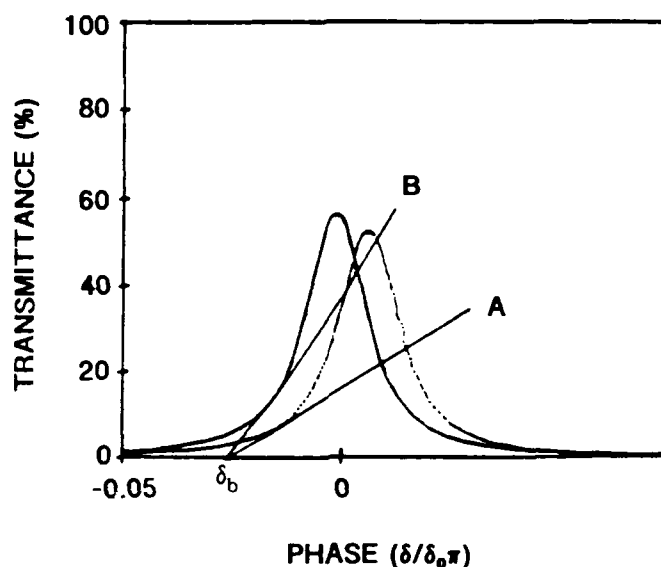

Figure 1. Transmittance peak measured at two points separated by 10 mm. $\delta_0 = m\pi$ is the phase thickness of the spacer. If straight line A is the maximum-irradiance load line, then δ_b is the maximum initial detuning for bistable operation on the spot with the right-hand transmittance curve. The spot with the left-hand transmittance curve will switch on with a much lower I_i, corresponding to the slope of load-line B.

The nonlinear experiment consisted of tuning the filter off resonance by roughly the halfwidth (FWHM) of the filter. The output intensity as a function of the input was then obtained for several locations. The beam from an argon-ion laser (2 W total output) is modulated either with an A-O modulator or a rotating halfwave plate, and has a spot size of roughly 50 μm at the bistable filter

Figure 2 is the observed minimum power in our experiments compared to the predicted power. There is qualitative agreement in the shapes of the two curves, which appear to converge for thicker cavities. Observed minimum threshold values are consistently smaller, by a factor of approximately 1/2, than the threshold prediction for an optimum cavity.
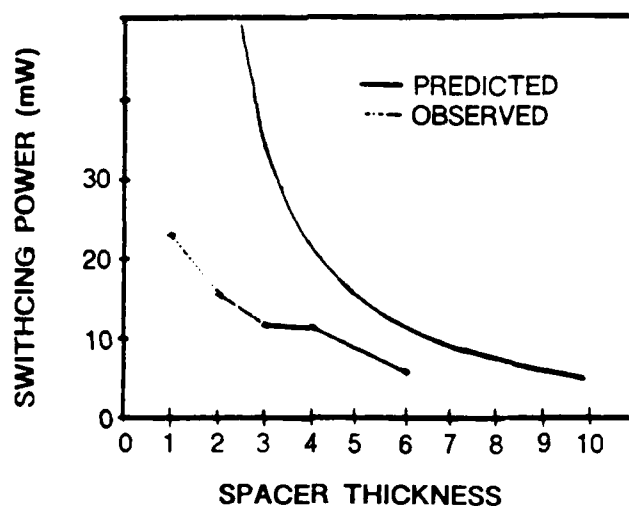
Figure 2. Predicted and observed threshold power as a function of spacer thickness in halfwaves.

Parallel Operation[14]

The filters showed constant operating characteristics for optical bistability over a 4 cm² area. The variation in switch-on time and intensity was less than 25% over 4 cm². The location of the transmission peak was within half of the instrument width over this area, as shown in Fig. 3.

Two-dimensional arrays of a large number of pixels have been envisioned to operate simultaneously in a parallel-processing device. Optical combinatorial logic, processor-to-processor communications, and crossbar interconnection are only a few of the possible parallel operations that can be addressed by a two-dimensional pixel array. Here attention was concentrated on 5145-Å ZnS interference filters because large Ar lasers with cw power in excess of 10 W are available, thus facilitating large-array processing. The array is defined here by dividing the beam and focusing on small areas on the device. Simultaneous switching of multiple pixels on the ZnS filter has been demonstrated using a fly-eye lens array. In the first experiment, three pixels were defined by illuminating three 8-mm focal length lenses cemented into an equilateral triangle geometry with 3-mm center-to-center separation, producing simultaneous bistable operation, as shown in Fig. 4.
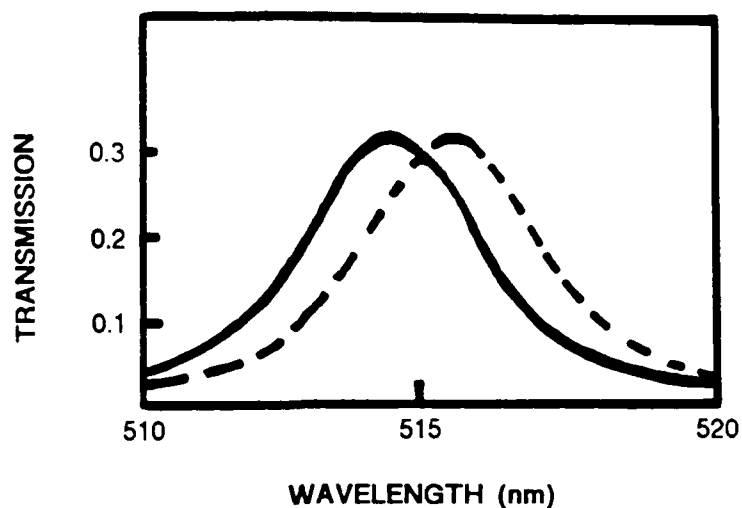
Figure 3. Spectrometer traces for two locations on a nearly uniform ZnS interference filter. Solid line for the center of a filter and dashed line for 20-mm radial displacement from center showing less than 12 Å shift in peak transmissions.
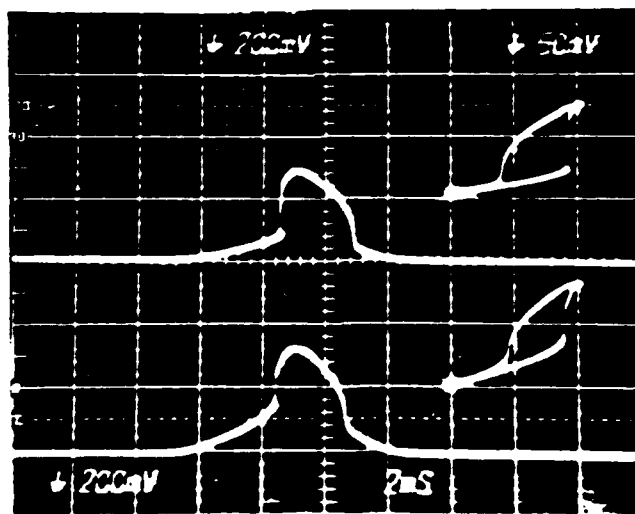

Figure 4. Simultaneous bistable operation of identical inputs separated by 3 mm on a ZnS interference filter.

First Observation of Kinks using Thermal Nonlinearity in a Color Filter[10],[11],[13],[15]

Because of the local nature of increasing absorption bistability (i.e., external feedback is not necessary), it is possible to observe partial sample switching in the propagation direction. If the input is ramped on, the discontinuity between the front

84

"off" portion and the remaining "on" portion jumps deeper and deeper into the filter (see Fig. 5). Color filters consist of semiconductor crystallites ($\cong 100$ to 1000 Å in size) embedded in glass in a concentration low enough that millimeter distances are needed for $\alpha L \cong 1$, compared with micrometers for pure crystals. Thermal kinks would be difficult to see in pure crystals because longitudinal conduction switches the whole sample simultaneously.
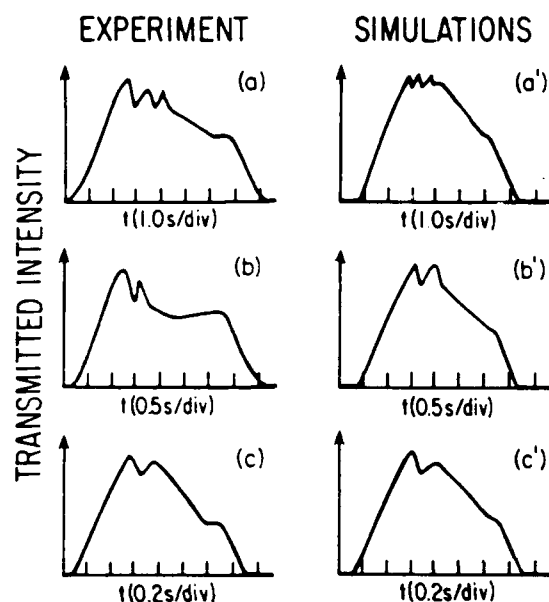

EXPERIMENT   SIMULATIONS

Figure 5. (a)-(c): Experimental kinks in a Corning CS3-70/No. 3384 sharp-cut color filter of thickness $L \cong 2$ mm for the same peak intensity. The rise time of the triangular input pulse is decreased from (a) to (c). (a')-(c'): Numerically calculated normalized $I_I(t)$ and $I_T(t)$ for three different values of $\Delta t / \tau$: (a') 350, (b') 175, and (c') 70. The thickness of $CdZn_xS_{1-x}$ is taken as 2.5 μm.

Interference Filter Optical-Bistability Demonstration[14]

A demonstration was constructed and operated at the OSA Topical Meeting on Optical Bistability (OB3) held in Tucson, on December 2-4, 1985. The demonstration consisted of an interference filter, air-cooled argon laser, and the optics required to permit visual observation of bistability as the input intensity was ramped up and down over a time span of a few seconds. The exhibit was a success, particularly as an explanation of bistability for the uninitiated.

Pattern Recognition[19]

A ZnS interference filter was used as an AND gate array for identifying the occurrences of two adjacent bright spots horizontally in an arbitrary 2×3 input array. The basic concept is define six input beams with a lens array, insert a mask to block

85

as many of those beams as desired, split the beams into two sets, shift one set right one position horizontally, and recombine them on an AND gate, as shown in Fig. 6. The output of the AND gate has a bright spot only if that spot received light from both the unshifted and shifted sets, so a bright spot appears on the right-hand spot of an adjacent pair. This simple pattern recognition was demonstrated at OB3 and emphasized parallelism (in contrast to the serial implementation of electronic analogs developed at Heriot-Watt).
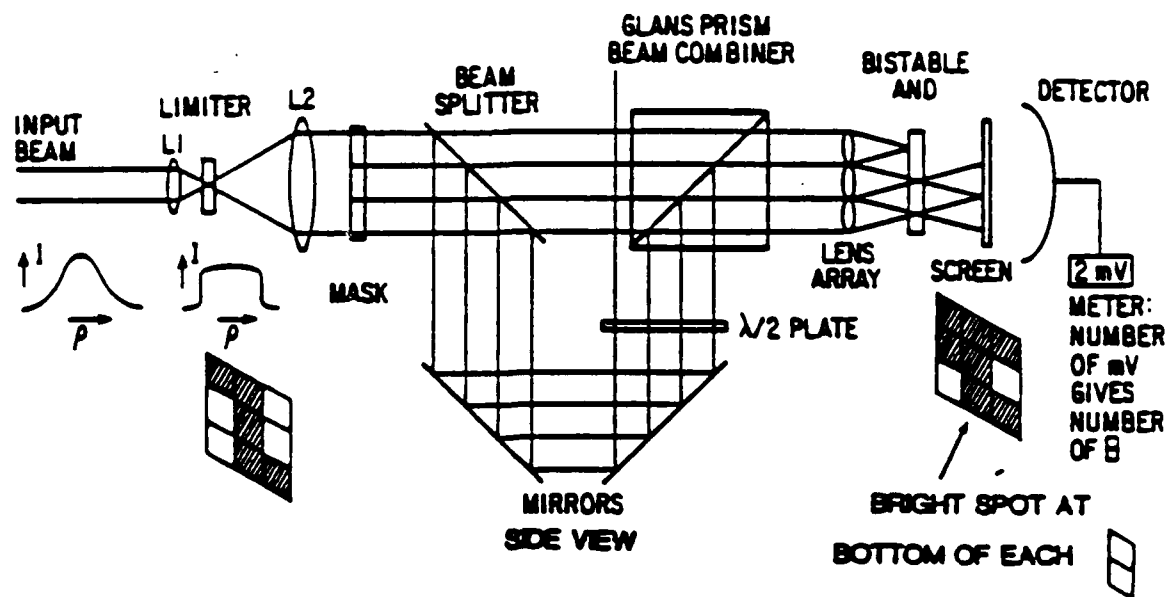
Figure 6. Pattern recognition.

Symbolic Substitution[23]

Alan Huang has shown that computations can be made by recognizing simple patterns and substituting other simple patterns. The first step is recognition of the occurrence of in an arbitrary 2×2 input (technique described above) and substituted if present and if absent as shown in Fig. 7. ZnS interference filters were used with 40 to 45 mW power switch-up; a 2 mW input then yielded an 8 mW change in output. Thus a fanout of 4 is theoretically possible.
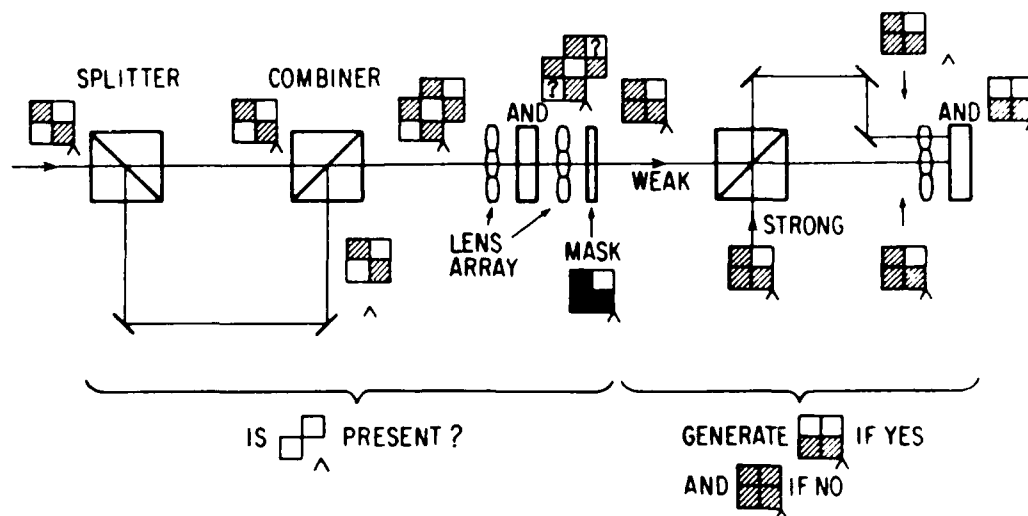
Figure 7. Symbolic substitution.

Conclusion

This project was funded by JSOP for only two years. Following its untimely termination, interference filters were used in several other experiments funded through other sources. These experiments include:

* one-bit addition by symbolic substitution[24,25]
* recognition of a three-spot pattern in a 2×9 input array[28]
* nonlinear decision-making in the correlation plane:
  fingerprint associative memory[28]
* comparison and exchange[29]

and are discussed in several of the publications listed previously.

ULTRASOUND-ASSISTED DEPOSITION OF DIELECTRIC FILMS

C. K. Hwangbo, M. R. Jacobson, H. A. Macleod, and R. H. Potoff

PUBLICATIONS

SCIENTIFIC PERSONNEL

C. K. Hwangbo

M. R. Jacobson

H. A. Macleod

R. H. Potoff

R. Swenson

RESEARCH FINDINGS

Introduction

Physical-vapor-deposited (PVD) optical thin films are often columnar and porous rather than solid and homogeneous and the shortcomings in performance of these films are largely caused by this microstructure. As a result, many new deposition techniques have been developed. In particular, mechanisms that increase the mobility of adatoms and admolecules have been shown to increase the packing density of thin films, which in turn inhibits the penetration of moisture. Direct radiant heating of substrates is one simple and effective means of mobilizing adatoms and admolecules, but it is limited by the ability of the substrate to endure high temperatures. Ion-assisted deposition has substanially improved the optical properties of several dielectric materials. Ultrasound irradiation is another means of directing energy to adatoms and admolecules. This project has shown that the vibration of the substrate transverse to the direction of columnar growth disturbs the growing columns and increases the packing density and homogeneity of the films.

Results

Films were produced at 2×10^{-6} torr in a Balzers 510 plant by resistive sources or electron-beam guns. An optical monitor measured film thickness and a quartz crystal

monitor measured evaporation rate. The glass or fused-silica substrates were glued to one end of a tubular piezoelectric transducer, to which a sine wave was applied. The transducer is tubular to permit transmission measurements without demounting the substrate. Radiative heating of substrates, with and without ultrasonic waves, was also performed to distinguish between purely thermal and ultrasonic wave effects. The film transmittance was measured on a Cary 14 spectrophotometer, and the optical constants calculated using Manifacier's method, which assumes that the film is homogeneous and weakly absorbing. To determine changes in the packing densities of coatings, metal-dielectric filters were employed to detect the vacuum-to-air shifts of their peak wavelengths. X-ray diffraction, Nomarski microscopy, and controlled temperature/humidity tests were performed to characterize film structure, texture, and durability.

In the following sections, findings for zirconium oxide, tantalum oxide, magnesium fluoride, and cerium oxide films are reported. The subscript x in the chemical formulae signifies uncertainty regarding the exact stoichiometry of the material. The acronyms CD, IAD, and UAD denote conventional deposition, ion-assisted deposition, and ultrasonically-assisted deposition, respectively, while T_s denotes substrate temperature.
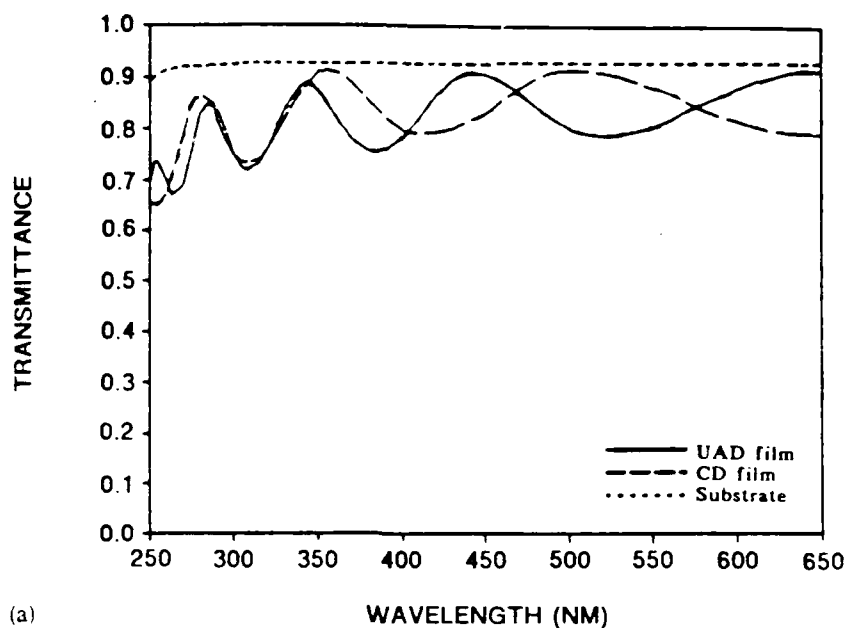
ZrO_x Films

Several ZrO_x single-layer films were deposited at ambient temperature and ultrasonic power densities of 30 W/cm² at 4.5 MHz. These films exhibited about 3% absorption in the UV (200 to 400 nm), as shown in Fig. 1a. For UAD films made at T_s = 150°C, and similar ultrasonic conditions, absorption increased to 88% in the UV and 3% in the visible (400 to 650 nm), as displayed in Fig. 1b. In both cases, the CD films did not absorb significantly. These effects, similar to those observed for IAD films under similar conditions, may be the result of a threshold effect, where conventional thermal heating of the 150°C substrates mobilizes the adatoms until they are more responsive to the additional energy input (in this case ultrasonic agitation).

Of course, UV absorption may not be desirable for many coating applications, so this effect was investigated further. Oxide films often absorb because of a lack of oxygen, and to determine if this caused the observed absorption in the UAD films, both the UAD and the CD films were baked in air at 400°C for 30 minutes, and their transmittances then remeasured. The T value of the UAD films increased to the levels of the CD films, while the T of the CD films were unchanged. Moreover, the k values of the UAD films fell from 1.3×10^{-3} to 1.9×10^{-4} after baking. This test

88

provided clear evidence that the enhanced UV absorption of the UAD ZrO_x films was caused by oxygen deficiency induced by the ultrasonic agitation. For this and other materials, reactive evaporation in oxygen can compensate for these deficiencies. Evaluation of the optimum oxygen pressure in the 1.2×10^{-5} to 10×10^{-5} torr range was attempted, but at present there are no reliable results.

(a)
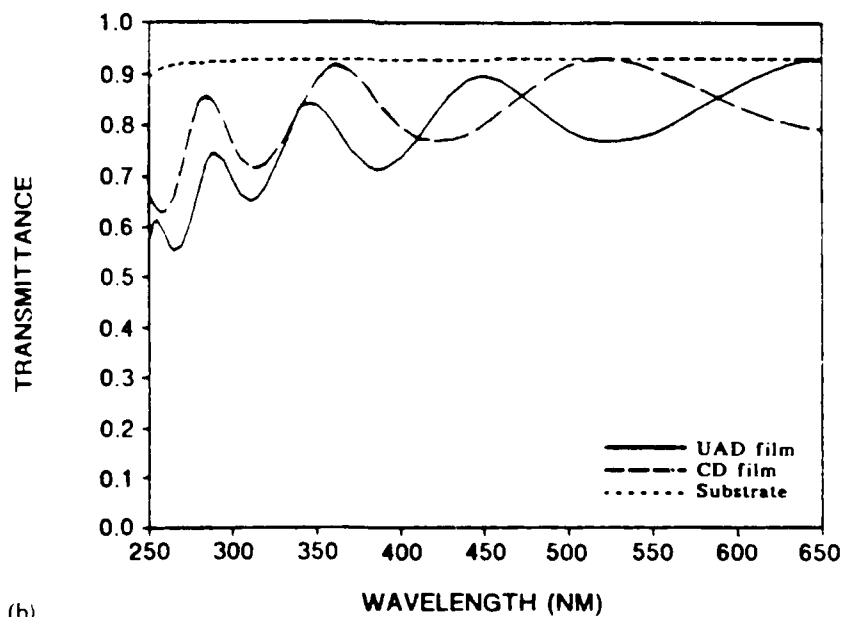
(b)

Figure 1. Transmittance of UAD and CD ZrO_x films at (a) ambient T_s and (b) $T_s = 150^oC$.

89

X-ray diffraction analysis indicated that both the UAD and CD films made with T_s at ambient temperature and at 150°C were amorphous. Since other workers have shown that ZrO_2 films display crystalline structures when deposited above $T_s = 300$°C, the conclusion here is that the ultrasonic wave energy is not enough to crystallize the amorphous structure.

As stated, film porosity can be gauged by the direct effect of water absorption on the optical performance of the film. Single layers, approximately 4500 Å thick, have fringe shifts of 2.5% and 2.7% for UAD and CD films, respectively. Several Ag-ZrO_x-Ag filters were made to determine the vacuum-to-air shift more accurately. In these filters, the silver has a geometrical thickness of 470 Å, while the optical thickness of the ZrO_x is $1.3\lambda_0$ at $\lambda_0 = 4500$ Å. The resulting vacuum-to-air shifts of the peak transmittance wavelength, λ_p are 3.32% and 5.10% for the UAD and CD films, respectively (see Figs. 2a and 2b). The effect of Ag on the peak shift is negligible, because the phase change between the λ_p values in air and in vacuum is less than 3 degrees.
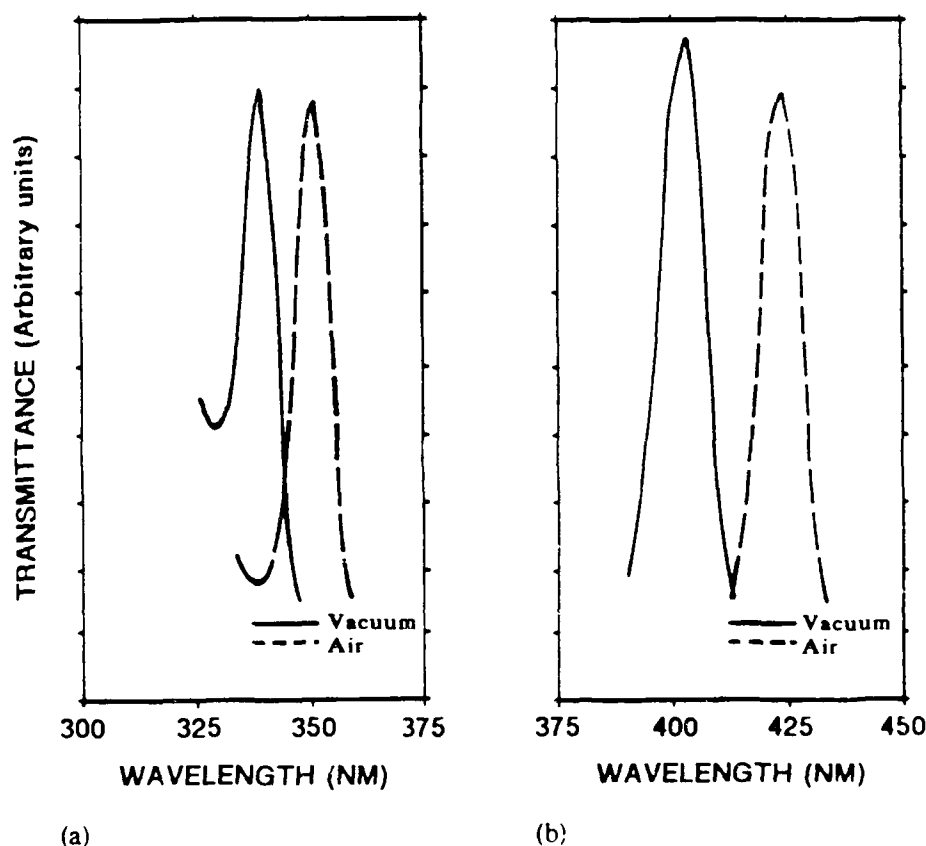

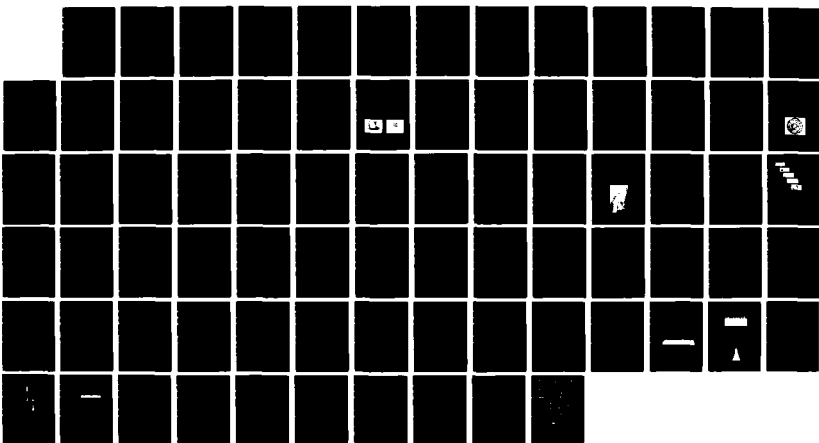Figure 2. *Vacuum-to-air shift of* λ_p *for a* Ag-ZrO_x-Ag *filter* *(a) UAD* *(b) CD.*

MICROCOPY RESOLUTION TEST CHART

NATIONAL BUREAU OF STANDARDS 1963-A
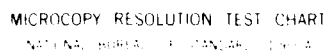
The packing density, p, of the film can be derived from the magnitude of the vacuum-to-air shift of the peak wavelength and the equation

$$n_f = (1 - p)n_w + pn_b \; ,$$

where n_f is the refractive index of the film in air, n_w is the refractive index of water, and n_b is the refractive index of bulk material, assuming that the film pores are filled with liquid water. If we assume that n_b is the same in air and in vacuum, p is approximately

$$p = 1 - 3n_f\Delta\lambda_p/\lambda_p \; .$$

From the above relations, the pairing densities of UAD and CD films are 0.808 and 0.694 respectively.

No significant differences between UAD and CD films were noted by Nomarski microscopy, nor by durability testing, under elevated temperature (50°C) and relative humidity (94%). The durability tests indicate that UAD does not enhance film stability under environmental stress.

TaO_x Films

Effects similar to those noted for ZrO_x were observed for TaO_x films. The lower absorption of the UAD films, however, allowed calculation of optical constants using Manifacier's method. The optical constants of UAD and CD films made at $T_s = 150^\circ$C are shown in Figs. 3a and 3b. The UAD films were subjected to 34 W/cm^2 of ultrasonic energy at 4.5 MHz. While n increased by 0.05 for UAD films, a helpful development, k for UAD films was double that of their CD counterparts. Again the obvious conclusion is that while UAD slightly increases p, it induces an oxygen deficiency.

When oxygen is bled into the chamber, reaching a pressure of 1.0×10^{-4} torr at ambient temperature, the n and k values of UAD films are found to be still higher than those of CD films, but the n and k values of both films decrease significantly, as depicted in Figs. 4a and 4b. The decrease of n is due to the low value of T_s and the imbalance between the O_2 pressure and the evaporation rate. The ultrasonic wave energy employed is apparently not sufficient to maintain high values of n, compared to the thermal energy associated with high T_s values. The significant reduction of k in UAD films, as compared to CD films, might be caused by the interaction of bled oxygen and ultrasonic vibration. As expected, the backfilled oxygen improves the transmission of UAD films by reducing k, but has little effect on n.

91

The relative vacuum-to-air shifts of UAD and CD $Ag\text{-}TaO_x\text{-}Ag$ filters were 2.3% and 2.6%, respectively. Using the method described above, p values were 0.862 and 0.844 for UAD and CD films. Although the magnitude of this improvement is presently small, larger improvements are expected as the process is optimized.

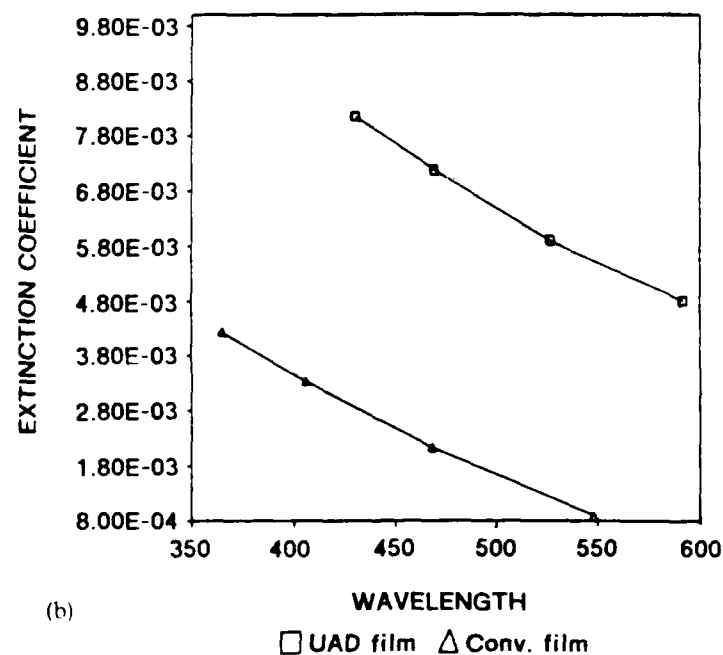
(a)

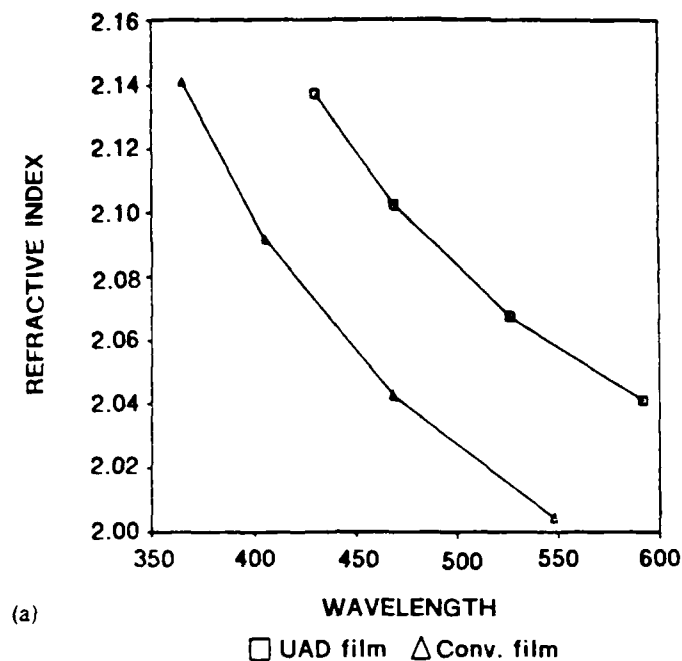□ UAD film △ Conv. film

(b)

□ UAD film △ Conv. film

Figure 3. (a) Refractive indices and (b) extinction coefficients of UAD and CD TaO_x films at $T_s = 150^\circ C$.
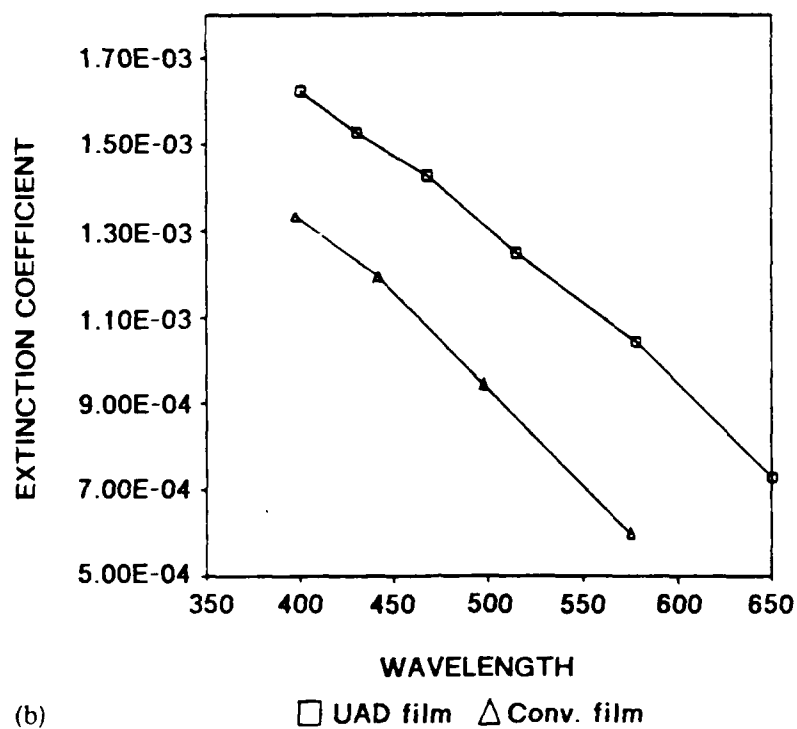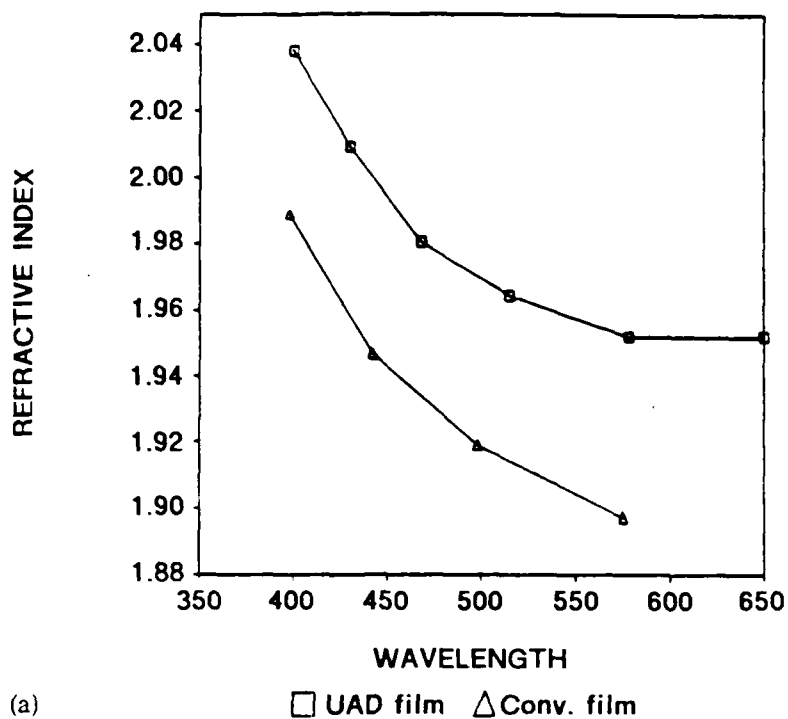
92

Figure 4. (a) Refractive indices and (b) extinction coefficients of UAD and CD TaO_x films at ambient T_s.

MgF_x Films

Single-layer UAD films deposited at ambient T_s showed minor UV absorption, but none in the visible region. At $T_s = 100°C$, strong UV absorption for UAD films appears. CD films did not absorb in either the UV or the visible. (See Figs. 5a and 5b.) This absorption was reversed by annealing the UAD films in air at 400°C for 30 minutes. When UAD films were deposited under an O_2 partial pressure of 2×10^{-5} torr, their absorption decreased somewhat but was still greater than that of CD films. This result agrees with the work of Saxe (1985), who noted that the absorption of MgF_x in the UV is caused by a lack of fluorine; the absorption is decreased by reactive evaporation in oxygen, which satisfies some of the anion vacancies. The optimum oxygen pressure for minimum absorption should be investigated.
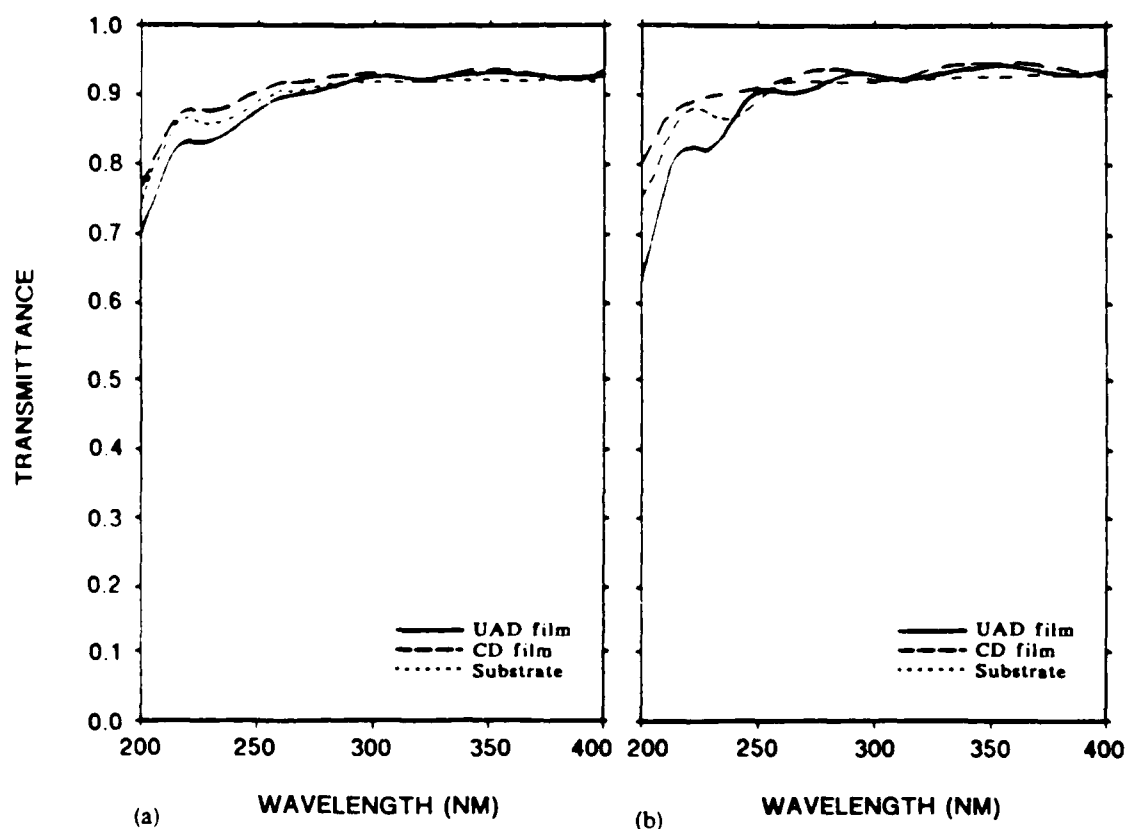

Figure 5. Transmittance of UAD and CD MgF_x films at (a) ambient T_s and (b) $T_s = 150°C$.

A UAD Ag-MgF_x-Ag filter exhibits a 2.19% vacuum-to-air shift of λ_p, significantly less than the 2.91% shift for a CD film. The packing density of UAD and CD films, derived as above, are 0.909 and 0.880, respectively, again showing a

benefit for UAD films. As for ZrO_x films, Nomarski microscopy and elevated temperature/humidity exposure revealed no systematic differences between UAD and CD films. Under X-ray diffraction analysis, UAD and CD films made at ambient temperatures were both amorphous; UAD and CD films made at 150°C showed similar polycrystalline structures. The thermal energy clearly caused the crystallization here; additional experiments to distinguish whether UAD had any effect on the type or degree of crystallization were not performed.

CeO_x Films

Single-layer UAD films deposited at ambient T_s showed no absorption in the visible region. But at T_s = 100°C, the UAD films absorbed about 3%. CD films did not absorb in the visible region. From the similar results of ZrO_x and TaO_x, the absorption is believed to be a result of the oxygen deficiency.

Discussion and Conclusions

Pairs of thin films of three important dielectric materials, deposited both conventionally and under ultrasonic agitation, were compared. At T_s = 150°C, the ultrasonic wave energy produced systematic differences between the films:

1. UAD films displayed increased UV absorption when compared to CD films, an effect attributed to oxygen or fluorine deficiencies. This effect was reversible for ZrO_x and MgF_x films under baking in air. Also, reactive evaporation reduced the observed UV absorption for TaO_x. The finding that this usually troubling absorption can be prevented or reversed enhances the prospects for this coating process.

2. UAD films had systematically higher refractive indices, and thus higher packing densities, than CD films. This preliminary but important development supports the predictions for this process, since increased values of p should eventually lead to improvements in optical performance and durability.

3. No important differences between UAD and CD films were noted by Nomarski microscopy, X-ray diffraction, or by high temperature/humidity testing.

The systematic, consistent nature of these observations on three different materials is encouraging. The lack of enormous changes in structure of these films, which would be detected by microscopy or X-ray diffraction, suggest that UAD may be a more subtle and controllable means of influencing film structure than other

95

methods such as ion-assisted deposition. The latter, while extremely effective for many materials, can significantly damage films if energies or fluxes are slightly too high. Moreover, IAD has rather unpredictable effects on some materials. These results therefore indicate a definite role for UAD along with other means of modifying film structure.

Acknowledgments

WAVEFRONT SENSING AND ADAPTIVE OPTICS

C. Koliopoulos

PUBLICATIONS

K. Freischlad and C. L. Koliopoulos, "A shearing interferometer for astronomical wavefront sensing." Proc. SPIE 627 (1986).

SCIENTIFIC PERSONNEL

C. Koliopoulos

K. Freischlad

RESEARCH FINDINGS

Introduction

The wavefront sensor was redesigned to make it more compact and easier to align. The properties of heterodyning in conjunction with the grating shearing interferometer have been investigated.

New Wavefront Sensor Design

The new design (Fig. 1) is based on the same principles as the previous wavefront sensor design.[1] It still uses only one linear diffraction grating and one detector array. giving it a high light efficiency.

A checkerboard beamsplitter is used to divide the pupil into areas of x-shear and y-shear measurements. depending on the direction of propagation through a loop path containing a Ronchi ruling as the shear producing element. This checkerboard beamsplitter is placed in the dividing plane of a Koester's prism, making the loop path very compact. The Ronchi ruling is now used in transmission. relaxing its alignment requirements.

A laboratory setup of the new wavefront sensor is almost completed; only the Koester's prism with the checkerboard mask remains to be fabricated.

Analysis of Heterodyne Procedures

The Ronchi ruling in the wavefront sensor generates multiple beam interference patterns.[2] Heterodyning with an integrated bucket technique will then produce a

97
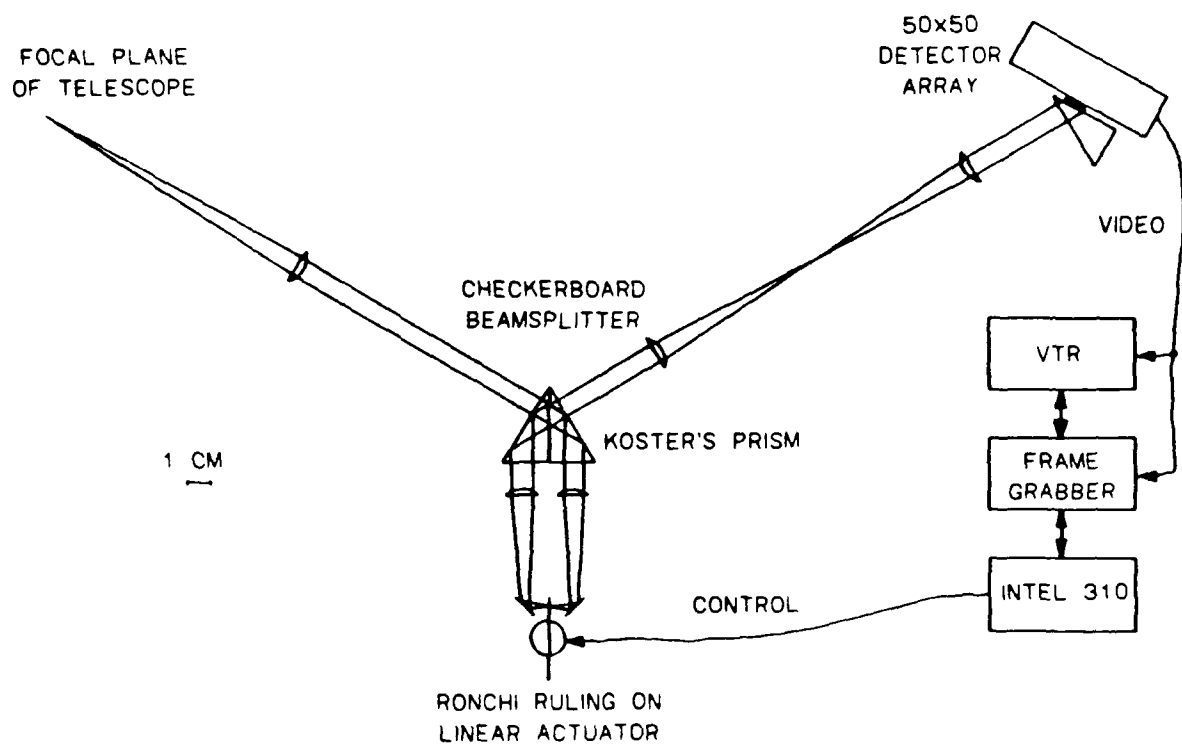
Figure 1. New wavefront sensor design.

systematic error in the phase measurement. This error will be smaller than $2\chi/56$.

In addition, the error propagation from noisy intensity data to the calculated phase has been analyzed for various heterodyning algorithms and the optimum has been chosen for the wavefront sensor.

REFERENCES

1. C. L. Koliopoulos, "Wavefront sensing of the turbulent atmosphere using a lateral shearing interferometer," JSOP Final Report (1985).

2. C. L. Koliopoulos, "Radial grating lateral shear heterodyne interferometer," Appl. Opt. **19**, 1523 (1980).

DEVELOPMENT OF AN ELECTRICAL-READOUT
X-RAY IMAGING SYSTEM

E. L. Dereniak and H. Roehrig

PUBLICATIONS

E. L. Dereniak, H. Roehrig, M. M. Salcido, D. H. Pommerenig, R. A. Simms, and J. M. Abrahams, "Image intensifiers with electrical readout," presented at the Photoelectronic Imaging Conference, London (1985).

SCIENTIFIC PERSONNEL

E. L. Dereniak

H. Roehrig

M. M. Salcido

RESEARCH FINDINGS

Introduction

Application of digital photoelectronic radiology has been widespread in recent years.[1-5] Figure 1 is a schematic of a typical photoelectronic x-ray imaging system. However, these systems lose spatial resolution because of the optical coupling of the x-ray image intensifier to the video camera tube for electrical readout. The limiting spatial resolution (10% MTF) of a typical x-ray image intensifier in the 9-in. mode is about 3.0 lp/mm, while the limiting spatial resolution of the overall system is only 1.5 lp/mm.
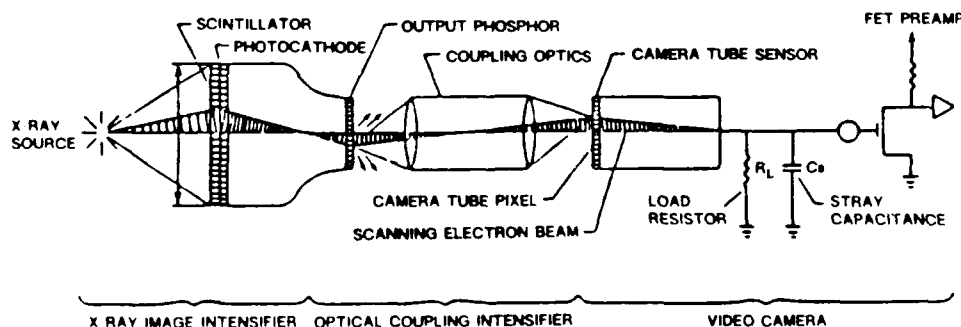
Figure 1. Conventional photoelectronic x-ray imaging system.

99

In addition, use of conventional digital x-ray imaging systems is impeded by their size, weight, and lag (attributable to the electron-beam-scanned video-camera tube and the output phosphor). Replacement of the output phosphor, optical coupling, and video-camera tube by a charge-coupled device (CCD) inside the vacuum envelope of the image intensifier is a possible solution, with benefits that extend beyond medicine to military applications, astronomy, or anywhere data is to be read from a remote image sensor (such as a satellite).

The idea is not new: CCDs and photodiode arrays have been used inside a vacuum envelope for electrical readout of image detectors previously.[6-9] However, in all cases, electron multiplication was at high kinetic energy of the photoelectron, which almost invariably caused damage to the delicate gate structure.[10] The approach investigated here operates the CCD in the charge-injection mode rather than by electron beam bombardment, similar to CCD operation in infrared (IR) hybrid focal plane arrays.[11] A schematic example is shown in Fig. 2.
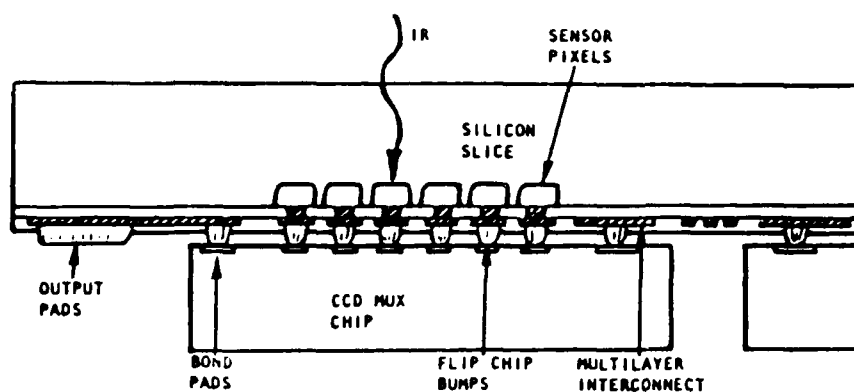
Figure 2. Hybrid silicon focal plane concept with CCD readout.

Methods and Procedures

Three 25-mm second-generation image intensifiers were modified (see Fig. 3). In each tube the output phosphor was replaced by a 100-pin multi-feedthrough header carrying two 32×32 CCDs designed for hybrid IR detectors.[11] Their center-to-center spacing is basically 0.088 mm, providing an area of 2.82×2.82 mm or 7.95 mm². The area of a charge-injection electrode, however, is only 0.025×0.025 mm, so the effective total active area is only 0.64 mm², or 8% of the total array area. The various voltages for clocks, phases, and gates are brought in on the multi-pin feedthroughs (see Fig. 4).

100
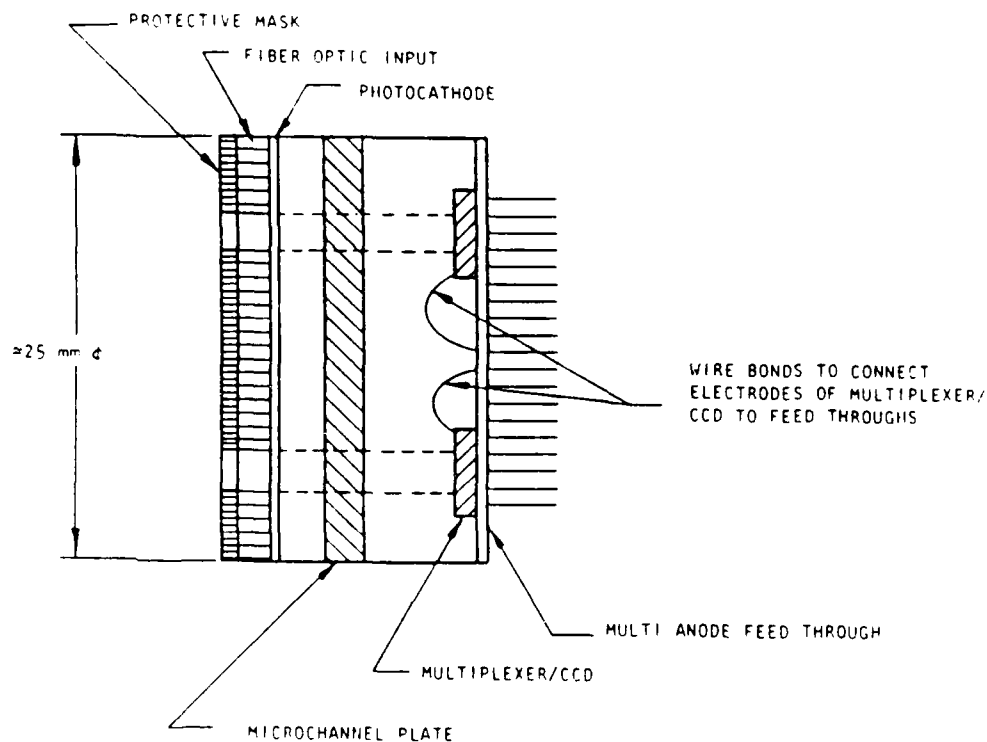
Figure 3. Modified second-generation image intensifier with two CCDs.

Before fabrication of the tubes, several CCDs were subjected to various temperature cycles and schedules, each exceeding those minimally necessary for electron tube production. The temperature levels ranged from 250°C to 300°C. The baking periods ranged from 6 to 12 hours. Because of limited resources, no tests were performed at the optimum baking temperature of 375°C. This was not considered critical since this study required only a working tube, and long lifetime was of secondary interest.

The spacing between CCD and microchannel plate (MCP) was a little less than 1 mm and was largely determined by the existence of wire bonds necessary for electrical connections (see Fig. 3). Masks were provided to restrict electron emission from the photocathode to the photocathode area opposite the active areas of the CCDs. This was important for operation of the tube as an imaging detector. The size and location of the apertures were varied on different masks, which permitted analysis of the landing of photoelectrons beyond the cathode locations opposite the CCD under test.

101
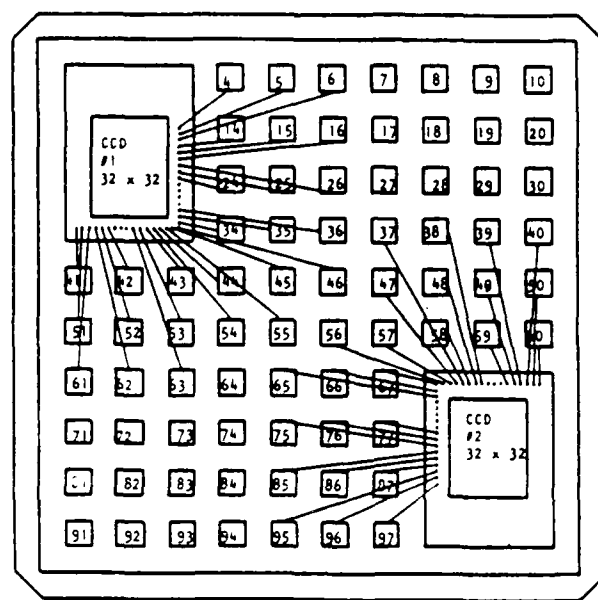
Figure 4. CCD arrays mounted on multi-pin feedthrough.

The tubes were set up with the anode (the CCD) at ground potential, and the cathode at high negative potential. The various voltage levels provided for were:

microchannel plate out: 0 to -200 V

microchannel plate in: -500 to -1100 V

photocathode: -700 to -1300 V

Electron energies at the CCD were never allowed to exceed 200 eV and the voltage from the photocathode to the microchannel plate was maintained at 200 V. Notice that the microchannel plate input was not covered by an ion barrier.

The operation of the tube was monitored in two ways:

1. With all the CCD electrodes shorted and floating, the current landing on all the CCD charge-injection electrodes was measured by inserting an electrometer between the substrate of the particular CCD and the ground, as shown in Fig. 5. Notice that the other (second) CCD was floating, as were all the other unused electrodes of the multi-pin feedthrough; in this mode, no imaging was possible, the CCD acted simply as a single detector.

2. With the CCD operating as an imaging device, the signal voltage developed by pixel 100 was observed.

Illumination was provided by a Gamma-Scientific RS10 standard light source, located about 75 cm from the image tube photocathode, and modified to be a

102
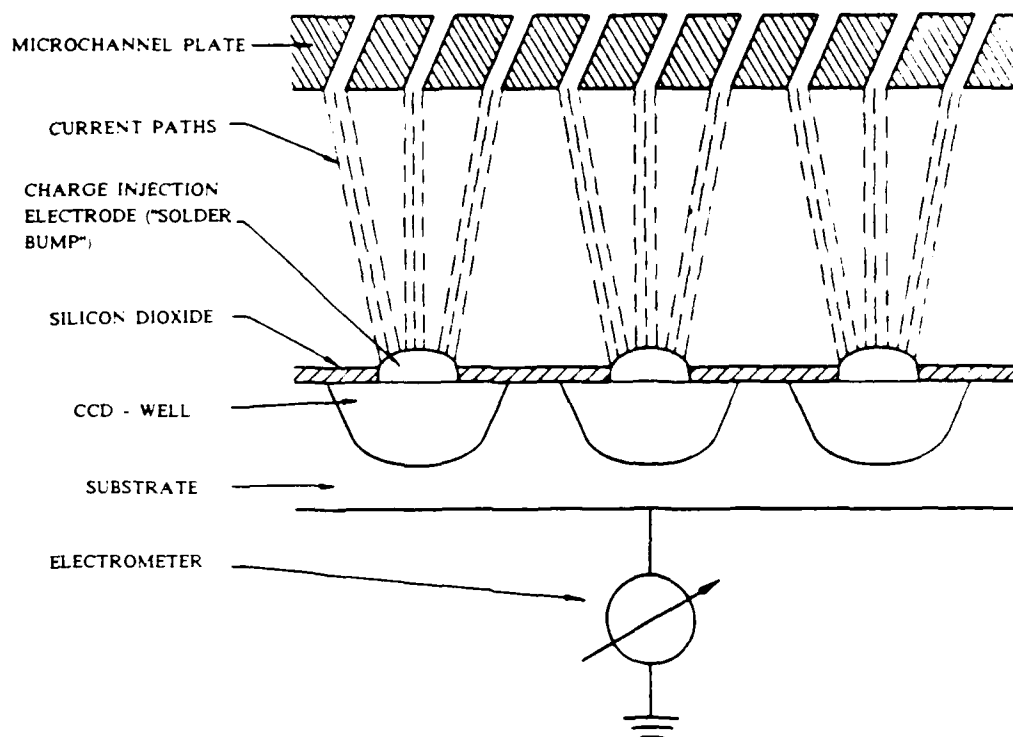
Figure 5. Schematic of charge collection on CCD injection electrodes and measurement of landing current.

variable-illumination source at low levels with a constant color temperature of 2875 K. The illumination was varied by changing the diameter of the aperture from 5 mm to 35 mm. The illumination of the photocathode was obtained from a calibration using an EG&G Radiometer-Photometer 550 in the photometric mode.

Results and Discussion

Tests with individual CCD arrays at various temperature levels to 300°C for up to 12 hours confirm that the CCDs can withstand the minimum temperature levels necessary for image tube fabrication.

Tests showed that electrons land at the CCD. The observed signal is linear with the light intensity on the photocathode and can be easily controlled by variation of the MCP gain. Figure 6 is a plot of the total landing current versus luminous flux at the cathode aperture opposite the CCD. The current was measured with an electrometer in the circuit from CCD substrate to ground, as shown in Fig. 5. The current was measured for four MCP voltages: 800 V, 900 V, 1000 V, and 1100 V.

Notice that the slopes of the four curves, plotted on double log paper, are almost unity. No saturation effects are observed at 1000 V or 1100 V, where the MCP gain is high, which indicates that the cathode response is extremely low. While the response immediately after fabrication of this particular tube was measured to be 137 μA/lm, the response dropped shortly thereafter. Most of the measurements presented here remained between 1 and 2 μA/lm.

(o) 1100 Volts MCP   (x) 1000 Volts MCP
(H) 900 Volts MCP   (•) 800 Volts MCP
Data taken 8/8/85
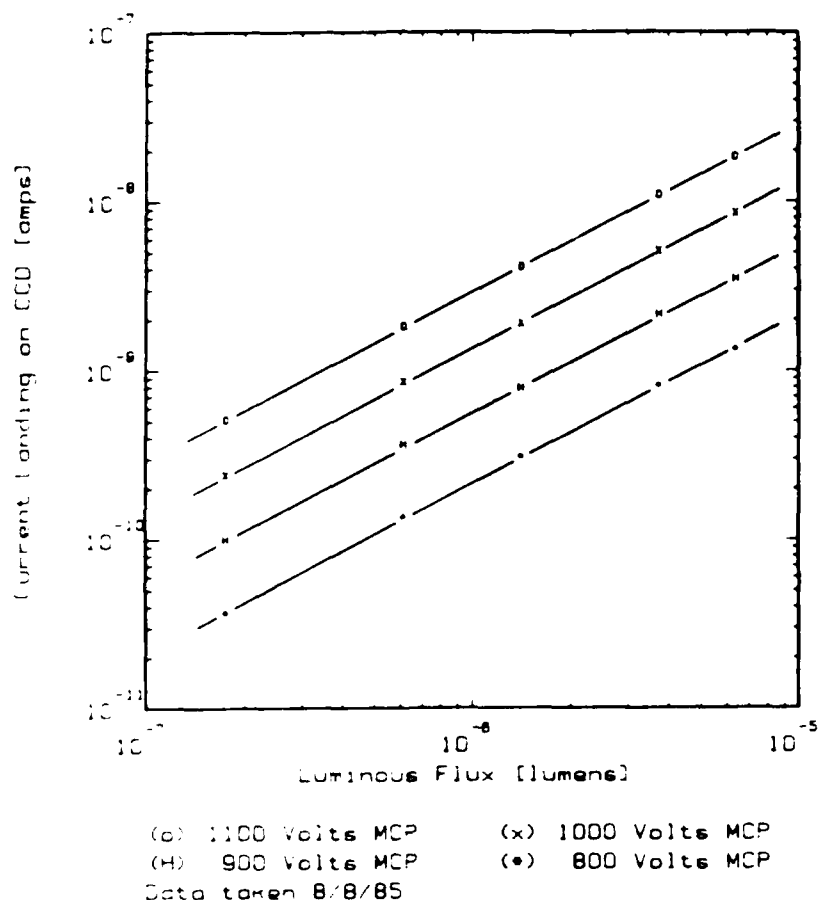
Figure 6   Current landing on CCD versus luminous flux on cathode for four MCP voltages

Similar linearity (with respect to input luminous flux) is observed with the signal as read from pixel number 100 when the CCD is operated as an imaging device (see Fig. 7). Figure 7 also indicates the linearity of the landing current versus the input luminous flux for comparison with Fig. 6. Now, however, the landing current is measured as a voltage drop across a 560-kΩ load resister, which replaced the electrometer in the substrate-to-ground circuit.

104
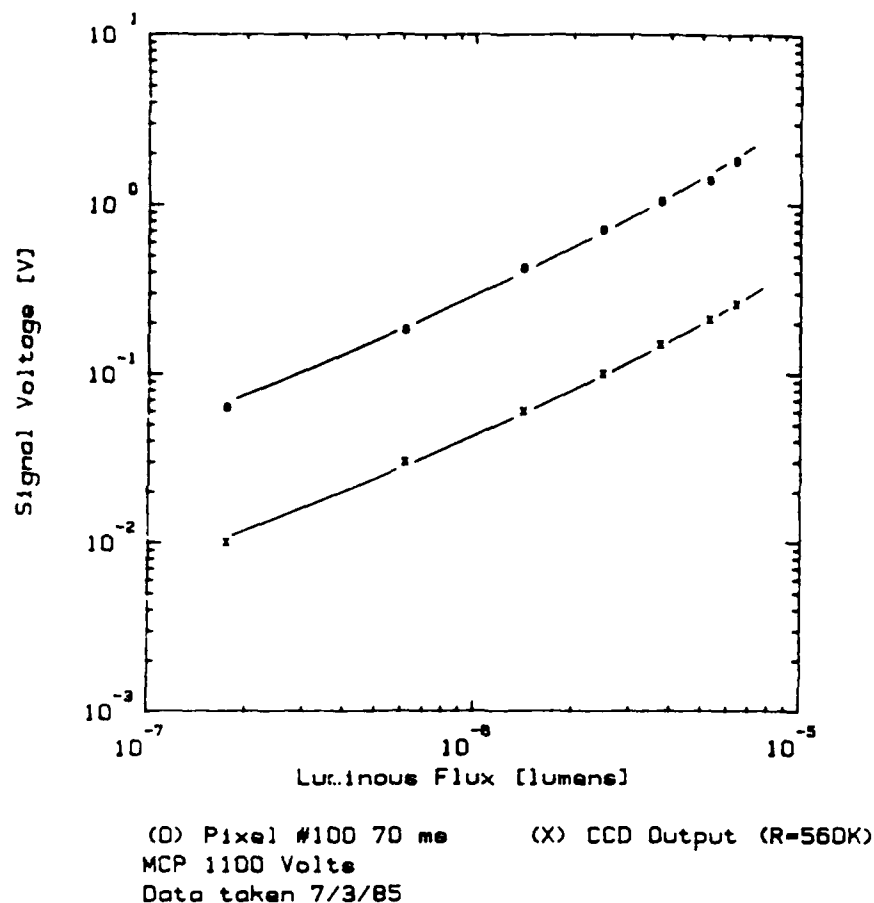
Figure 7. Signal voltage developed by pixel 100 and current landing on CCD (measured as voltage drop across R = 560 kΩ) versus luminous flux on cathode.

There seems to be complete balance of the current, indicating that all current leaving the MCP lands on the charge-injection nodes. This occurs even though their total area is only 8% of the total active area of the CCDs. Attempts to observe charging effects on the insulating SiO_2 surrounding the charge-injection electrodes using moderately fast equipment ($\cong 10^4$ Hz) were not successful.

The dependence of the signal developed by pixel 100 on the integration time for constant luminous flux was also investigated. It is not linear, as shown in Fig. 8. However, this slight deviation from linearity can be related to effects of the dark current. Two curves are presented, one for an MCP voltage of 900 V and one for an MCP voltage of 1100 V. The curves are parallel.

105
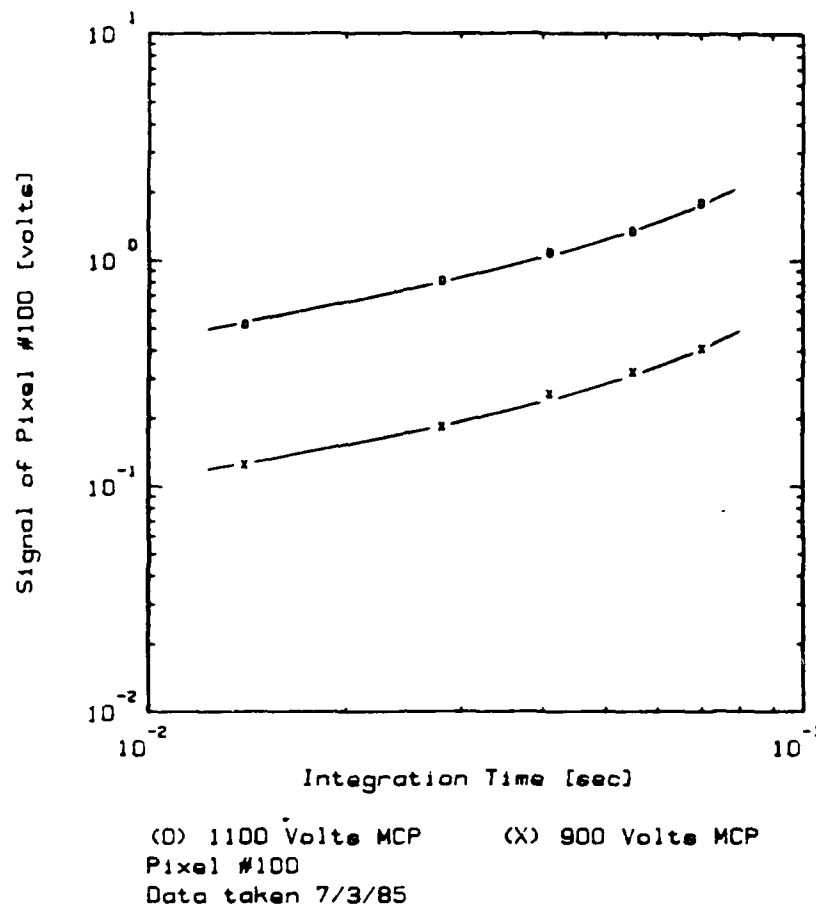
Figure 8. Signal developed by pixel 100 as a function of integration time.

Of particular interest was the dependence of the landing current on the electric field in the space between the anode and the MCP. The measurement was made three times with an MCP voltage of 900 V and the anode-to-MCP out voltage ranged from 15 V to 200 V. The results are shown in Fig. 9. The general shape of the curve follows the normal expectation, namely a gradual increase up to a saturation at around 150 V. However, an indication of two saturation points was apparent, one at approximately 60 V and the other at approximately 150 V. No explanation is available at this time.

To provide some information on the electron paths, the landing current was analyzed as a function of the cathode area, which was illuminated. As shown in Fig. 10, the landing current is slightly superlinear with the illuminated area. This clearly demonstrates that the landing current does not consist solely of electrons originating at the cathode location opposite the CCDs.

106
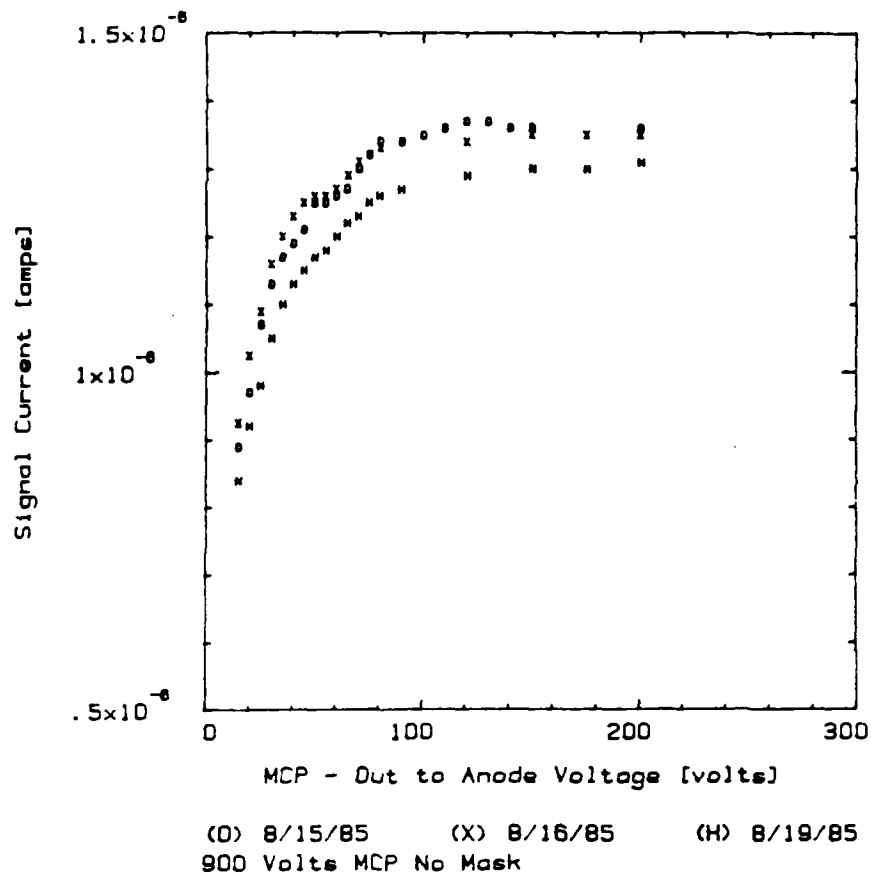
Figure 9. Current landing on CCD versus voltage between CCD and MCP out.

Tube life was also investigated. Figure 11 is a plot of the cathode response versus time in units of days for the first and third tubes. For both tubes, the responsivity dropped. The first tube dropped from 200 μA/lm to 37 μA/lm over a period of 200 days. For the third tube, responsivity dropped from 130 μA/lm to 3 μA/lm over 50 days. It is not clear whether the CCD itself caused the outgassing.

Also of interest was the imaging capability of the tube. From the imaging geometry for proximity focusing (1-mm spacing and 200-V potential), one would not expect more than a few line pairs per millimeter limiting resolution.[12] This was confirmed by the images shown in Fig. 12.

This project succeeded in determining that electrons can land on the charge-injection nodes of CCDs and be used for direct electrical readout. Questions of tube life, optimum processing schedule, and tube and CCD design will be addressed in subsequent projects.

107
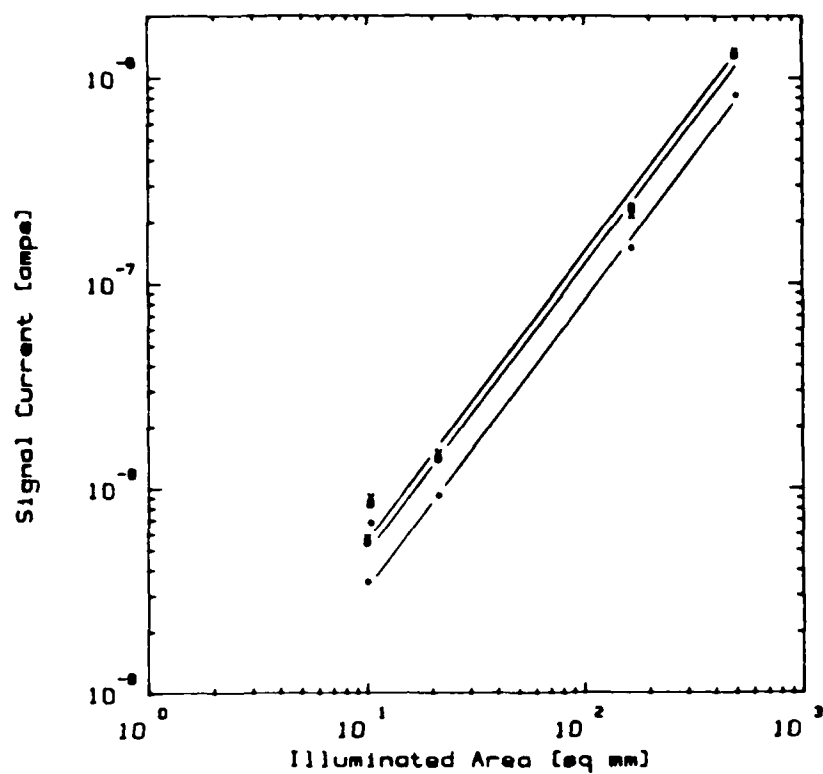
Figure 10. Current landing on CCD as a function of cathode area, illuminated with constant illumination.
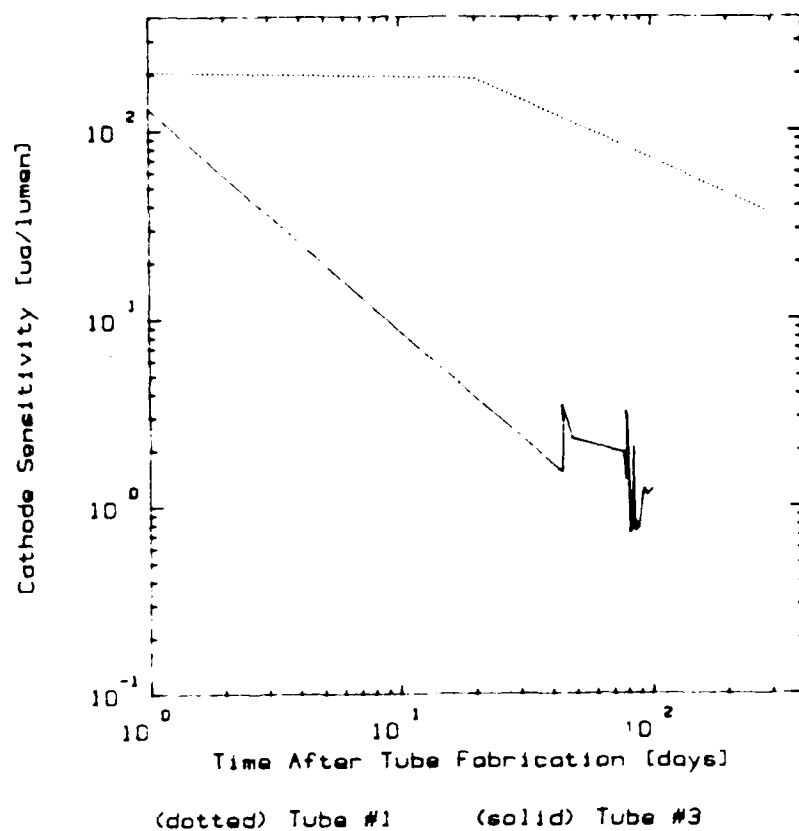
Figure 11. Cathode sensitivity versus time after fabrication.
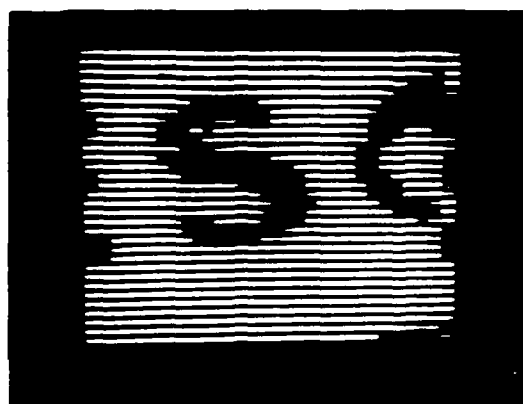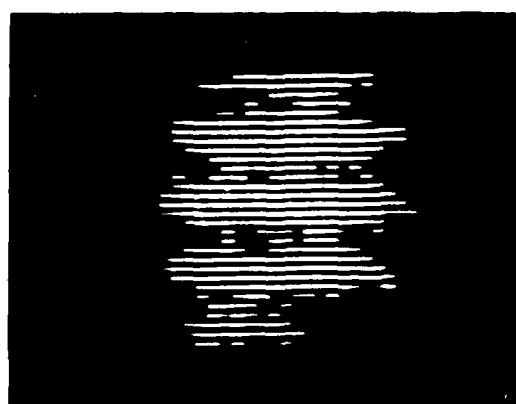
(a)   (b)

Figure 12. Images produced by image tube with electrical readout. (a) test pattern letter "S"; (b) bar pattern at a frequency of about 1 lp/mm.

109

References

1. P. C. Christenson. T. W. Ovitt, H. D. Fisher, M. M. Frost, S. Nudelman, and H. Roehrig, Am. J. Neuroradiol. 1, 379 (1980).

2. M. M. Frost, H. D. Fisher, S. Nudelman, and H. Roehrig, Proc. SPIE 127, 208 (1983).

3. P. H. Heintzen and R. Brennecke, *Digital Imaging in Cardiovascular Radiology* (Thieme-Stratton, New York, 1983).

4. S. Nudelman, "Photoelectronic-digital radiology. Past, present, and future," in *Digital Imaging in Cardiovascular Radiology*, P. H. Heintzen and R. Brennecke, eds. (Thieme-Stuttgart, New York, 1983).

5. B. J. Hillman and J. D. Newell, "Symposium on digital radiography," The Radiologic Clinics of North America, Vol. 23 (1985).

6. J. Lowrance and P. Zucchino, Proc. SPIE 172, 232 (1979).

7. P. Everett et al., "Texas Instruments' virtual phase charge coupled device (CCD) imager operated in the front side electron bombarded mode," Proc. SPIE 331, 151 (1982).

8. J. Chossier, "Recent developments in the use of parallel and self-scanned diode arrays to detect photo electrons," in *Advances in Electronics and Electron Physics*, Vol. 40B, B. L. Morgan, R. W. Airey and D. McMullen, eds. (1976).

9. P. A. Gottshall, "Electro optics and devices," private communication on the RCA-Intensified CCD Model C21205 (1985).

10. Proceedings of the IEEE special issue on the Effects and Uses of Energetic Radiation in Electronic Materials, Vol. 62, 1974.

11. D. H. Pommerenig, T. Meinhardt, and J. Lowe, "Hybrid extrinsic silicon focal plane architecture," Proc. SPIE 244, 9 (1980).

12. E. H. Eberhardt, "Image transfer properties of proximity focused imaging cubes," Appl. Opt. 16, 2127 (1977).

SURFACE FIGURE PROBE

Robert E. Parks

PUBLICATIONS

S. Wong, R. E. Parks, and L. Shao, Proc. SPIE **680**, 62 (1986).

SCIENTIFIC PERSONNEL

R. E. Parks
S. Wong, Student
Genrui Cao, visiting scientist

RESEARCH FINDINGS

Introduction

This task consisted of two principle parts: direct determination of the figure of a ground surface using a floating spherometer; and determination of the wavefront of an optical system from information in the image plane. Because these were fairly disparate tasks, they will be discussed separately.

Spherometer

Background on spherometer

Previous work[1] had shown that it is possible to determine the figure of a ground surface using a spherometer (a device that measures the curvature of a surface) by integrating the curvature data twice. This technique speeds the manufacturing process for aspheric optics because it is difficult to measure the shape of the aspheric surface during the grinding stages of manufacture.

Although the feasibility of determining the figure from spherometer measurements had previously been demonstrated, the process was not in any way optimized for rapid data taking. In the previous method, a bar-type spherometer such as that shown in Fig. 1 was used to take the data. A grid pattern was laid out on the work and the spherometer used to measure the curvature of the surface at the nodes of the grid, first in the x-direction and then the y-direction. While making any single curvature measurement is not a difficult or time-consuming task, the measurement of 100 or more data p ints in two directions is rather painstaking. The

111

goal of this program was to devise a spherometer that could be used more rapidly and to test the new device on a simulated aspheric optic.
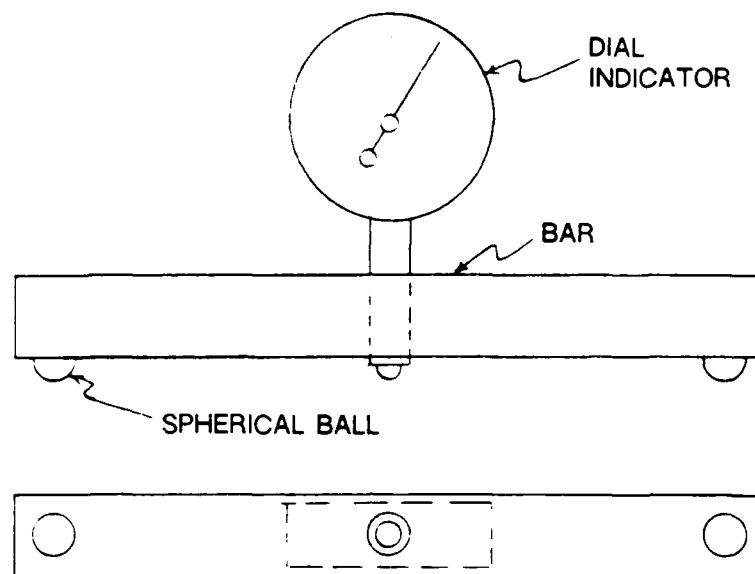
Figure 1. Standard bar-type spherometer.

Spherometer theory

The most usual spherometer is the three-ball type used in optical shops for determination of the radii of lens curves. However, it can be shown that the three-ball spherometer is insensitive to azimuthal variations in surface height about its central probe point, making this type of spherometer unsatisfactory for use in determining the shape of aspheric surfaces.

Since the linear or bar-type spherometer is sensitive to azimuthal variations in surface height, it was natural to examine this type next. However, this type of spherometer is designed to be rocked about its lengthwise dimension to get the maximum (or minimum) reading. It is this rocking of the spherometer that makes data taking with the bar spherometer rather tedious. The operator must be positioned over the work piece with wrists braced on the work in order to rock the spherometer. A smooth rocking motion is necessary because of the sensitivity of the spherometer which can be read to microinches (or tenths of microns).

The goal then was to come up with a spherometer design that would not require the tipping motion to be read accurately and that could be easily positioned about the surface being measured without the need for the operator to remain in

112

close proximity to the instrument. In addition, it was essential that the spherometer not damage the surface as it was moved about.

Since the three-ball spherometer would not work on theoretical grounds, the new design had to be based on the bar-type spherometer. This type normally has balls at either end that serve as reference points and an indicator centered between the balls both longitudinally and laterally. The spherometer thus measures directly the height of the indicator tip relative to the average height of the two balls. This measured height, h, is related to the radius of the work under test by

$$h = (R - r) - \sqrt{(R - r)^2 - y^2} \, ,$$

where y is the distance from the center of a ball to the center of the indicator tip, R is the radius of curvature of the work, and r is the radius of the balls on the spherometer. This expression can be recast to give R as a function of h in the form

$$R = \frac{h^2 + 2rh + y^2}{2h} \, .$$

This expression is the heart of the spherometer technique for determining surface figure.

Floating Spherometer Design

To give the bar spherometer the characteristics necessary to meet the requirements outlined above, it was decided to float the spherometer in a frame supported by three air-bearing pads. Since the entire frame of the spherometer was to float, the end balls in the conventional spherometer could no longer be used and had to be replaced by two additional indicators. The new spherometer is shown in Fig. 2.

To maintain sufficient load-bearing capacity in the air support pads, these pads have to be lapped to the approximate radius of curvature of the part under test. Air is supplied at 15 psi and the pads have a diameter of one inch. This is sufficient for a 5% mismatch between the radius of the work and pads.

The spherometer itself works like the normal bar spherometer except that the end balls are replaced by indicators. The measured sag, or h, is obtained by electronically subtracting the average of the outer two indicator readings from the reading of the central indicator. The new spherometer reads

$$h = \left[\frac{z_1 + z_2}{2} \right] - z_3 \, ,$$

where z_3 is the reading of the central indicator, and z_1 and z_2 are the readings of the outer two.
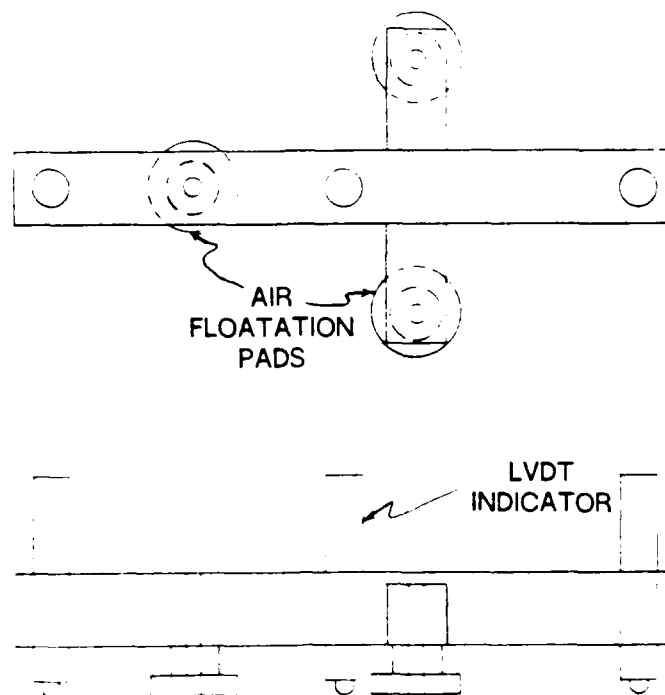
Figure 2. Floating type spherometer.

The indicators are air-bearing-type linear variable differential transformer (LVDT) devices with 15 gm plunger pressure. They are individually sensitive to motions as small as 0.1 μm.

A "black box" was built to combine the three LVDT outputs, as indicated by the equation above, avoiding the need for three electronic readout indicators.

Test of the Floating Spherometer

The floating spherometer was tested to determine the repeatability and sensitivity of the unit by measuring the sag of a large piece of plate glass as it was rotated on a large bearing. The spherometer was placed on the glass and the spherometer constrained with a piece of string in the direction of rotation of the glass.

As the glass was rotated, the spherometer came to an equilibrium position and then measured the curvature along the same circumferential path rotation after rotation. The output of the "black box" was recorded for two consecutive rotations and the sag readings compared for like azimuthal orientations on the two rotations.

Sag repeatability was 0.1 μm over the entire rotation, while sag variation was 15 μm over the path. While the total sag variation was not great (although it did correspond to ±26.666 inches in radius) the repeatability is as good as the resolution

of the LVDTs themselves.

Because the very light pressure of the indicators did not damage the polished glass and because of the excellent repeatability of the spherometer, the test was considered a success.

Future Plans

After demonstration of the hardware for the floating spherometer, the next logical step is to build a cruciform-type spherometer so that the two principle curvatures of a surface can be determined simultaneously. This information is necessary for integration of the curvature data to determine the actual shape of the surface. The cruciform spherometer would provide this data about the central indicator tip simultaneously for both the radial and tangential curvature of a surface.

This type of instrument could then be used in conjunction with the Large Optical Generator (LOG) to measure the shape of a work in progress. This measurement would be completely independent of the machine accuracy.

The spherometer would be positioned at the vertex of the work. As the table is rotated, the spherometer would gradually be pulled radially, so that measurements would be made in a spiral pattern. The spherometer would be oriented so one leg was in the radial direction. A continuous flow of data would then be produced by the spherometer about both the radial and tangential curvature of the surface.

Software would have to be written to coordinate the flow of data from the spherometer to the data reduction program FRINGE. This should be rather straightforward because software has already been written to analyze height data taken directly with the LOG in a continuous fashion.

Conclusion

In has been demonstrated that a three-ball spherometer will not work for measuring the principle curvatures of a surface and so a two-ball or bar-type spherometer must be used. A working model that floats over the surface to be measured without damaging the surface has been built. The instrument shows high sensitivity and repeatability to 0.1 μm in sag. The design is easily expandable to simultaneously take data for both principle curvatures, and it appears that the data could be captured in a real-time mode for analysis as soon as the last data point was read. For these reasons, the task is felt to be a complete success.

Wavefront Analysis from Image Plane Data

This sub-task was an attempt to obtain information about the wavefront in the pupil plane using intensity information in the image plane. Although this research is

115

not complete. a method has been devised to describe the intensity distribution in the image plane for both one and two dimensions, knowing the phase in the pupil. Progress thus far indicates a solution is possible given the time and money to pursue the problem further. The technique would permit wavefront sensing in the image plane without employing an elaborate method to obtain a reference wavefront.

Background

Initial interest in this project began with the Multiple Mirror Telescope (MMT) project on Mt. Hopkins. In 1979 when the telescope was first operated, a series of photographs were taken in the image plane to assess the image quality. Some of these photographs were taken with the telescope substantially out of focus. In these out-of-focus images, the ring structure of the zonal errors in the mirrors (the result of residual manufacturing errors) were clearly visible as intensity variations. In addition there was the hint of a square grid pattern that corresponded to the egg-crate core pattern used in the construction of these lightweight mirrors. It was known from interferometric data that the effect of this core structure was less than $1/50\ \lambda$ and probably more like $1/100\ \lambda$. Yet here in the simplest of tests was evidence of figure errors that could not be seen with state-of-the-art interferometers. Figure 3 is an example of the intensity pattern observed at the MMT.

Figure 3. Photograph of intensity distribution 76 cm inside best focus at the MMT

116

Approach to the Problem

Before one could work from the image plane back to the pupil plane, it was necessary to know how to work from the pupil plane to the image plane. To determine this, a simple geometrical optics model was constructed, showing the location and slope of rays in the image plane, given their location in the pupil plane. Uniform intensity in the pupil plane was assumed and conservation of energy used.

Once an approach to describe the intensity pattern in the image plane was established, it was felt that the problem could be solved using an influence function approach. A series of intensity distributions would be constructed in the image plane using known phase errors. Then for an arbitrary intensity distribution, a linear superposition of phase errors could be constructed that would produce the image plane intensity distribution in a least-squares sense.

A more modest though also very useful goal was to help establish a quality criterion for the amount of ripple or midspatial frequency roughness allowable in a wavefront. The approach used to describe the intensity variation in the image plane gives a very easily implemented criterion for wavefront ripple.

Analysis

Using the geometry shown in Fig. 4, it is easy to show[2] in one dimension that the intensity distribution in the image plane is the product of two terms. The first is the average intensity due to the convergence of the light beam from the pupil to the focal region. The second term is the square of the first derivative of the error in the wavefront and the second derivative in the denominator. Since the first derivative will be small, the square will be inconsequential. Thus the variation in intensity in the image plane is proportional to the inverse second derivative of the wavefront. This is seen as the connection between this work and the first task; the spherometer measures curvature, while in this task it is again the curvature of the wavefront as evidenced in the second derivative that is important.

After making several realistic simplifying assumptions, the intensity in the image plane is given by

$$I = \frac{d}{d + R^2 h''},$$

where the quantities are defined in Fig. 4 and h'' is the second derivative of the wavefront error. Since the denominator can go to zero if the second term becomes large in relation to the distance from observation plane to the Gaussian image, this is the condition on the geometrical optics limit of this approach. If d becomes small to the point that the second term makes the denominator go to zero, the diffraction

117
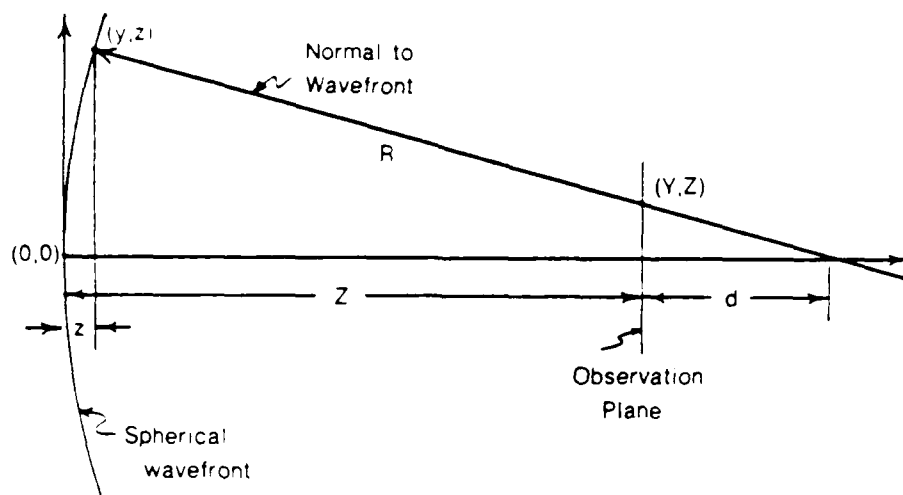
Figure 4. Converging nearly spherical wavefront and observation screen.

regime has been entered and this present approach is no longer valid.

Since the change in contrast in the image plane is more easily measured than the intensity itself, a slight rearrangement of terms and the assumption that the errors on the wavefront can be represented by sinusoids yields

$$C = \frac{kf^2AR^2}{d},$$

where C is the contrast, k is a constant, f is the spatial frequency of the sinusoidal variation in phase error, A is the amplitude of the error, R is the distance from pupil to image plane, and d is the distance of the observation plane to the image plane.

The degree of ripple in the wavefront can now be assessed in terms of spatial frequency and amplitude, and high spatial frequency errors will be evident even with very small amplitudes. Also, d is a means of controlling the sensitivity of the test. In fact, because of the diffraction limit, varying d allows "tuning" of the test for various spatial frequency errors. The test is sensitive to the highest spatial frequency errors furthest from focus. On the other hand, the test is not very sensitive to low spatial frequency errors called figure errors. Thus this new test does not change the interpretation of the classical tests for wavefront error but rather complements them.

118

In addition to this work, the intensity distribution in the image plane in two dimensions has been determined so that it is possible to analytically describe the intensity pattern rather than having to do a spot diagram based on ray trace data. This type expression will be useful for those trying to predict the intensity distribution on a CCD array, for example. There will be no need for interpolation, as the intensity on each pixel can be directly calculated by integrating the intensity over the pixel area.

Progress in working back from the image plane to the pupil plane was slowed because the intensity distribution in the image plane is given in terms of the spatial coordinates of the pupil plane, making it difficult to work backward. Some breakthroughs occurred here but none were significant and none occurred in time to be incorporated into this report.

Conclusion

An analytical method of describing the intensity distribution in the image plane given an error in the pupil plane has been developed. The description has been made in both one and two dimensions. It was further shown how this description of the intensity variation can be used to assess the degree of ripple or midspatial frequency error in a given wavefront. The test is simple to implement and interpret.

This work will continue, funded through other sources, because of the value of the results. While the work has been more difficult than originally expected, confidence remains that a solution can be found.

REFERENCES

1. R. E. Parks and D. S. Anderson, "Surface profile determination using a two-ball spherometer," Optical Fabrication and Testing Workshop, Technical Notebook, OSA, Tucson, AZ (1979).

2. S. N. Wong, R. E. Parks, and L. Shao, "Intensity distribution in out-of-focus images of a rotationally symmetric optical system," Proc. SPIE **680**, 62 (1986).

GUIDED-WAVE OPTICAL LIMITERS

G. I. Stegeman and C. T. Seaton.

PUBLICATIONS

C. T. Seaton, J. D. Valera, and G. I. Stegeman, "Integrated optics optical limiters," Proceedings of AGARD Conference on Guided Waves in the Military Environment, Istanbul, Turkey (1985).

C. T. Seaton, G. I. Stegeman, and H. G. Winful, "Nonlinear planar guided wave interactions and devices," Proceedings of AGARD Conference on Guided Waves in the Military Environment, Istanbul, Turkey (1985).

G. I. Stegeman and C. T. Seaton, "Numerical and experimental studies of nonlinear EM guided waves," invited paper, Proceedings of Second International Conference on Surface Waves in Plasmas and Solids, Ohrid, Yugoslavia (1985).

G. I. Stegeman, C. T. Seaton, A. Boardman, and P. Egan, "Nonlinear guided waves," Proceedings of NATO Summer School on Surface Electromagnetic Excitations, R. F. Wallis and G. I. Stegeman, eds. (1986); also Proceedings of NATO Summer School on Nonlinear Optics: Materials and Devices (1986).

J. Ariyasu, C. T. Seaton, and G. I. Stegeman, "Power-dependent attenuation of nonlinear waves guided by thin films," Appl. Phys. Lett. **47**, 355 (1985).

G. I. Stegeman and C. T. Seaton, "Nonlinear guided waves: Physics and applications," invited paper, Proceedings of the Trends in Quantum Electronics '85," Bucharest, Romania (1985).

G. I. Stegeman and C. T. Seaton, "Nonlinear integrated optics," invited paper, Proceedings of Fifth International Conference on Integrated Optics and Optical Fibre Communication, Venice, Italy (1985).

C. T. Seaton and G. I. Stegeman, "Intensity-dependent waveguide phenomena," Proceedings of Second Conference on Integrated Optical Engineering, Cambridge (1985).

J. D. Valera, B. Svensson, C. T. Seaton, and G.I. Stegeman, "Power-dependent waveguide phenomena with liquid crystal claddings," Proceedings of Fifth International Conference on Integrated Optics and Optical Fibre Communication, Venice, Italy (1985).

G. I. Stegeman and C. T. Seaton, "Nonlinear integrated optics," Appl. Phys. Rev. (J. Appl. Phys.) 58, 57 (1985).

C. T. Seaton, J. Ariyasu, G. I. Stegeman, and T. P. Shen, "Nonlinear thin film guided waves in non-Kerr media," Appl. Phys. Lett. 47, 1254 (1985).

G. I. Stegeman, C. T. Seaton, J. Ariyasu, and T. P. Shen, "Nonlinear waves guided by the interface of a non-Kerr-like medium," Opt. Commun. 56, 365 (1986).

J. D. Valera, B. Svensson, C. T. Seaton, and G. I. Stegeman, "Bistability and switching in thin film waveguides with liquid crystal cladding," Appl. Phys. Lett. 48, 573 (1986).

J. V. Moloney, J. Ariyasu, C. T. Seaton, and G. I. Stegeman, "Stability of nonlinear stationary waves guided by a thin film bounded by nonlinear media," Appl. Phys. Lett. 48, 826 (1986).

J. V. Moloney, J. Ariyasu, C. T. Seaton, and G. I. Stegeman, "Numerical evidence for non-stationary nonlinear guided waves," Opt. Lett. 11, 315 (1986).

J. Ariyasu, C. T. Seaton, G. I. Stegeman, and J. V. Moloney, "New theoretical developments in nonlinear guided waves: Stability of TE_1 branches," IEEE J. Quant. Electron. QE-22, 984 (1986).

G. I. Stegeman, E. M. Wright, C. T. Seaton, J. V. Moloney, T. P. Shen, A. A. Maradudin, and R. F. Wallis, "Nonlinear slab-guided waves in non-Kerr-like media," IEEE J. Quant. Electron. QE-22, 977 (1986).

J. D. Valera, C. T. Seaton, G. I. Stegeman, and B. Svensson, "Switching and bistability in liquid crystal cladded waveguides," Proceedings of SPIE Conference on Liquid Crystal and Spatial Light Modulator Materials (1986).

SCIENTIFIC PERSONNEL

G. I. Stegeman

C. T. Seaton

E. M. Wright

B. Svensson

J. D. Valera

RESEARCH FINDINGS

Introduction

This research program was initially funded by the MICOM Army Labs as a three-year program supplement to the Joint Services Optical Program. Following budget cuts at MICOM, the program was discontinued (after one year). It was then transferred to the task "Physics and Applications of Surface Guided Fields" (without an increase in funding for that task) and progress subsequent to the initial year is summarized in that report.

A series of experiments was performed on waveguides with liquid crystal media as the cladding medium on top of the guiding film. For the liquid crystal E-7, optical limiting of the transmitted guided wave was obtained as a result of the generation of leaky waves into the cladding. When K-18 was used, optical bistability and subsequent optical limiting attributable to phase changes in the liquid crystal medium were observed.

Theoretical calculations for highly nonlinear waveguide media showed that hard optical limiting could be obtained when a self-defocusing medium was used as the cladding medium. Absorptive loss and saturation in the refractive index change have both been included. Excessive amounts of either were found to be detrimental to the limiting process.

Objectives

The goal of this program was to investigate the application of guided waves to optical limiters. The detailed goals were as follows:

1. To continue the investigation of the propagation of guided waves through liquid crystal media where limiting had been previously observed.

2. To investigate, first theoretically and then experimentally, nonlinear guided-wave geometries for implementing optical limiting action.

Results

A very promising new geometry for guided-wave optical limiters has been identified. It consists of a thin film bounded on one or both sides by self-defocusing nonlinear media. As the guided-wave power in a given mode is increased, the waveguide cuts off at some power level, and will not transmit any more power in that guided-wave mode. If the film thickness is chosen so that only the lowest-order TE_0 mode can be propagated, then the cutoff for this mode is absolute in the sense that no other mode is allowed. Calculations based on $GaAl_xAs_{1-x}$ multiple-quantum-well (MQW) waveguides have been carried out. The numerical results show that the cutoff power can be tuned by varying the film thickness, or the index difference, between the film and the nonlinear medium. For this MQW system, limiting action in the range of a few milliwatts per millimeter of beam width is predicted. Preliminary considerations indicate that this phenomenon should be extendable to channel waveguides, and hence could, in principle, be implemented for detectors consisting of multiple small elements. A search is underway for a self-defocusing material in which to verify these concepts.

The role played by loss was estimated by assuming that the field distributions calculated in the absence of loss are still valid for small losses. The net result is a strong dependence of the wave attenuation on guided-wave power.

Saturation effects have now been included in our calculations on optical limiters based on these nonlinear guided waves. Saturation does not appear to affect the projected operation of the optical limiters based on self-defocusing nonlinearities. Examination of the effect of nonlinearities which vary as E^p, where E is the optical field and p is greater than 2.5, indicates that optical limiting action is still expected. This result is important because most materials with large negative nonlinearities, namely semiconductors, are not Kerr-like (i.e., $p = 2$).

Recent work has concentrated on the stability properties of these analytical solutions. The stability calculations were performed by assuming that the field distribution associated with a point on one of the nonlinear guided-wave branches is incident onto the endface of the waveguide, and then propagating the wave numerically down the film under the influence of the nonlinear wave equation. Preliminary results indicate that the waves required for switching and thresholding all belong to stable branches. There were, however, two types of instabilities found on some of the branches. In the first, the field energy remains bound within the film and the field distribution oscillates with propagation distance down the guide. These correspond to new, non-stationary solutions to the nonlinear guided-wave equations. The second type of instability is characterized by the emission of spatial

123

solitons which leaves stable guided-wave fields propagating down the film. These soliton systems appear intriguing for soliton-based guided-wave devices.

The research into the transmission properties of a waveguide with different liquid crystal media on top was continued. Among the interesting behaviors observed were conditions under which increasing the guided-wave power led directly to leaky waves, and hence reduced transmission with increasing power. For materials with thermal nonlinearities which cannot maintain large temperature gradients, the increase in index of the cladding medium eventually leads to leaky modes, which radiate into the cladding medium, and thus lead to optical limiting action.

Another interesting result was a classical bistable response when the liquid crystal K-18 was placed on the film between input and output coupling prisms. The glass film index and thickness were chosen so that the TM_0 mode was extremely lossy and no transmitted power was measured at low powers for the nematic liquid crystal state. As the input power was increased, switch-up from essentially zero to a finite power was obtained. As power decreased, switch-down occurred at a lower incident power. The stability of both upper and lower states was verified, and the physical mechanism identified as resulting from the nematic-isotropic phase transition (and its accompanying critical opalescence). Similar, but more complex, results were obtained and interpreted for the TE_0 mode. This phenomenon can be applied to threshold and two-level devices.

ROOM-TEMPERATURE CW OPERATION OF A BISTABLE
GaAs ETALON USING A LASER DIODE LIGHT SOURCE
(An ARO add-on project)

H. M. Gibbs and N. Peyghambarian

PUBLICATIONS/REFERENCES

1. S. S. Tarng, H. M. Gibbs, J. L. Jewell, N. Peyghambarian, A. C. Gossard, T. N. C. Venkatesan, and W. Wiegmann, "Use of a diode laser to observe room-temperature, low-power optical bistability in a GaAs-AlGaAs etalon," Appl. Phys. Lett. **44**, 360 (1984).

2. H. M. Gibbs, J. L. Jewell, N. Peyghambarian, M. C. Rushford, K. Tai, S. S. Tarng, D. Weinberger, A. C. Gossard, W. Wiegmann, and T. Venkatesan, "Advances in optical bistability of semiconductors: GaAs-AlGaAs superlattices, bulk GaAs, CuCl, ZnS, ZnSe, and GaSe." Proceedings of the Royal Society Meeting, London (1984); and "Semiconductor Nonlinear Etalons," Phil. Trans. R. Soc. Lond. A **313**, 245 (1984).

3. N. Peyghambarian and H. M. Gibbs, "Optical nonlinearity and bistability in semiconductors," invited paper, Proceedings of the International School on Nonlinear Phenomena in Solids, Varna, Bulgaria (1984); and in *Nonlinear Phenomena in Solids*, A. F. Vavrek, ed. (World Scientific Publishing, Singapore, 1984).

4. H. M. Gibbs, J. L. Jewell, Y. Lee, G. Olbright, S. Ovadia, N. Peyghambarian, M. C. Rushford, M. Warren, and D. A. Weinberger, "Controlling light with light using semiconductor etalons," invited paper, AVP Specialists meeting on Optical Circuit Technology, Munich, West Germany (1984).

5. M. Ojima, A. Chavez-Pirson, Y. H. Lee, J. F. Morhange, H. M. Gibbs, N. Peyghambarian, S. Y. Juang, P. K. Bhattacharya, and D. A. Weinberger, "Optical NOR gate using diode laser sources." Appl. Opt. **25**, 2311 (1986).

SCIENTIFIC PERSONNEL

H. M. Gibbs

N. Peyghambarian

Y. H. Lee (Ph.D. 1986)

Chih-Li Chuang

M. Ojima, Hitachi, Visiting Scientist

J. F. Morhange, Univ. Paris, Visiting Scientist

RESEARCH FINDINGS

Goal

The goal of this project, as stated in the title, was not fully achieved: pulsed bistability and NOR-gate operation were achieved. Since pulsed rather than cw applications seem most likely, the heat sinking required for true cw operation was not pursued.

Observation of Optical Bistability at Room Temperature using a Diode Laser Light Source[1-4]

The details of this success, reported in the previous three-year summary, were published early in this three-year period.[1]

Optical NOR-Gate Demonstration[5]

A stable optical NOR gate was demonstrated in a small ($\cong 30$ cm) optical setup using two diode lasers. It was found that a Faraday isolator (Hoya M500) has better isolation (32 dB) than a polarization beamsplitter and quarter-wave plate combination. The isolation eliminated mode-hopping problems arising from the feedback of laser light.

The optical gate consists of a GaAs/AlGaAs multiple-quantum-well crystal sandwiched between two dielectric mirrors. The front mirror has low reflectivity ($\cong 30\%$) at 825 nm and high reflectivity (97%) at 850 nm; the rear mirror has high reflectivity (94%) at both wavelengths. This design allows efficient pumping and high finesse at the probe wavelength.

Miniature current drivers for laser diodes were designed and installed. All that is necessary to observe the operation of the NOR gate is a simple oscilloscope. The setup is quite portable, as shown in Figs. 1 and 2.
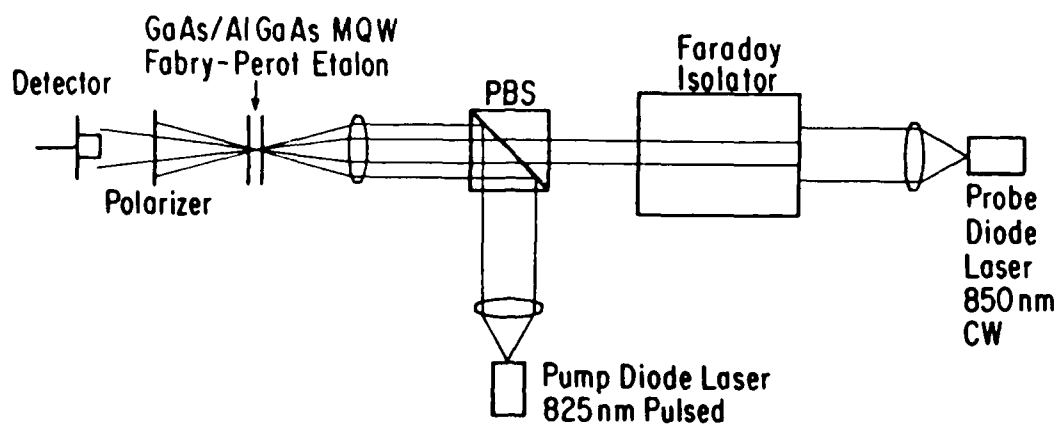
126

Figure 1. Configuration for optical NOR-gate operation with two diode laser sources, using a Faraday rotator as the optical isolator.
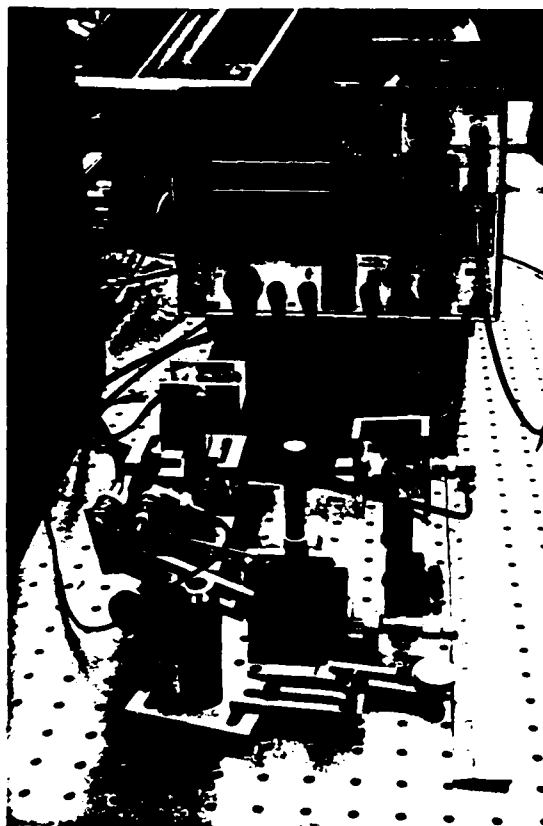
Figure 2. Setup for optical NOR-gate demonstration with two diode lasers and a Faraday isolator. The NOR-gate signal can be seen on the oscilloscope screen.

ION-BEAM PROCESSING FOR OPTICAL COATINGS ON PLASTICS

Ursula Gibson

PUBLICATIONS

Charles M. Kennemore III and Ursula J. Gibson, "Ion beam processing for coating MgF$_2$ onto ambient temperature substrates," Appl. Opt. **23**, 3608 (1984).

Charles M. Kennemore III and Ursula J. Gibson, "Ion beam processing for coating MgF$_2$ onto ambient temperature substrates," Technical Digest of the Third Topical Meeting on Optical Interference Coatings, Monterey, CA (1984).

U. J. Gibson and C. M. Kennemore III, "Ion beam assisted deposition for coating of ambient temperature substrates," Thin Solid Films **124**, 27 (1985).

S. D. Jacobs, A. L. Hrycin, K. A. Cerqua, C. M. Kennemore, and U. J. Gibson, "Adhesion enhancements and internal stress in MgF$_2$ films deposited with ion beam assistance," Thin Solid Films **144**, 69 (1986)

Ursula J. Gibson and Charles M. Kennemore III, "Ambient temperature deposition of MgF$_2$ with noble and chlorofluorocarbon ion assistance," Proc. SPIE **678**, 130 (1986).

C. M. Kennemore III, Ion Assisted Deposition of MgF$_2$, Ph.D. dissertation (University of Arizona, 1987).

SCIENTIFIC PERSONNEL

U. J. Gibson
C. M. Kennemore III (Ph.D. 8/87)

RESEARCH FINDINGS

Objectives

To apply the process of ion-assisted deposition (IAD) to the production of MgF$_2$ thin films on ambient temperature substrates, particularly plastics, to improve their mechanical properties.

To determine the chemical and microstructural changes associated with ion-assisted deposition (IAD).

Results

Magnesium fluoride (MgF_2), because of its chemical stability, wide transparency range, and low index of refraction, is desirable as a single-layer AR coating, particularly for low-index plastics. However, it has poor mechanical properties when deposited onto an unheated substrate. Use of low-energy ion bombardment during deposition of these layers has resulted in dramatic improvements in their durability, with little change in their optical performance.

In collaboration with Stephen Jacobs at the Laboratory for Laser Energetics in Rochester, New York, quantitative results were obtained on the improvement of adhesion of the ion-assisted films to quartz substrates. The measurements are made by contacting the translating films with a stylus to which a constantly increasing load is applied. An acoustical transducer receives the shockwave that results from film failure or substrate damage. A subsequent correlation of the acoustical signal with a photograph of the trace allows determination of the load at which failure occurred and the nature of the failure. The results of a series of MgF_2 films deposited onto quartz substrates are shown in Fig. 1. The run numbers of the IAD films are correlated with refinement of the technique, and represent a progression to lower energies and ion fluxes. In the most recent run (ID29C), the film is seen to adhere to the substrate three times better than a film deposited by the accepted state-of-the-art method (heated substrate). The film adheres so strongly that the substrate is damaged before the film is abraded away.

The experiments on the adhesion of the films also revealed altered stress levels in films deposited by IAD. The reduction of stress using IAD is sufficient to allow deposition of 1.6-μm layers without crazing. This is equivalent to a $\lambda/4$ layer at the long-wavelength transparency edge of MgF_2. Samples deposited onto annealed glass substrates have been studied to quantify the changes in stress, and the results published.

Comprehensive studies were also made of the chemical and microstructural changes in MgF_2 resulting from the use of IAD. Normal processing conditions, which led to transparent coatings, also led to a slight fluorine deficiency, and the incorporation of a few percent of oxygen in the films. These films had a shift of the UV absorption edge to longer wavelengths, as might be expected if some MgO was formed by residual oxygen incorporation. Pursuing the hypothesis that the oxygen was saturating dangling bonds left by preferential sputtering of the fluorine,

*007 KgF

- MSS2B - Cold substrate no ion assisted deposition IAD
- Stress relief type buckling on scratch channel edge
- Initial failure at 0.07 Kg

*0 2 KgF

- ID4A - Cold substrate IAD
- Poor substrate cleaning observed
- Initial failure at 0.11 Kg

*0 3 KgF

- MSH3C - Substrate at 300°C no IAD
- Stress relief type buckling
- Initial failure at 0.11 Kg

*0 5 KgF

- ID18C - Cold substrate IAD
- Minor coating lifting on substrate cracks at 0.5 Kg

*0 9 KgF

- ID29C - Cold substrate IAD
- Substrate cracking no coating lifting

KgF value indicates load at which photograph
was taken but not necessarily the load where
initial damage occurred

Coatings deposited by C. Kennemore and
U. Gibson, Optical Sciences Center, University
of Arizona

Figure 1. Scratch test results for magnesium fluoride coating on fused silica.

depositions were made at lower partial pressures of oxygen and water vapor. These film had less oxygen, and greater absorption at visible wavelengths. Use of a fluorocarbon as the bombarding gas reduced the absorption somewhat. X-ray photoelectron spectroscopy revealed the presence of a peak for oxygen, which corresponds to oxygen incorporated into Mg-O-F complexes.

Ion bombardment during deposition resulted in smaller grains of MgF_2, as determined by x-ray and transmission electron diffraction. The finer grain size, as well as the energy supplied during deposition, are believed responsible for the reduced stress levels.

In summary, the results are:

1. The first demonstration of the applicability of IAD to deposition of MgF_2.

2. Determination that the incorporation of small amounts of oxygen is important in determining the optical properties of the films (slight shift of UV edge, and little visible absorption).

3. Relation of this incorporation to the healing of dangling bonds left by preferential sputtering of fluorine.

4. Quantification of large improvements in the mechanical properties of the films, and relation of these to changes in the microstructure.

5. Application of durable antireflection coatings to a wide variety of plastic substrates, including acrylic, polycarbonate, polystyrene, and CR39.

131

ABERRATED GAUSSIAN BEAMS

R. V. Shack

SCIENTIFIC PERSONNEL

B. T. Landesman (M.S. 1983)
R. V. Shack

RESEARCH FINDINGS

Introduction

The effects of aberrations on Gaussian beams was studied by re-examining the first-order descriptions of such beams. This study included both a geometrical model and an unapproximated scalar diffraction analysis. The goal was to obtain a series-expansion representation of both the phase and amplitude distributions on which aberrations would be imposed, so that the power concentrations in the beam in the near and far fields could be determined.

Summary of Results

The approach to developing an aberration theory for the propagation of Gaussian beams was twofold. First, a new geometrical model was developed that provides a simpler and more powerful means of conceptualizing Gaussian beams. This model lends itself well to an aberration construct that includes "rays" and fixed reference wavefronts. In addition, the model provides a simple and powerful means of calculating the first-order properties of a Gaussian beam in an optical system. Further, since Gaussian beams are a phenomenon of scalar diffraction theory, a geometrical model alone will not suffice to understand the higher-order terms in a propagating beam. For this purpose, the diffraction problem was reworked by convolving an initial disturbance with the Fourier transform of the transfer function using no approximations and without truncating the beam. The initial disturbance is a plane wavefront with Gaussian amplitude distribution. The convolution provides a series-expansion representation of both amplitude and phase distributions in the beam for the purpose of studying how these change with the imposition of aberrations.

132

Work Performed

A literature search at the beginning of this research revealed that the effects of aberrations on the propagation of Gaussian beams have been virtually unexplored. Yoshida and Asakura[1,2] dealt with the value of the Strehl ratio for an off-axis pencil with Gaussian amplitude distribution. A more pertinent paper by Hopkins[3] developed a wave-aberration function for skew rays having a hyperbolic envelope. However, it is assumed here that the wavefront has a constant amplitude distribution and that the center of curvature of the spherical wavefront is fixed at the waist location; neither of these assumptions is true for the Gaussian beam under consideration.

The current first-order description of the Gaussian beam derives from the resonator-mode analysis of Fox and Li.[4] They obtained the steady-state field distribution across the resonator mirrors using successive approximations to numerically evaluate the Rayleigh-Sommerfeld diffraction integral with the usual approximation ($R \gg \lambda$). The amplitude distribution for the TEM_{00} mode was found to be Gaussian (within the limits of integration), with the phase surface a constant across the spherical mirrors. This normal or lowest-order mode became the ideal wavefront of a Gaussian beam.

Kogelnik and Li[5] later derived a more rigorous mathematical description of the beam. Starting with the scalar wave equation, they postulated a solution having a nonuniform intensity distribution, a curved wavefront, and a complex phase shift associated with propagation. Characteristic equations for the propagating fundamental mode were established, including the nature of the hyperbolic envelope (locus of constant relative amplitude), the radius of wavefront curvature with distance from the waist, and the phase-shift difference between the Gaussian beam and an ideal plane wave. This description can also be deduced another way, as shown by Kogelnik.[6] Beginning with the expression for a spherical wave, $\exp[(ikR)/R]$, where $R^2 = x^2 + y^2 + z^2$, and the z variable is made complex instead of purely real, the radius R is approximated using the lowest-order term in a binomial expansion and then substituted back into the wave expression. The resultant form is that of the Gaussian beam. This exercise demonstrates that higher-order terms exist not only in the phase distribution but also in amplitude, and that both change upon propagation of the Gaussian beam.

The first-order description of a beam is the usual starting point for a mathematical treatment of its aberrated terms, since aberrations can be properly understood only in relation to ideal wavefronts and their normals or rays. In this case, difficulties arise in attempting to model the beam to include ray-like phenomena

133

and expand wavefronts with a single center of curvature. The locus of constant relative amplitude in a plane containing the axis of propagation describes a hyperbola. Not only is the idea of a curved ray impossible in a homogeneous medium, but a family of spherical surfaces (i.e., wavefronts) is not orthogonal to a family of hyperbolas (i.e., rays). The other problem posed by the model concerns the center of curvature of the expanding wavefronts. This center varies in a nonlinear fashion along the axis with the asymptotic wavefront curvature centered at the waist. Likewise, the radius changes nonlinearly, decreasing to a minimum from the waist and then increasing again. This significantly complicates the development of a wave aberration theory which assumes a reference sphere centered at the geometrical focus, and a ray aberration theory for wavefront normals directed to the same point.

The model developed here consists of a skew line rotated about the axis. This process sweeps out a hyperboloid of one sheet, the envelope of a Gaussian beam. If this skew line is projected onto a plane where the axis of propagation is a point, the first-order properties of the beam can be calculated easily.[7] Since the skew line is tangent to the hyperbolic envelope everywhere, it is the locus of constant amplitude in a plane skewed to the axis of propagation.

Consider a segment of length r of one such skew line with one endpoint on the plane of the waist and the other in a plane a distance z from the waist. The endpoints are located at different radii from the axis and with an angular separation α. If the line segment is moved toward the axis in such a way that it maintains contact with both radii joining the axis and the original endpoints, and maintains a constant length r, it will sweep out an elliptical cap to the plane at z. This elliptical cap is a section of an oblate ellipsoid rotated about the axis of propagation and having the same foci as the hyperboloid. A family of such ellipsoids forms the orthogonal family to the hyperboloid. If this ellipse is considered a wavefront, a skew line lying on the orthogonal hyperboloid between any two "wavefronts" possesses the ray-like property of maintaining a constant optical path length.

The skew line, and therefore the hyperbolic envelope, is easily described by the tangent of the angle it makes with the axis of propagation. This is also the beam divergence angle. Indeed, the radius of curvature of the spherical wavefront in the traditional beam description, R_o, is related to the radius of vertex curvature of the ellipse, R_e, by the cosine of the beam divergence angle, δ, or $R_e \cos\delta = R_o$.

This illustrates the small difference between a spherical wavefront and the postulated ellipse. In most beams, δ is small and the radii of curvature are almost identical. The differences would not be apparent except in very fast beams with large divergence angles. Insights such as these demonstrate the usefulness of the

134

model, which is still being expanded and explored.

In addition, the Gaussian beam as a diffraction problem has been reconsidered from a different perspective. The field distribution in a plane at a distance z from an initial disturbance is the convolution of the initial disturbance with the Fourier transform of the transfer function, $\exp[ik\gamma z]$. This transform can be expressed in many forms, including the traditional Green's function of the Rayleigh-Sommerfeld integral,

$$2\pi \left[\frac{\hat{z}}{\hat{r}}\right] \left[\frac{1}{2\pi\hat{r}} - i\right] \frac{e^{2\pi\hat{r}}}{2\pi\hat{r}} ,$$

where

$$\hat{r} = \frac{r}{\lambda} \text{ and } \hat{z} = \frac{z}{\lambda} .$$

If the usual assumption is made that $r \gg \lambda$, this becomes

$$-i\left[\frac{\hat{z}}{\hat{r}}\right] \frac{e^{i2\pi\hat{r}}}{\hat{r}} .$$

The term $\hat{z}/\hat{r}$ is the obliquity factor. As shown by Shack,[8] making the approximation this way eliminates not only the evanescent components but some of the propagating terms as well. The effect is somewhat akin to approximating an integrand containing derivatives of functions by the functions themselves. At the very least, an unapproximated analysis would permit an estimation of the amount of error introduced by the absence of these terms. It may also provide much useful insight into both the "ideal" wavefront (lowest-order term) and the higher-order terms.

The kernel of the diffraction integral can also be written in terms of spherical Bessel functions,

$$i2\pi \; \frac{\hat{z}}{\hat{r}} \; \{j_1 (2\pi\hat{r}) - iy_1(2\pi\hat{r})\} .$$

The convolution integral is then

$$\int_{-\infty}^{\infty}\int_{-\infty}^{\infty} e^{-a^2\hat{r}^2} \; i2\pi \; \left[\frac{\hat{z}}{\hat{r}}\right] \; \{j_1(2\pi\hat{r}') - iy_1(2\pi\hat{r}')\}d\hat{x}d\hat{y} ,$$

where

$$\hat{r}^2 = \hat{x}^2 + \hat{y}^2 ,$$

$$\hat{r}'^2 = (\hat{x}' - \hat{x})^2 + (\hat{y}' - \hat{y})^2 + \hat{z}'^2 ,$$

$$\hat{z} = 0 .$$

The variable $\hat{z}'$ is the distance along the z axis from the initial plane. Although the overall integral converges because of the Gaussian term, intermediate steps in the

135

solution that involve integral representations may diverge depending on the nature of the argument and the order of the Bessel function concerned. This divergence problem can be avoided if the expression for $\hat{z}'$ is made complex after the manner of Kogelnik. This technique has proved useful, and it appears that a series-expansion solution to the diffraction integral does exist. Further study should reveal the amplitude and phase distributions in an unapproximated first-order description.

REFERENCES

1. A. Yoshida, Appl. Opt. 21, 1812 (1982).

2. A. Yoshida and T. Asakura, Opt. Comm. 14, 211 (1975).

3. H. H. Hopkins, Proc. Phys. Soc. 65B, 934 (1952).

4. A. G. Fox and T. Li, Bell Sys. Tech. J. 40, 453 (1961).

5. H. Kogelnik and T. Li, Proc. IEEE 54, 1312 (1966).

6. J. Gordon, "Elements of laser theory," in *Laser Technology and Applications*, S. Marshall, ed. (McGraw-Hill, New York, 1968).

7. R. Shack, Class notes, 1983.

8. R. Shack, Class notes, 1983.

APPENDIX

MODULATED EMITTANCE SPECTROSCOPY

B. O. Seraphin and J. D. Mueller

MODULATED EMITTANCE SPECTROSCOPY

B. O. Seraphin and James D. Mueller

Summary

During the last two decades, modulation spectroscopy has developed into a family of analytical techniques of considerable diagnostic value. The electronic bandstructure of most materials of technological merit has been determined with an accuracy sufficient to interpret, design, and optimize their optical properties technologically. In all of these techniques, light is directed towards the sample, and the changes that an external modulation parameter imposes on the bandstructure are analyzed. This has limited the range of applications to room temperature or slightly above. In contrast to conventional techniques, a novel version of modulated emittance spectroscopy attempts to analyze the light emitted from a sample whose temperature was modulated. An attempt was made to find the resonances that relate to the key parameters of the electronic bandstructure in the temperature derivative of the blackbody curve. Although the resonances must be present in all optical observables such as emittance, the major difficulty consists in separating the thermodynamically determined background described by the Planck function from the emittance that carries the bandstructure information. A computational scheme was tried that counteracted the temperature modulation by a corresponding change in the wavelength, keeping the product $\lambda \cdot T$ constant. However, the charge-coupled device (CCD), although state-of-the-art, was too noisy by two orders of magnitude as compared to the size of the expected

resonances to serve as a computational element in this procedure. An alternative approach is described that will use Fabry-Perot tunable filters to perform the arithmetic necessary to separate thermodynamic background from the bandstructure-related resonances. If successful, the novel spectroscopy will extend the established diagnostic value of the other modulation techniques up to the melting temperature. The use, design, and optimization of optical materials at elevated temperatures will then significantly profit from a knowledge of the electronic bandstructure at these temperatures.

Introduction and Background

In the first decades of this century, quantum theory interpreted the spectra of atoms and molecules with dramatic success in terms of the energy eigenstates of the electron assembly and the optically induced transitions between them. Although the optical spectra of solids involved identical theoretical concepts, their interpretation in similar terms took nearly half a century longer. Unlike the sharp spectral lines generated in systems that interfere little with each other, the spectra of solids are featureless, and little profile is available to indicate a possible correlation to the energy spectrum of the electrons. A strong interaction between the closely spaced atoms in a solid spreads the energy levels into bands and increases the number of possible transitions between eigenstates to the point where symptomatic features in the spectra are washed out. As a result, the theoretical interpretation of the spectral profile of the optical properties of solids created band structures that had error margins equal to the energies of the optical interaction itself.

The situation improved drastically in 1965 when it was observed that the periodic modulation of any parameter that entered into the determination of the band structure, pressure, temperature, electric, and magnetic fields, resulted in a synchronous and phase-related resonance response of the optical properties.[1]

This modulated spectrum consisted of a spectral sequence of sharp resonances that are related to singularities in the density-of-states profile of the electron assembly. The high spectral resolution indicated the energy value of the singularity.[2] The line shape and the response of the resonance to external perturbation corresponded to the electron momentum at the singularity. The amount of experimental information improved considerably as compared to the static spectrum. Figure 1 illustrates this improvement by comparing the static reflectance curve of GaAs with the modulated electro-reflectance spectrum.[3]
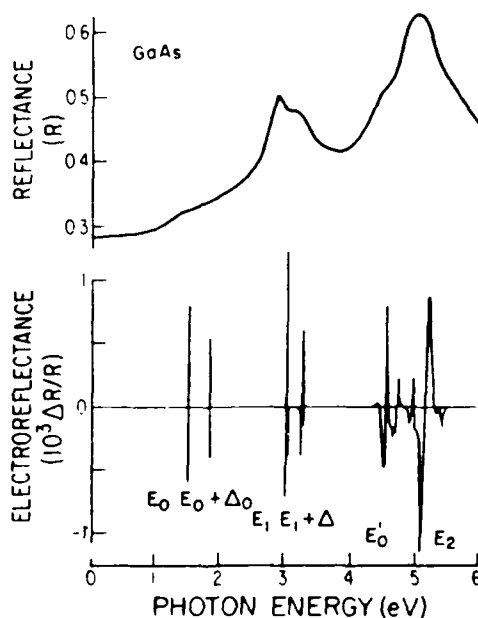
Fig. 1. Reflectance and electro-reflectance of GaAs as a function of photon energy.[3]

Within a decade, theorists used the sharp resonances with remarkable success to adjust their parametric calculations of band structures. Based on the modulated spectrum, the band structure of a solid can now be calculated with the accuracy that experimentally reproduces the observed spectral profile of the optical properties.[4]

The new spectroscopy has found its place among other diagnostic techniques and has been applied to most materials of scientific and technological interest. Like most optical techniques, however, it has been used only for temperatures around and below ambient. Little information is available on the static and modulated spectra of solids at elevated temperatures. As a result, the optical properties and the electronic band structures from which they are derived, are unknown above room temperature. Also, little is known about the optical constants of the more popular optical materials (such as gold, silver, and aluminum) at elevated temperatures, and the few available data scatter widely. It is difficult to separate the actual temperature change of the optical property from the thermal expansion of the apparatus or from the thermally induced contamination of the surface, to name just two major error sources.

Modulated emittance spectroscopy addresses the problem by expanding the known diagnostic power of the other modulation spectroscopies to the emittance of a material. Instead of directing a probe beam to the sample, the radiation from a hot surface of a modulated sample is analyzed (a configuration much less susceptible to the vagaries of high-temperature reflectance or transmittance spectroscopy). Little doubt exists about the presence of symptomatic resonances in the emittance spectrum of a solid. They are created by a modulation of the dielectric function which, through the optical constants, enters into all "observables" such as reflectance, transmittance, or emittance. Since they are so well established in reflection and absorption, and since the emittance is as much a function of the optical constants as they are, the spectral profiles of the radiative output from a hot surface must carry them as well. However, observing them in the presence of a strongly temperature-dependent background, that is of a different nature than in reflectance, is the subject of this study, and will be described in detail below.

Once the techniques are developed under this project, we will have a novel version of modulation spectroscopy available that is not subject to the limitations of existing techniques at high temperatures. The singularities in the density-of-states function, and

thus the key features of an electronic band structure, will be open to the spectroscopic analysis over a temperature range extending up to the melting point of the material. The relative position of energy bands as a function of temperature, their shifting and crossing over as the temperature is changed, the effects of alloying, dilute admixture of additional components, and phase changes on the optical properties will be possible in terms of a temperature-dependent band structure. The knowledge of the band structure has led to an understanding, and subsequent design and optimization of, the optical properties of new and existing materials. To have this facility available over a wide range of temperatures up to the melting point will be of great scientific and technological significance at a time when the number of high-temperature and high-radiation-load applications increases.

We will show in the following sections that the thermodynamically determined background of the radiative emission exceeds the size of the resonances by four orders of magnitude. To separate the two, and make the bandstructure-specific resonances emerge from the background, the wavelength must be counter-modulated to the temperature, so that their product stays constant. The thermodynamical background remains unmodulated, permitting us to separate and amplify the emittance modulation which is not invariant to the product of wavelength and temperature.

The countermodulation was attempted with a "smart" CCD controlling an IBM PC and worked to our satisfaction. However, the time fluctuations of the output from a given pixel of the CCD exceeded the size of the expected resonances by two orders of magnitude. Since the CCD operated as a computational element rather than a detector, averaging over numerous runs could not remove this limitation. As we will show in the section on experimental results, the stability of present-day CCDs appears to rule out the approach used in this study, and the project is on hold. We will outline an alternative, however, based on the use of tunable Fabry-Perot narrow-band filters that may open the possibility to develop this novel and powerful version of modulated spectroscopy.

Reflectance Modulation vs Emittance Modulation

The modulation of the reflectance $R(\epsilon_1, \epsilon_2)$ by a parameter X (pressure, temperature, electric or magnetic fields) can formally be described by the total differential

$$\frac{dR/R}{dX/X} = \alpha \cdot \frac{d\epsilon_1/\epsilon_1}{dX/X} + \beta \cdot \frac{d\epsilon_2/\epsilon_2}{dX/X} . \tag{1}$$

The "weight" of the modulation with respect to a change in either ϵ_1 or ϵ_2 (real and imaginary part of the dielectric function from which the optical constants are derived) is given by the two coefficients α and β which, through ϵ_1 and ϵ_2, are functions of the wavelength. Their dependence on the wavelength is slight, however, for the case of GaAs as illustrated in Fig. 2. Over the width of the spectral resonances, a few milli electronvolts, they can be assumed constant. In addition, the modulation changes the ϵ_i so little that $d\epsilon_i/\epsilon_i \ll 1$. Both facts together support the approximate assumption that the observed dR-line shape reflects the X-induced modulation of the dielectric function that can then be evaluated in terms of the electronic band structure.[5]
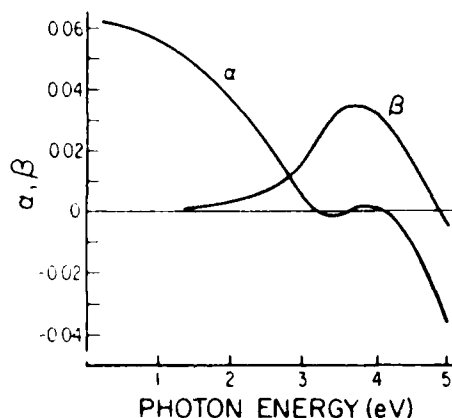

Fig. 2. The coefficients α and β of Eq. (1) for GaAs.

For the temperature-induced modulation of the radiative output from a hot surface, the situation is more complex. Writing the output as

$$I_r(\lambda, T) = \epsilon(\lambda, T) \cdot P(\lambda \cdot T), \tag{2}$$

where $P(\lambda \cdot T)$ is the Planck function multiplied by the Stefan-Boltzmann constant and $\epsilon(\lambda, T)$ is the emissivity of the solid, we can find the temperature response by differentiating

$$\frac{dI_r}{dT} = P \frac{d\epsilon}{dT} + \frac{dP}{dT} \epsilon \quad . \tag{3}$$

The differential $d\epsilon/dT$ carries the band-structure information. This term is overpowered, however, by the much larger temperature differential of the Planck function, which is of thermodynamical origin and not bandstructure related. We trust that the reader is not confused by the same symbol ϵ being historically used for the dielectric function and emissivity, respectively.

However, the separation can be accomplished on the strength of the fact that ϵ depends separately on λ and T, while P is invariant to modulation that leaves the product $(\lambda \cdot T)$ unchanged. A few transformations of Eq. (3) lead to

$$\frac{dI_r/I_r}{dT/T} = \frac{d\epsilon/\epsilon}{dT/T} + \phi(\lambda T). \tag{4}$$

in analogy to Eq. (1). Note that the emissivity modulation now emerges from the background once the temperature modulation is accompanied by a correlated change in wavelength that leaves the product (λT) invariant.

To separate the bandstructure-related information given by the first term in Eq. (4), we must ask for its magnitude, and that of the thermodynamic background $\phi(\lambda T)$ on which it rides, as given by the second term in Eq. (4).

The second term is, of course, an expression of Wien's Displacement Law for the blackbody. If $\epsilon(\lambda, T)$ is a constant on the wavelength as well as the temperature scale, the first term disappears, and the temperature modulation of the emitted intensity is constant as well, if observed under the condition that $\lambda \cdot T$ is constant. It is straightforward to evaluate $\phi(\lambda \cdot T)$ from tables of the Planck function to

$$\frac{dI/I}{dT/T} = \phi(\lambda \cdot T) = X(1 - e^{-X})^{-1} \tag{5}$$

where $X = b/\lambda T$, with $b = hc/k = 1.44 \cdot 10^{-2}$ (mK) .

The function expressed in Eq. (5) assumes the value one for $X = 0$, and approximates a straight line $Y = X$ as X increases. Typical limiting values for the experiment are given by $\lambda = 1\ \mu m$ and $T = 3000$ K, and $\lambda = 0.4\ \mu m$ and $T = 1000$ K. For these limits, the ϕ-function assumes the values

$$5.7 < \phi < 43 . \tag{6}$$

We will show in the next section that the contribution of the first term in Eq. (4) is of the order 10^{-4} at the most. The noise performance of the modulation and detection system must therefore be such that this small bandstructure-related contribution to Eq. (4) can emerge from a background that is typically five orders of magnitude larger.

This task is not too formidable. Conventional modulation spectroscopy routinely separates signals that are 10^{-6} times smaller than the background on which they ride. In some cases, this limit has been pushed to the 10^{-9} range.

However, a basic difference exists between conventional modulation spectroscopy and the emittance-based approach considered here. The conventional technique resolves a slope singularity in the joint-density-of-states function from the rather smooth background of the noncritical transitions all over the Brillouin zone. The modulation therefore acts in a singular manner on the resonance without affecting the background to the same extent.

The temperature modulation in the emittance version affects both the resonance and the background. As a matter of fact, Eq. (6) implies that this modulation effect can be one million times stronger on the background than on the resonance. To separate the two, the invariance of the background with response to $(\lambda \cdot T) = $ constant must be used to separate a resonance that is not subject to this invariance. This places a more demanding requirement on modulation and detection, as we will see in the following

sections. At first, however, we will briefly describe how this separation can in principle be accomplished.

Separation of Resonances
from the Thermodynamical Background

Equation (6) implies that the temperature modulation of the thermodynamical background is very strong. The difficulty of the new spectroscopy consists then in retrieving the band-structure resonances from a background that is 4 to 5 orders of magnitude larger. The central concept of this project is that this separation be accomplished by synchronously countermodulating wavelength and temperature so that their product stays constant.

This is done by operating along the hyperbolas $\lambda \cdot T$ = constant, where the thermodynamical term in Eq. (4) is constant. For a blackbody with wavelength- and temperature-independent emissivity or a real blackbody outside the resonances, the effect of the temperature modulation on the emitted intensity can be suppressed by going to a corresponding wavelength. To accomplish this, horizontal motion compensates for the temperature modulation (vertical motion in the diagram of Fig. 3) and leads the readout back to the initial hyperbola. In our initial approach described below, a microcomputer readdresses the pixels of a CCD detector in the exit-slit plane of a monochromator such that the new address reads out the initial intensity. If the modulation $\phi(\lambda T)$ can be restored to its center value, we operate at a region of the spectrum for which the emissivity does not display a strong temperature variation. If this cannot be accomplished, however, a resonance in the emissivity is observed (Fig. 4).

The actual data processing will proceed on the basis of a triplet of wavelengths sliding over the blackbody curve as shown in Fig. 5. For the outer points of the triplet, the invariance condition is forced on the modulation in approximate fashion. If the center point can be "leveled," the blackbody differential is smooth. If the region of a
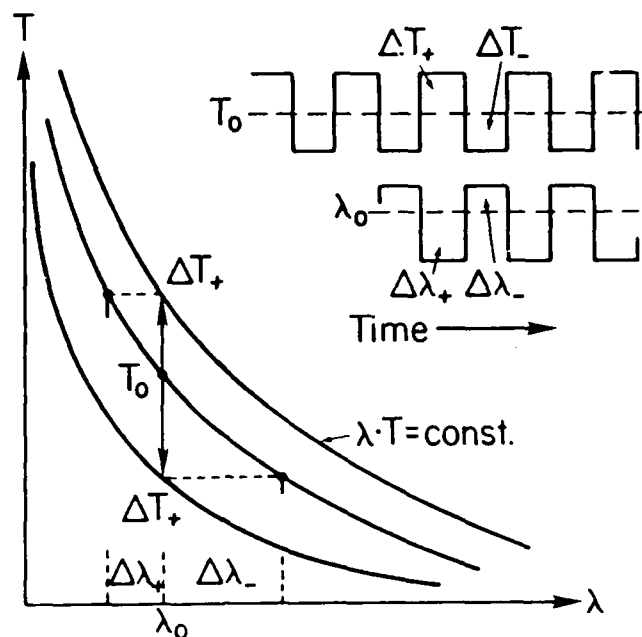
Fig. 3. Temperature modulation $\Delta T_+/\Delta T_-$ and the ϕ-function
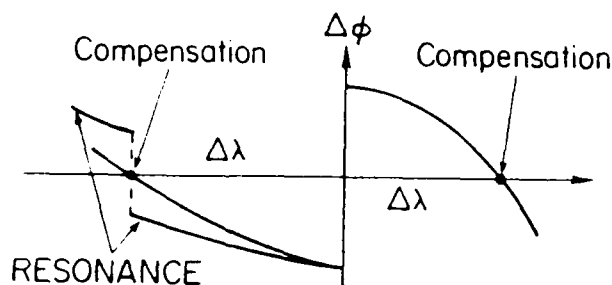

Fig. 4. Wavelength compensation of the temperature modulation, or lack thereof, outside and at a resonance, respectively.

resonance is at the center-point position, however, the "normalization" performed at the outer points of the triplet will not be possible. The temperature response of the emissivity will upset the average normalization performed in the smooth parts, and the spectral line shape will be indicative of the temperature modulation of the optical constants that lead to a diagnosis of the energy band structure. The computer program will insure that the process is not confused by a resonance at one of the outer points.
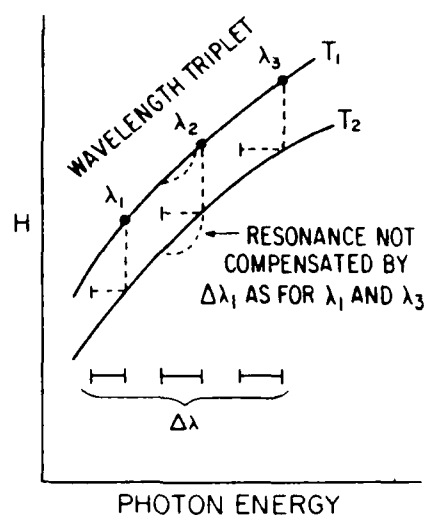
Fig. 5. Visualization of the data analysis of the temperature-modulated radiative output I_r under condition $(\lambda \cdot T)$ = constant.

We will scan the spectral profile of the radiative output for energies at which it resonates in response to the temperature modulation by sliding the wavelength triplet along the spectral scale incrementally and for each position trying to force the invariance normalization on the outer points. The resulting spectrum should resemble that of a regular thermoreflectance scan, although the line shapes are expected to be different because in one case the radiative output is modulated and in the other a probe beam is directed against the modulated sample. Unlike the thermoreflectance scan, however, the emittance experiment can be performed over a wide temperature range up to the melting point, indicating in spectral shifts and strengths the response of the band structure to temperature changes.

Estimate of the Size of the Expected Emittance Resonances

By its very nature, modulated emittance spectroscopy resembles the thermoreflectance version of the conventional technique. To determine the effect of a temperature change on both optical constants n and k, two separate measurements or a very complex Kramers-Kronig analysis must be performed.

For the sake of an order-of-magnitude estimate, we will assume that the effects of the temperature modulation are of the same order on both optical constants. We can then evaluate the expected contributions to the first term of Eq. (4) from known thermoreflectance spectra such as shown in Fig. 6 for gold.
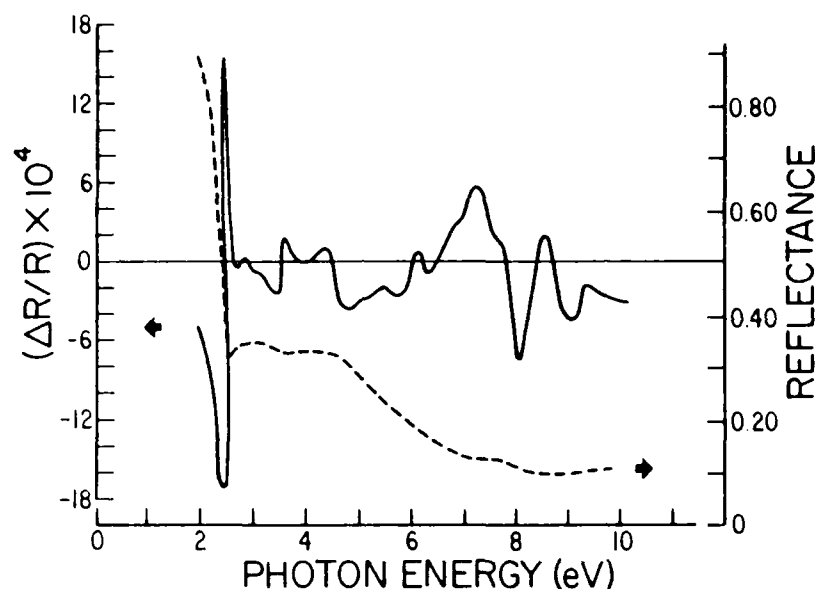

Fig. 6. Static (broken line) and thermoreflectance spectrum of gold (Ref. 4).

No thermoreflectance spectra have yet been measured for the refractory metals tungsten, tantalum, and molybdenum which, by virtue of their high melting points, will be the first candidates investigated by the novel spectroscopy. We will assume that spectra similar in size to that of gold will be obtained once they have been measured.

From the modulated reflectance of gold shown in Fig. 6, changes in the optical constants n and k are expected on the order of

$$\Delta n \approx \Delta k \approx 10^{-2} \quad .$$

Feeding this into the expression for the emissivity modulation

$$\Delta \epsilon = \frac{4}{[(n + 1)^2 + k^2]^2} \{[k^2 - n^2 - 1]\Delta n + 2nk \cdot \Delta k\}$$

we obtain at the strong resonance at 2.4 eV the value of

$$\frac{\Delta\epsilon}{\epsilon} = 2 \times 10^{-2} \ .$$

For a temperature modulation of dT/T = 0.01, we therefore expect a resonance contribution to the thermodynamic modulation on the order of

$$\frac{d\epsilon/\epsilon}{dT/T} \sim 10^{-4} \text{ to } 10^{-5} \ .$$

Values in this range must be separated from a background that according to Eq. (6) is 10^6 times bigger.

Experimental Method

The basic principle of a separation of the bandstructure-related emissivity from the thermodynamical background consists in modulating the temperature T while countermodulating the wavelength λ in such a manner that the product $\lambda \cdot T$ remains constant. Figure 7 shows a schematic of the experimental approach: each wavelength of the emitted intensity is assigned a "pixel address" on a CCD located in the exit-slit plane of the monochromator. Once the spectral distribution of the emission is varied by a change in the temperature, a computer-controlled search readdresses the pixels so that $\lambda \cdot T$ returns to the same product as before the temperature change.
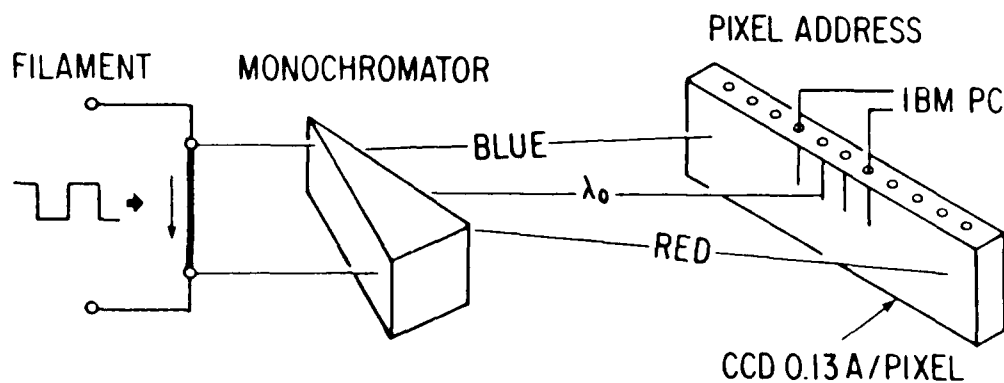

Fig. 7. Schematic of the experimental approach.

The "re-addressing" of the spectral scale is accomplished by means of the charge-coupled device CCD) that is controlled and read out by a microcomputer. The emitted intensity from the hot sample is displayed spectrally by a monochromator into the conventional "color band" in the plane of the exit slit. However, instead of sampling this color band by means of the exit slit, the plane of the CCD intercepts the color band. Each "pixel" of the CCD corresponds to a narrow spectral range for which the average intensity can be read out at the terminals of the device. As a result, each narrow spectral range has a pixel number as its "address." After the temperature of the sample is increased, the intensity distribution along the pixel sequence changes accordingly. A program can then direct the microcomputer to search for a new spectral address around the previous one (for the visible range it will always be on the short-wavelength side of the previous address) until a wavelength is found for which the invariance condition is fulfilled.

Optical and Detector Facilities

A Spex 1702 monochromator was set up, adjusted, and isolated from vibration. Mechanical linkages and wavelength-drive motor uniformity within the monochromator were tested. A sample holder was designed and built that holds a filament of the material to be studied between two spring-loaded mounts that maintain constant tension on the sample. This ensures accurate alignment on the optical axis while the filament length changes with temperature. The vacuum system for the sample holder was built and tested. A programmable power supply, which provides a controllable filament current and achieves the temperature modulation, was purchased and connected to the computer. The filament temperature can be varied under computer control.

A CCD linear array detector Fairchild Model 122 was placed in a holder, mounted inside the monochromator without affecting monochromator performance.

The replacement changes the mechanism that ordinarily selects a wavelength at one position of the exit slit. The projection of the spectrum along the CCD may not relate to the wavelength in a compensatable linear fashion, impairing the spectral fidelity of the selection. The holder was designed with this possibility in mind, giving a sufficient range of adjustment.

Electronic Data Collection, Storage, and Display

Light emitted by the sample passes through a window in the vacuum chamber into the monochromator where it is dispersed onto the 1728-element linear CCD array. This allows a portion of the spectrum to be observed almost instantaneously (limited by the scanning speed of the CCD). The output of the CCD is processed by circuits that select three elements from each scan, digitize them to 12-bit resolution, and send them to the computer.

The processors for the CCD readout system enable the computer to read any three pixels of the CCD and change these three as necessary. This gives the three-point grid (two calibration points surrounding the data point) that is moved along the spectral contour of the radiant output in search of modulated fine structure.

Collection of approximate data and its storage and display were accomplished by software written in compiled BASIC. The collection of accurate amplitude data will ultimately depend on the writing of an assembly language program that will be fast enough to gather all the needed values in one scan of the CCD. The slower program currently in use does give accurate wavelength information.

A nearly real-time intensity profile of any section of the CCD array can be scanned. The program allows a new scan of 209 pixels every 4 seconds. This is fast enough to perform the necessary steps of fine tuning the optical setup and to calibrate the CCD in wavelength terms. Figure 8 shows the spectral display of the sodium D doublet generated by the computer scans. From the known 5.93 Å spectral separation of

the two components displayed over 43 pixels, the spectral resolution is determined as 0.138 Å per pixel. This implies that resolution is presently limited more by the monochromator than by the separation of adjacent pixels. No side bands are presently evident.
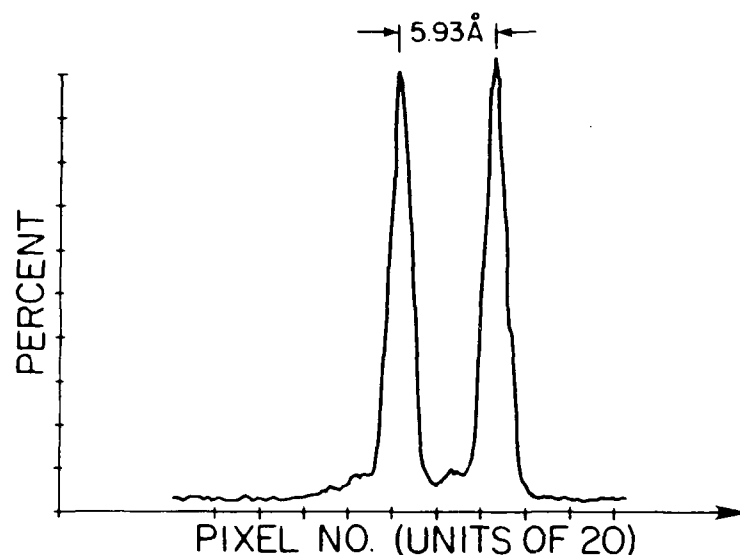

Fig 8. Sodium D-doublet as resolved by CCD detector behind Spex 1702 monochromator.

Data Processing and Invariance Arithmetic

To perform the operations on the data that lead to an invariance of the product $(\lambda \cdot T)$, parameters must be adjusted to lie within specific interrelated ranges. The most important ones are the modulation frequency and depth, spectral resolution of the monochromator and CCD, scan rate of the CCD readout, and the speed of the computer operations that perform the data gathering and arithmetic.

To establish the basic interrelation of some of these parameters and to define suitable ranges of their values, a simulation program was undertaken.[6] Its execution led to the realization that the CCD detector was by far the weakest link in the detection

chain. The stability of the individual pixel over the scanning and computing time is about two orders of magnitude below that needed to separate the signal from the background. We performed elaborate tests described in the following section to ascertain the problem was CCD related. Since we had planned to use the CCD as a logical element that controls the data analysis on the basis of a return to an original value once another parameter, the temperature, had been changed, we could not rely on its proper function once it was shown to be incapable to recognize this original value in a noise level that is one hundred times larger.

The noise performance of CCDs is not something that interferes with their general usage. As a matter of fact, our observations can be traced back to the manufacturers specifications. We simply had planned to use a CCD far beyond its state of the art, and must either await improved devices or turn to a different approach which we will describe at the end of this report.

Experimental Results

Initial studies showed that in low resolution the CCD control could indeed lead the readout back to the original hyperbola of the constant $(\lambda \cdot T)$ product once the temperature was changed (Fig. 3). Size and magnitude of the changes corresponded well with what could be expected from the line shape of the blackbody curve. Increasing the temperature required wavelength reduction and vice versa, with the size of the reduction properly correlated to the base temperature.

However once the temperature amplitude of the modulation was reduced and higher read-out resolution was required, it became evident that intrinsic CCD noise buried the values of the emitted intensity changes that the CCD was to recognize. We performed a number of tests described below that led to the conclusion that our approach could not be carried through to fruition using present-day CCDs.

Spatial Uniformity and Temporal Stability
## of the CCD Detector

Spatial Uniformity

To test the spatial uniformity of the CCD detector, i.e., the uniformity of the response along the line of 1728 pixels, we placed the detector against the face of an ultrastable uniform light source (ULS) developed by Eustace Dereniak of the Optical Sciences Center. It consists of a 300 W tungsten-halogen lamp illuminating a screen through a tunnel of mirrors, filters, and diffusers. The light source is energized by a power supply that is stable to within 0.006%, resulting in a uniform illumination of the 6-in. screen to within 0.2%. The temporal stability was tested to better than 0.01% by means of a photomultiplier and an oscilloscope.

The illumination of the CCD in all of the tests described in the following is "white." Variations of the spectral sensitivity of the CCD array are not accounted for and further tighten the limitations of the CCD.

Since the illuminated area of the ULS is much larger than the linear dimension of the CCD, we placed it on the screen together with United Detector Technologies PIN DP 325-1 monitor. We tested the entire length of the CCD array by intercepting the analog signal before the A/D converter and running it into a lock-in amplifier. The reference signal was taken off the power supply.

We expected variations of the sensitivity along the length of the array, and planned to calibrate the response by means of a table that could be stored, used as a reference, and calibration in the subsequent data analysis. We quickly learned, however, that the limited temporal stability of each individual pixel rendered such an approach useless. In addition, the test described here refers to white illumination. Our calibration table, even if feasible for a very stable array, would have to consider the variations in the special sensitivity of each individual pixel which may be a function of illumination intensity, and therefore of modulation depth.

Figure 9 shows the relative response of the pixel array along its length. Note that towards each end, the sensitivity drops considerably. However, incisions as deep as 5% in the center region are common as well. The variations exceed non-uniformities of the ULS source considerably. We confirmed this by placing the CCD against different portions of the screen, observing the same spatial profile shown in Fig. 9. Placing the CCD at different angles to the screen confirmed that the drop-off was not caused by shadowing or mounting of the CCD. Our initial plan to store the profile of Fig. 9 as a multiplicative correction factor for each pixel would have met with considerable limitations, even if the array had turned out to be stable in time. Tests confirmed that each pixel has a slightly different spectral response, as function of illumination intensity. A full correction table would by far have exceeded the available memory capacity and speed of the system.
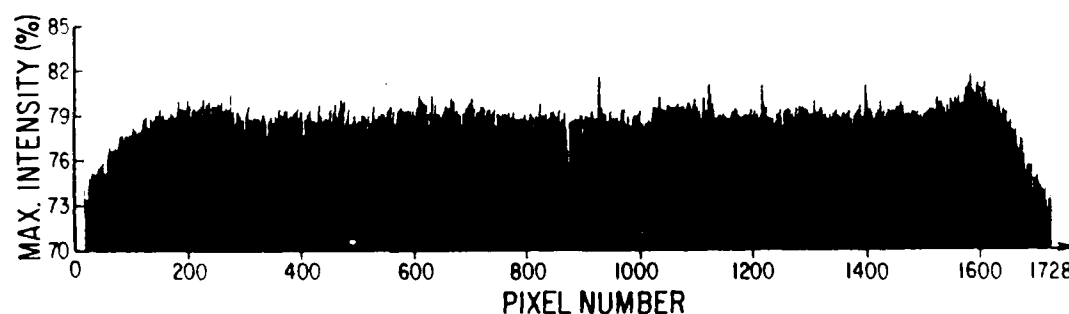
Fig. 9. Response of CCD to a constant uniform illumination.

Short-Time Temporal Stability

Over 4 s and at a sampling rate of one per every 7 ms, the output of 26 pixels out of a total of 1728 was measured. They were evenly distributed over the face of the CCD. The time profile of their response did not show any significant variations, so that it is sufficient to show the profile for just one of them (No. 1111) in Fig. 10. Note that the response varies with time in the range of 0.5 to 1.0% of maximum intensity, as defined at the output of the CCD at 2.0 V saturation voltage.
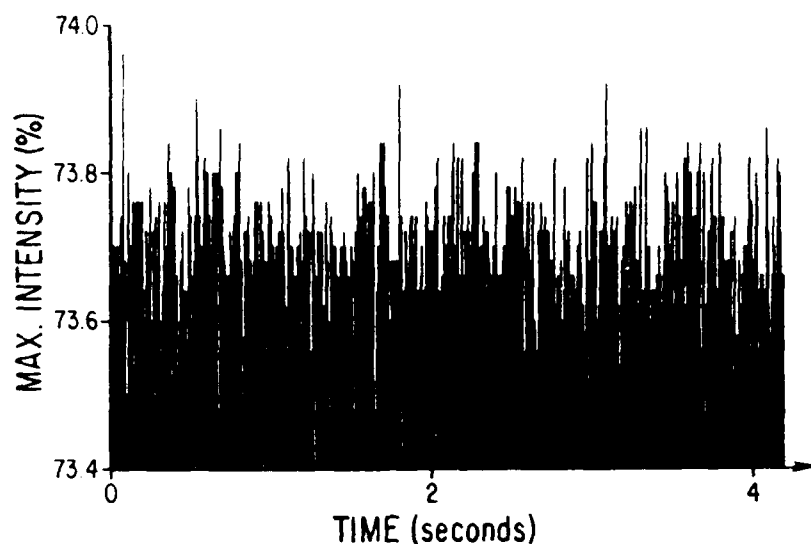
Fig. 10. Response of a pixel over time to a constant intensity light source. Values are taken every seven milliseconds.

The variations of the output intensity follow a square-root law, as shown in Fig. 11. In principle it appears feasible to flatten out the profile by repeated runs over an extended period of time. To arrive at a flatness of better than 0.01% of maximum intensity, as prescribed by the size of the resonances to be resolved, would require sampling typically over several minutes.

Fig. 11. Distribution of intensity values of successive sampling runs of one individual pixel. See Fig. 12 for scale.

To reduce the variations in one single pixel by repeated runs would not serve a purpose, however. The method is based on a search for the wavelength (= pixel address) that fulfills the condition $(\lambda \cdot T)$ = constant value before the temperature T was changed to the new value. This requires that several pixels, typically on the order of 50, are scanned, starting from the initial pixel. For each one, the runs would have to be repeated over several minutes until the uncertainty is reduced to a value that allows the initial ϕ function to be recognized, or the resonance identified. Sampling times on the order of hours would result, and the questions must be asked whether or not the rest of the equipment is sufficiently stable over such length of time. We will see in the next section that this is not the case.

Before proceeding to this test, however, we must point out that the stability tests were performed with white light. Using the pixel array in monochromatic light would introduce the non-uniform spectral response of the pixels, expanding the sampling space by one more dimension.

Long-Term Temporal Stability

Even if the above limitations would not apply, repeated sampling requires that the profile of Fig. 10 stays constant for a certain length of time on the order of minutes. This is not the case, however, as shown in Fig. 12. The output from a pixel was followed in the form of an intensity histogram over several minutes. Although random in their occurrence, jumps were found to occur. The light source cannot be responsible for these jumps, since we measured its stability and found it stable to better than 0.01% of its output. We suspect that internal changes in the CCD are causing these jumps that prevent us from scanning the array in repeated runs for much longer than several seconds.
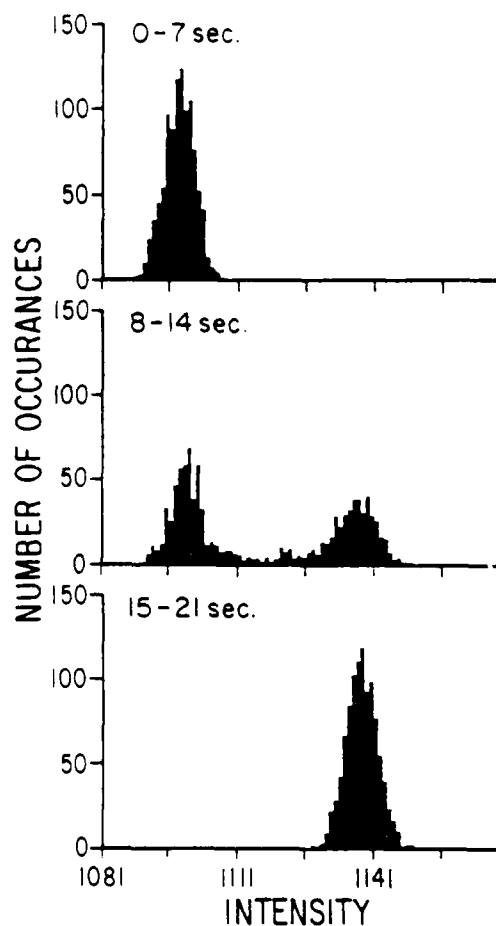
Fig. 12. Distribution of intensity values over successive 7-s intervals, as recorded by one pixel. Values are taken every 7 ms. Intensity is measured on a scale of 0 to 4095; 0 corresponds to 0 volts (dark), 4095 corresponds to 2.0 volts (saturation).

Replacing the CCD with a Resistor

To identify the contribution to the noise of control and supply electronics, the CCD was replaced by a resistor. When the same test was performed that resulted in the data of Fig. 10, the noise spectrum was reduced to approximately 1% of the former values, as shown in Fig. 13. Note that the ordinate gives intensity values on the same scale as Fig. 10; it is evident that the CCD contributed about 100 times as many fluctuations as the electronics. This indicates that the CCD is the source of the fluctuations.
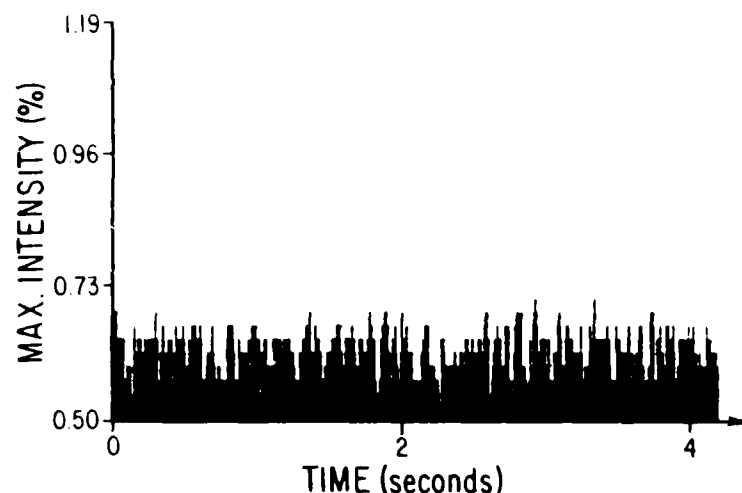
Fig. 13. Noise (in terms of CCD intensity) seen when the CCD is replaced by a resistor circuit.

Conclusions

From the tests reported above, we concluded that the noise performance of the CCD does not permit us to resolve the resonances from the background. To demonstrate this more clearly, we will schematically compare with each other the resolving power of the two versions of modulation spectroscopy: the new emittance version and the conventional one.

The data to be separated from the background in conventional modulation spectroscopy consist in a slope singularity of the joint-density-of-states function superimposed on the smooth background of all other optical transitions. The situation is sketched in Fig. 14, showing the square-root singularity of a critical point in the joint-density-of-states function superimposed on the integral of all optical transitions throughout the Brillouin zone. As the modulation, consisting of the variation of any parameter that affects the electronic band structure, is moved across the singularity, it resonates sharply, causing a signal much larger than the response of the non-critical profile below. A lock-in amplifier easily separates the two responses which are so widely separated in magnitude.
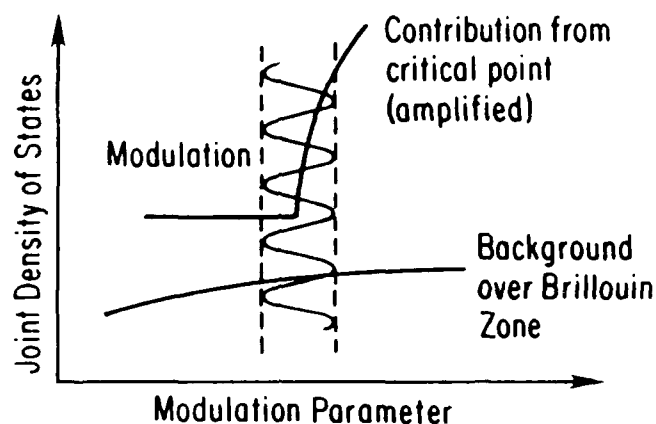
Fig. 14. Schematic representation of the separation of slope-discontinuities in the joint-density-of-states function in conventional modulation spectroscopy.

To visualize the situation for the emittance-based spectroscopy, we have to resort to topographical terms. The thermodynamical function ϕ can be plotted as a hyperbolical terrain over the $\lambda \cdot T$ plane, with the contour lines $\lambda \cdot T$ being hyperbolas of equal "elevation" in planes parallel to the base plane.

For a blackbody, modulation along these contour lines strictly does not affect the value of the emitted intensity. For a real body, however, for which band structure information is superimposed on the thermodynamical component, the contour line is not perfectly smooth, but has a "roughness" superimposed on it, that represents in its profile the band structure information embedded in the emissivity that is not invariant to $(\lambda \cdot T)$ = constant. In particular, spikes are expected along the contour line that represent the critical points in the joint-density-of-state function.

It is important to realize that the terrain on either side of the contour line changes very steeply. Leaving the contour line in the direction of a temperature change modifies the ϕ function very quickly on the scale of ten-thousand times the size of the expected resonances. Unless the gauge for changes in "elevation" above the base plane is very

sensitive, and in particular very stable over the time range of a measurement, little chance exists to find with sufficient precision the way back to the contour line, to determine whether or not it has a spike. For the case of the CCD we are certain that the time variation of the output fluctuates one hundred times more than the amplitude of the roughness of the contour line. With this in mind, we have decided to put the experiment on hold, in spite of the certainty that the sought-after resonances must ride on the contour lines.

Since modulation of the temperature affects the resonances, as in the conventional spectroscopy, and in contra-distinction causes much stronger changes in the background attributable to movements in the very steep terrain of the background, a significant difference in the resolving power of the modulation is established. Unless a sensitive and stable probe is found that leads a logical element with precision back to the contour line after the temperature has been modified, we cannot determine whether this contour line represents a "blackbody value" or has bandstructure information riding on it.

Present-day CCDs apparently do not provide such a probe. In the appendix, we will sketch why we expect tunable Fabry-Perot interferometers to provide an alternative. As with the CCD, we will stretch again the state of the art in an application for which neither the CCDs nor the Fabry-Perots were designed.

The project challenge here is that the diagnostic resonances are riding on the temperature-derivative of the emitted intensity profile. These resonances must be there for very fundamental reasons, confirmed by the large volume of modulated reflectance spectra. Their value in determining the electronic band structure, and thus the optical performance of materials, over the temperature range to the melting point stresses the imagination. To separate them from the background challenges the experimentalist and recalls the situation of the early sixties, when the empty schemes of band-structure calculations had to await modulation spectroscopy to connect them to the experimental reality.

Acknowledgements

The new approach described in the Appendix emerged in discussions with Dr. Victor Mizrahi. We gratefully credit him with his helpful contribution. Robert Rauchmiller and Karl Chao have helped as students with the project.

Appendix -- Future Work

We will state the aims of this project in a manner that outlines the restrictions of the present experimental approach, but identifies alternatives at the same time.

Find the singularities that are superimposed on the smooth profile of the temperature derivative of the intensity emitted from a hot surface.

For a black or grey body, the temperature derivative of the emission has the same value along contours $(\lambda \cdot T)$ = constant, if the ranges of variation of temperature T and wavelength λ are small. Once a detector determines this value for a given temperature, it is possible to find this same value again for a different wavelength after a change of temperature, if the product $(\lambda \cdot T)$ is maintained constant.

It is the reason for the failure of the CCD-based approach that the signal-to-noise ratio of the detector did not give this determination sufficient reproducibility in successive measurements to find the deviations that are characteristic for the presence of a resonance.

It is proposed in a preliminary manner that the CCD detector be replaced by a tunable Fabry-Perot interferometer that looks into a photomultiplier followed by a lock-in amplifier. The tunable Fabry-Perot is set to a starting wavelength λ_0 for which the photomultiplier registers a modulation $(\Delta I/\Delta T)_0$ in response to a temperature modulation ΔT of the filament. The temperature T_0 on which this modulation rides, is then set to a new value T_1, and the Fabry-Perot is instructed to search for a new wavelength for which the modulation of the emitted intensity is restored to its initial value $(\Delta I/\Delta T)_0$.

This procedure would be arbitrary if performed for one wavelength only. However, if a sequence of wavelengths is scanned in this manner, a smooth base line is obtained from which the resonance emerges, if present.

The new approach is superior to the previous one in more aspects than potentially improving on the insufficient signal-to-noise ratio of CCDs. Two advantages emerge:

1. The method is "static" in the sense that the base temperatures T_0 and T_1 can be maintained over a long period of time, so that the filament reaches equilibrium. Should it sag under the new temperature, or should the field of view scan an inhomogenious distribution of temperatures, the effect will be less severe than in the previous approach.

2. Doubly tunable Fabry-Perots have the potential of wavelength modulation of the observation using one surface as the static adjustment and the other to modulate the wavelength periodically.

This adds an additional parameter of registration. Not only can the interferometer be instructed to search for the initial value of the emittance modulation, it can also register the wavelength derivative of this emission. This makes the topographical evaluation of the surface shown in Fig. 15 two dimensional, since this surface is symmetrical in wavelength and temperature.
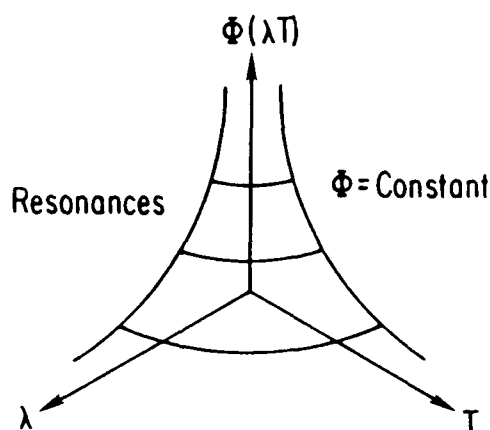

Fig. 15. Schematic representation of resonances as "10^{-4} roughness" on the contour lines of the $\Phi(\lambda T)$ function

This application is as novel for Fabry-Perot interferometers as it was for CCDs. We may encounter similar precision and reset limitations with respect to tunable Fabry-Perot interferometers as we have with CCDs.

Literature cites a scan linearity of 0.1% for the tunability, so that only one order of magnitude may separate us from the expected value of the resonances. It is not clear, however, whether scan linearity is our critical parameter. Rather, we must discover the limits within which a Fabry-Perot returns to an initial setting once it has been detuned.

The novel approach has the advantage, however, that the "static" nature makes it now possible to scan repeated runs until a sufficient value of the precision is obtained.

We are presently discussing the method with manufacturers of Fabry-Perot interferometers and will solicit sources of funding for the project once we are sufficiently certain of its merits.

References

1. Seraphin, B. O. and R. B. Hess, Phys. Rev. Lett. **14**, 138 (1965).

2. Seraphin, B. O., Phys. Rev. A **140**, 1716 (1965).

3. Aspnes, D. E. and A. A. Studna, Phys. Rev. B **7**, 4605 (1973).

4. Christensen, N. E. and B. O. Seraphin, Phys. Rev. B **4**, 3321 (1971).

5. Seraphin, B. O., and N. Bottka, Phys. Rev. **145**, 628 (1966).

6. We gratefully acknowledge the suggestion of R. R. Shannon for this simulation.

END

DATE
FILMED

6-88

DTIC